ADAPTIVE SIGNAL SUBSPACE DIGITAL RECEIVERS FOR COMMUNICATION IN TIME-VARYING NOISE

by

Jerry Roger Mitchell, Jr.

Thesis submitted to the Faculty of the
Virginia Polytechnic Institute and State University
in partial fulfillment of the requirements for the degree of

Master of Science
in
Electrical Engineering

APPROVED:

A. A. (Louis) Beex, Chairman

H. F. VanLandingham

J. S. Bay

April 1992
Blacksburg, Virginia

ADAPTIVE SIGNAL SUBSPACE DIGITAL RECEIVERS FOR COMMUNICATION IN TIME-VARYING NOISE

by
Jerry Roger Mitchell, Jr.

Committee Chairman: A. A. (Louis) Beex
Electrical Engineering

(ABSTRACT)

We develop a general three stage Moving Average Matched Filter (MAMF) receiver system for digital communications in an environment where the noise conditions are *unknown a priori and change constantly and significantly* with time. The MAMF is a subset of the class of matched filters which are optimal with respect to enhancing the signal energy relative to the noise power in order to improve discrimination between signals at the receiver. In a time-varying noise environment, a fixed signal cannot be designed and used for transmission which will provide optimal performance at the receiver under all noise conditions. Designing a signal for optimality in a particular noise environment will typically lead to deteriorated performance in another noise environment relative to a signal which is chosen for the new environment. This deterioration in performance can be so severe that the signal-to-noise ratio (SNR) from the input to the output of the filter is degraded. Ideally, to achieve performance which is more nearly optimal under all noise conditions, the transmitted signal should change or *adapt* in response to variations in the noise environment.

For practical reasons it is desirable to concentrate all adaptivity in the receiver rather than the transmitter. Typically, a MAMF receiver consists of two stages - a *filtering* stage and a *detection* stage. We develop the general design expressions for a three stage MAMF receiver in which the additional stage is a *linear pre-filter* placed before the filtering and detection stages.

Obviously, if the MAMF is optimal for a given noise condition, any

operation performed on the received signal plus noise prior to filtering will potentially reduce performance at that given noise condition by some amount. We accept this performance loss in favor of a pre-filtering operation which can effectively manipulate the transmitted signal upon arrival at the receiver and provide more *robust* performance in the time-varying noise environment.

Specifically, we compare a pre-filter consisting of a unity gain with a pre-filter which linearly combines k $M \times 1$ partitions of the transmitted signal vector (i.e. transmitted signal vector of length $N = k \times M$). Proper design of the transmitted signals can ensure that the partitions are linearly independent. In this case, we can view the transmitted signal as representing a k-dimensional subspace of the original M-dimensional signal space. By linearly combining these partitions at the receiver we can achieve any vector within this subspace. We show that we can select these partitions such that the resulting signal vector represents an optimum signal subspace for k noise environments. This is contrasted with the fixed 1-dimensional subspace of the original N-dimensional signal subspace when the pre-filter is a constant gain.

The two MAMF receivers are compared by measuring the signal-to-noise ratio improvement (SNRI) of the filters. The SNRI is defined as the output signal-to-noise ratio (OSNR) measured at the output of the filtering stage over the input signal-to-noise ratio (ISNR) measured at the input to the pre-filtering stage. We demonstrate through simulation that the signal subspace version can be more robust with respect to deviation from the absolute maximum SNRI achievable by either system.

Using maximum likelihood techniques, we derive an optimal detector for an arbitrary bank of L linear pre-filter and MAMF sections. This is shown to outperform a detection scheme which has been derived for use solely in an optimal binary communication scenario.

Acknowledgements

I would like to thank my advisor and friend Dr. A. A. (Louis/Indiana) Beex for his patience and sense of humor in dealing with me over the last couple of years. He has earned both my respect and admiration and it has truly been a pleasure to work with him. Thanks also to Dr. Hugh VanLandingham and Dr. John Bay for agreeing to sit in judgement as my committee and to the Naval Surface Warfare Center for providing the funding for the project.

A special thanks to my parents Jerry and Katie, my brother Doug, and my sister Connie, who through their love and actions six years ago set in motion the events which led to this work.

Most especially, thank you Karla for standing by me through it all and providing the love and companionship which gave me the strength and motivation to complete my degree.

I dedicate this work to the late Mr. Bird, my cockatiel who died last fall, but was with me for the five or so years it took to finish my B. S. and M. S. degrees.

TABLE OF CONTENTS

LIST OF FIGURES

LIST OF TABLES

1.0 INTRODUCTION

Any communications system can be separated into three primary segments - the *transmitter*, the *channel*, and the *receiver* (Figure 1). The transmitter accepts and encodes the data symbols using a finite library of L signals (i.e. $L = 2$ for binary communication), which are then sent or transmitted to the receiver. The transmitted signal must pass through some medium or channel, where it is subject to corruption (noise), prior to arrival at the receiver. Examples of various communication channels would be the atmosphere, water, coaxial cables, or optical fibers. At the receiver the noise corrupted signal is accepted and a determination is made as to which of the L signals is most likely to have actually arrived, following which it is decoded into the appropriate data symbol.

In a digital communications system, we have available a finite library of L signal vectors at the transmitter with which to encode the data symbols. These signal vectors are used in some fashion to modulate the actual signal waveform which is transmitted through the channel. Several methods by which this channel encoding procedure may be accomplished for the L-ary communications system are *amplitude shift keying* (ASK), *phase shift keying* (PSK), or *frequency shift keying* (FSK) [29]. These three methods use the coefficients of the signal vector to modulate the amplitude, phase, or frequency respectively, of the actual transmitted sinusoidal waveform. Similarly, at the receiver the channel decoder converts the corrupted signal waveform back into a vector of corrupted measurements which is viewed as a function of the original signal vector and the channel noise. This process is fixed in the system design and has no direct influence on any subsequent processing of the corrupted signal vector. Without any loss of generality we can refer to the transmission of signal vectors and the reception of corrupted signal vectors understanding that they are converted in

actual transmission or reception by the channel encoder and channel decoder respectively.

If there were no corruption or *noise* effect on the signal in the channel then there would be little problem in determining which signal was sent. In practice this is rarely the case and the channel noise can cause severe problems with respect to making this decision. These problems are in part due to the lack of *a priori* knowledge relative to the noise characteristics (i.e. mean and autocorrelation) which require that we estimate the necessary information in some fashion from samples taken of the channel noise. The noise characteristics may be fairly constant, vary significantly but slowly (due to natural causes) or vary significantly and rapidly (due to man-made causes) with time. Therefore, in keeping with the worst-case scenario, the time interval in which noise samples can be taken must be kept short in order to ensure the "short term" wide sense stationarity of the noise. The resulting small number of noise samples may lead to poor estimates of the desired noise characteristics.

This thesis is concerned with the performance of moving average matched filter (MAMF) receiver systems in time-varying noise environments. MAMF receivers are a subset of the class of matched filter receivers. They offer the advantages of guaranteed stability, efficient design process, easy implementation, and the fact that they are optimal given the restriction of a MA solution to the matched filter problem. The two MAMF receiver systems we compare fit within a general three stage receiver framework consisting of a *pre-filtering stage*, a *filtering stage*, and a *detection stage* (Figure 3).

The MAMF performance can be measured by comparing the SNR at the output (OSNR) of the MAMF to the SNR at the input (ISNR) of the MAMF receiver system. The ratio of OSNR to ISNR is defined as the SNR improvement (SNRI) of the MAMF receiver. Given that the channel noise conditions match the assumed conditions under which the signal vector set was designed, the MAMF can produce the maximum SNRI under the MA restriction. Of course, the practical performance of a MAMF receiver is ultimately determined by the number of bit errors made in transmission or the bit error rate (BER).

The *filtering stage* of the receiver system is the MAMF itself. The goal of

the MAMF is to enhance the ratio of signal power relative to the noise power in an effort to maximize the probability of detection and the discrimination of known signals in colored noise. The MAMF receiver relies heavily on the assumed or estimated noise characteristics of the colored channel noise and the set of L available signal vectors ($\{\underline{s}_i\}$ $i = 0, \ldots, L-1$) which may be transmitted. The available set of signals is often designed under the assumption that some particular type of colored noise will actually exist in the channel. Conventionally, when the channel noise characteristics change rapidly with time, design of such a signal set cannot be made optimally and may cause significant degradation in the performance of the MAMF. This is primarily due to the inability of the receiver and the fixed signal set to change in response to existing channel noise conditions.

We desire an alternative which will allow the receiver to *adapt* in response to changes in the channel noise environment. It is desirable to concentrate all adaptation in the receiver for practical reasons. If the adaptation were to reside in the transmitter, this would necessitate some form of error free link to the receiver in order to inform the receiver of changes in the signal set. Obviously, such an error free link cannot be established in many applications (or we would use it for transmission) and the problem of communicating in a time-varying noise environment arises.

The function of the *pre-filtering stage* is to **incorporate this adaptability into the receiver.** Since the MAMF is designed around the knowledge of the actual set of signal vectors available, if we apply a pre-filtering operation which manipulates the signal vectors in response to the existing channel noise conditions, we are in effect *adapting* the signal vectors to the noise which may yield more consistent or *robust* performance in a time-varying noise environment. Often, in the attempt to provide robust performance under a variety of conditions, there is a sacrifice made relative to the maximum performance at a particular condition when that particular condition is actually present. Intuitively we might expect that since the MAMF is optimal under the assumptions made for a particular colored channel noise, any pre-filtering operation (other than a constant gain) will reduce the absolute maximum performance of the receiver for that particular colored channel noise.

The output of the pre-filtering stage is fed to the MAMF whose output is

in turn fed to the *detector*. The detector is often designed based on some fundamental assumptions concerning the colored channel noise and knowledge of the pre-filtering and filtering operations which occur prior to it. Ultimately, the goal of the detector is to decide (hopefully in some optimal fashion) which transmitted signal has most likely arrived at the receiver system. This is where the practical measurement of performance in terms of BER is conducted.

Traditionally, MAMF receivers have a pre-filter defined as a unity gain and there is no manipulation of the N-dimensional transmitted signal vector at the receiver. For this system we are transmitting a 1-dimensional subspace of the N-dimensional signal space. A MAMF receiver in which the signal vector is fixed at transmission and using a constant gain pre-filter at the receiver will be referred to as a fixed vector MAMF (FVMAMF).

In this work we compare the FVMAMF with a MAMF receiver whose pre-filter is not a constant gain. It should be apparent that there are an infinite number of possible pre-filters which could be used in the receiver. We restrict our attention to the subset of linear pre-filters, specifically one which will linearly combine various partitions of the transmitted signal in some fashion.

We construct the transmitted N-dimensional signal vector from k M-dimensional sub-vectors ($k \times M = N$) which are concatenated for transmission. By choosing the sub-vectors to be linearly independent, we can effectively transmit a k-dimensional subspace of the original M-dimensional signal space. A MAMF system in which the signal vector is fixed in this fashion at the transmitter and which has a pre-filter that linearly combines the sub-vectors at the receiver shall be denoted a signal subspace MAMF (SSMAMF). Note that both the FVMAMF and the SSMAMF transmit a signal vector of length N.

At the receiver, the pre-filter linearly combines the k sub-vectors of the SSMAMF signal vector and its associated channel noise components in an attempt to maximize the OSNR of the SSMAMF (Figure 4). The resulting length of the pre-filtered signals in the FV and SSMAMF receiver systems is N and M respectively. Since the length of the pre-filtered signal is exactly the length of the MAMF, we can see that the SSMAMF sacrifices the longer filter length (and the potential for noise cancellation) of the FVMAMF for the added flexibility of

manipulating the received signal and channel noise at the receiver.

As mentioned earlier the MAMF design relies also on the assumed transmitted signal vector. It is reasonable then to have available at the receiver a pre-filter and MAMF designed around each one of the L possible signal vectors; in other words a bank of L pre-filter and MAMF sections which will then feed their outputs to a detector for signal determination (see Figure 5). A detection scheme was presented by Kontoyannis [5] to accomplish this task in the specific case of an optimal binary communication system.

The major purposes of this thesis are to, a) derive the design equations for the general three stage MAMF receiver system; b) develop methods by which the highly non-linear OSNR of the SSMAMF receiver can be maximized; c) derive an optimal detection method for an arbitrary bank of L linear pre-filter and MAMF sections; d) determine methods for the design of optimal signal vectors for the SSMAMF in the case of given colored channel noise(s); and e) investigate the design of "robust" signals for the FV and SSMAMF in the case of time-varying colored channel noise.

The theoretical development of the general three stage MAMF receiver (including OSNR maximization, signal design and optimal detection) is presented in Chapter 2. Chapter 3 describes the specific communication system (i.e. signal vectors, channel noise, and MAMF receiver) which we chose to simulate. In Chapter 4 results of the simulations in terms of SNRI are examined to compare the response of the FV and SSMAMF receivers to changes in the noise environment. Additionally, we verify that the BER performance of the detection scheme derived in Chapter 2 is equivalent to the method derived [5] for the optimal binary communication case and superior when this condition is not met. A discussion of the overall performance of both systems and recommendations for future work are found in Chapter 5.

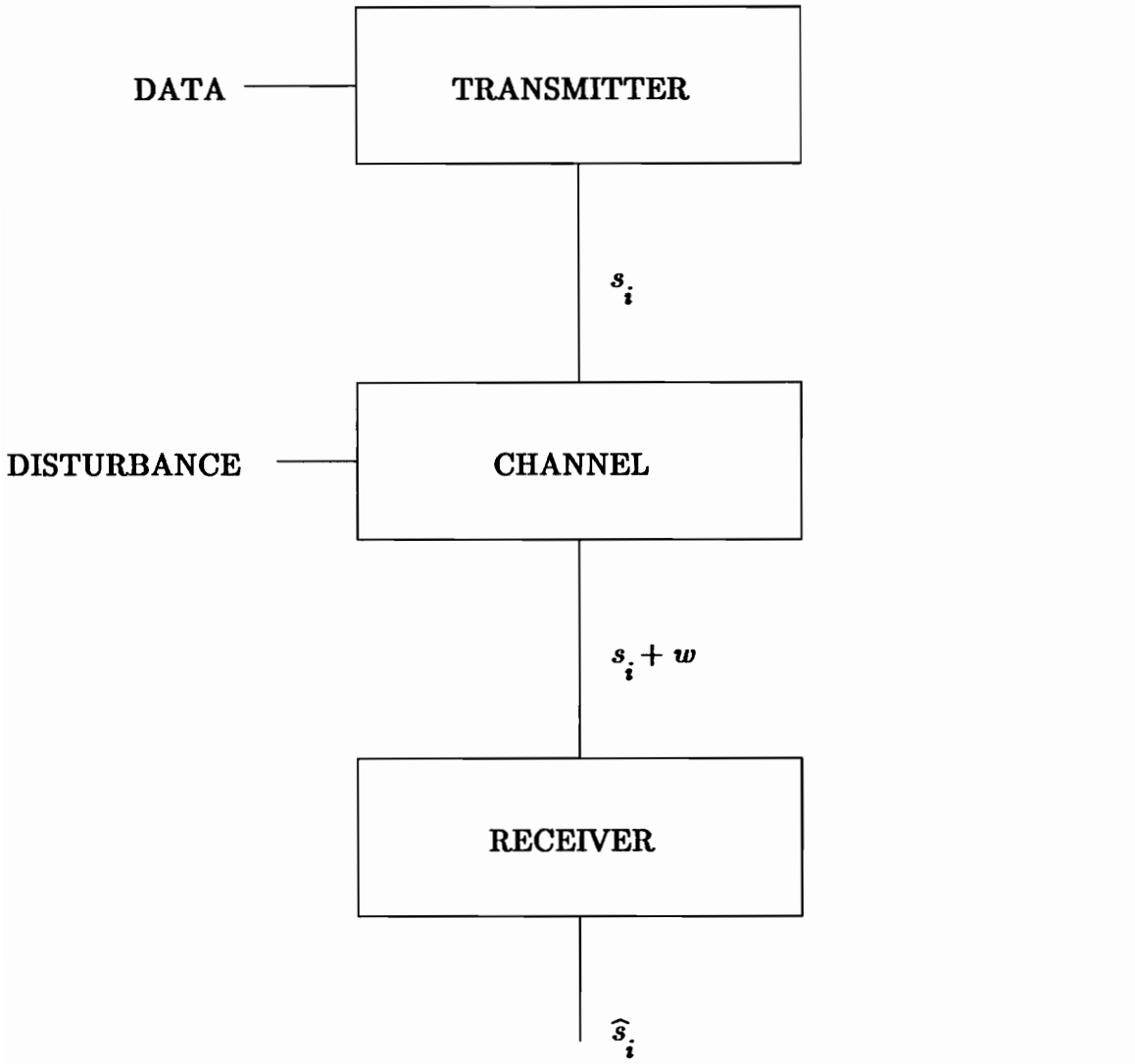

FIGURE 1: General Communication System

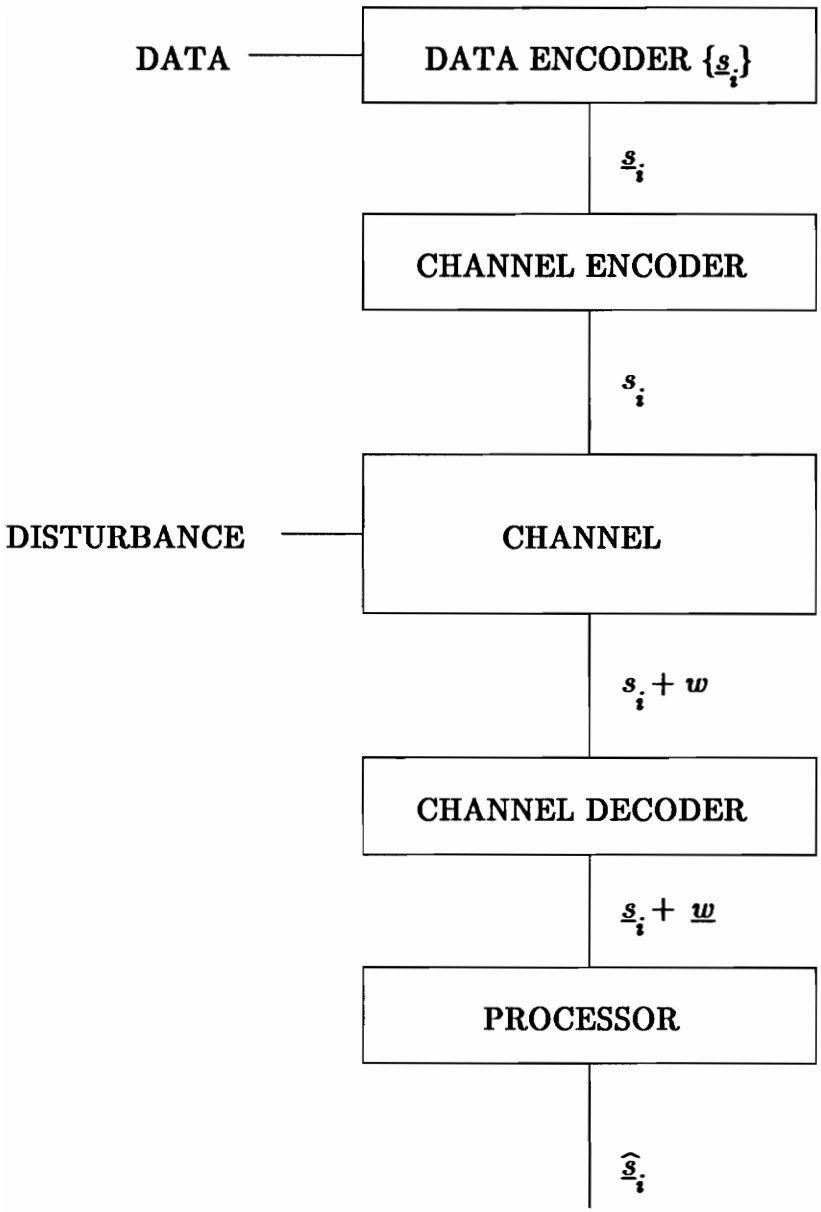

FIGURE 2: General Digital Communication System

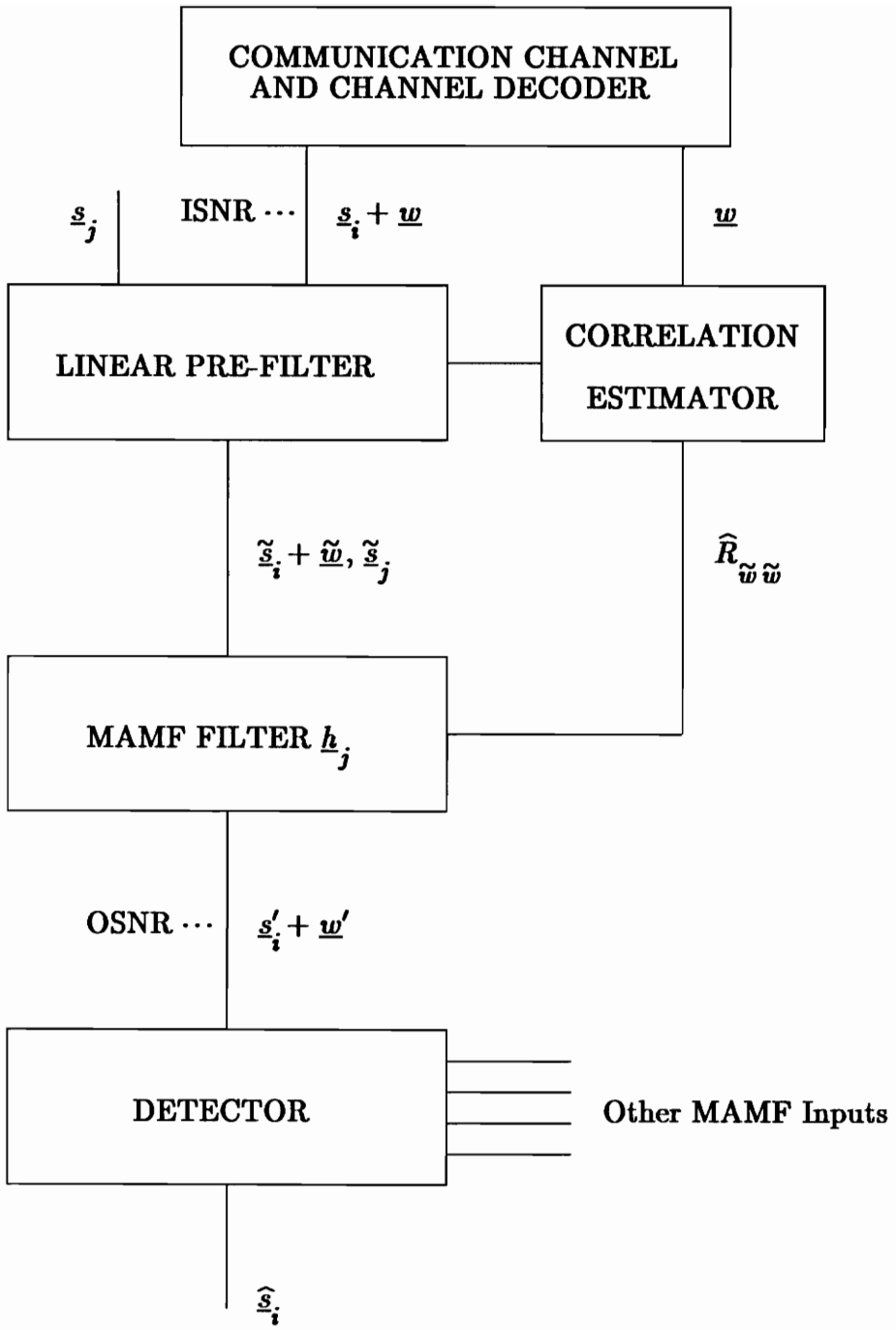

FIGURE 3: Three (3) Stage MAMF Receiver System

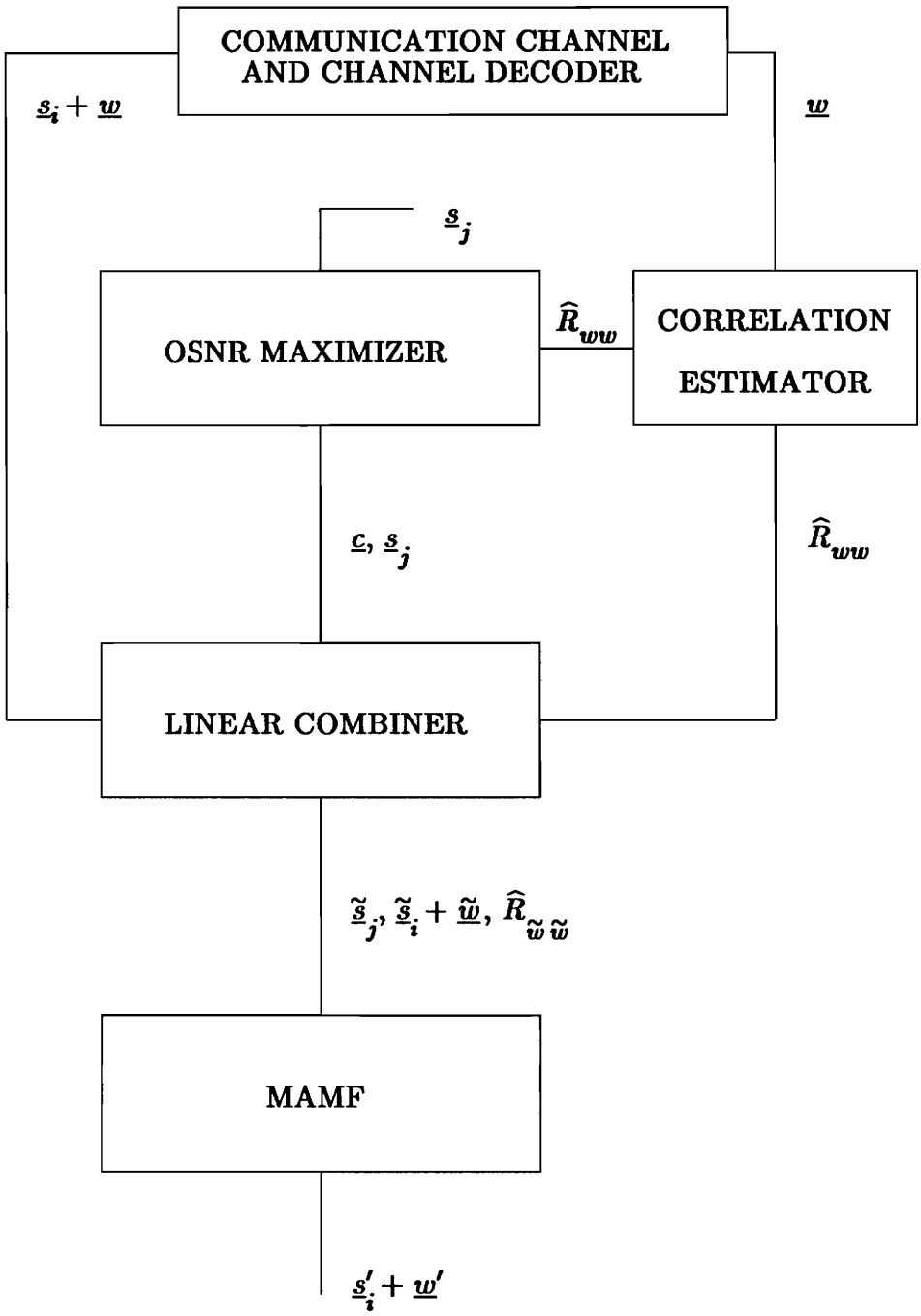

FIGURE 4: SSMAMF Receiver System (Linear Combination, OSNR Maximization, and MAMF)

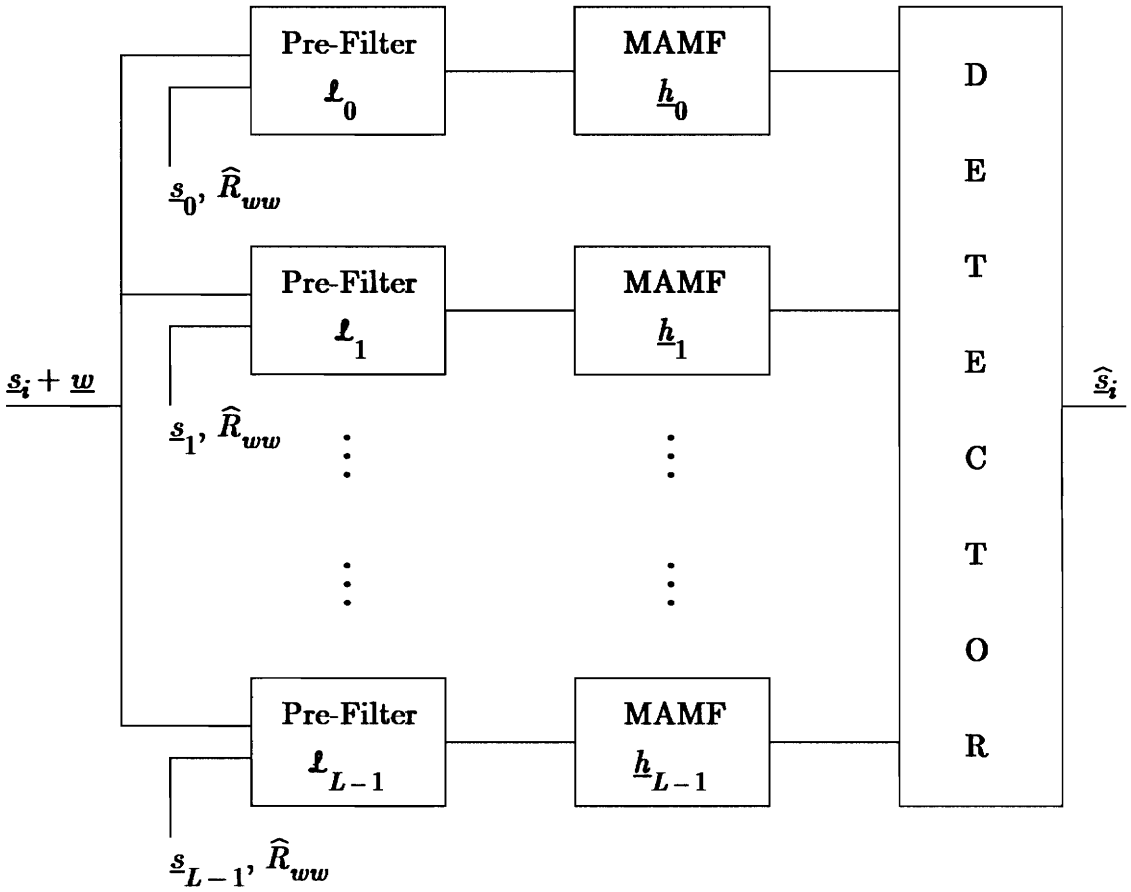

FIGURE 5: Bank of L Pre-filter and MAMF Sections with Detector

2.0 THEORETICAL DEVELOPMENT

This chapter develops the theory underlying the FVMAMF and SSMAMF systems from the design of transmitted signal vectors to their arrival and subsequent processing at the receiver. The channel noise characteristics are presented along with various channel noise correlation estimation procedures. Some estimation procedure is necessary for any practical implementation of either MAMF system. The design requirements, the performance criterion, and the optimal signal design are derived first for the general three stage MAMF receiver and then modified to incorporate the specific effects of the linear pre-filter used by the FVMAMF and SSMAMF. Techniques for maximizing the highly non-linear OSNR function of the SSMAMF are derived and their relative merits discussed. The SSMAMF can be "optimized" for multiple noise conditions indicating its more robust nature. The SSMAMF is shown to be a more general form of the FVMAMF. Making some assumptions about the channel noise, an optimal detection scheme is laid out for a bank of L arbitrary MA filters.

2.1 SIGNAL VECTOR TRANSMISSION

This thesis compares two MAMF receiver systems which transmit a given fixed N-dimensional signal vector. The method in which these signal vectors are designed and subsequently used in the design of the MAMF receiver differs significantly.

For the FVMAMF we have available at the transmitter a set of L possible signal vectors of dimension N with which to encode data symbols

$$\left\{\underline{s}_i\right\} \quad i = 0, \ldots, L-1 \tag{2.1}$$

where $N \geq L$. The value of L depends on the type of communication system in use (i.e. $L = 2$ implies a binary system, etc.). For convenient use in later sections we shall define the signal vector as the time reverse of the transmitted signal sample values, i.e.,

$$\underline{s}_i = \begin{bmatrix} s_{i,N-1} & \cdots & s_{i,1} & s_{i,0} \end{bmatrix}^{\mathrm{T}} \tag{2.2}$$

The dimension of the signal vector, N, is at the discretion of the designer but in practice would be constrained by considerations arising from available hardware, desired transmission rates and receiver processing speed.

Once transmitted the signal is subject to the channel noise w, leading to the definition of the noise vector $\underline{w}$ analogous to the above signal

$$\underline{w} = \begin{bmatrix} w_{N-1} & \cdots & w_1 & w_0 \end{bmatrix}^{\mathrm{T}} \tag{2.3}$$

The noise corrupted signal r, arriving at the receiver is some function of both the transmitted signal and the channel noise, in vector form

$$\underline{r}_{FV} = f_F(\underline{s}_i, \underline{w}) \tag{2.4}$$

The comparable SSMAMF also has available for transmission a set of L signal vectors of dimension N defined in reverse order as described for the

FVMAMF. We partition each of the L N-dimensional signal vectors into k M-dimensional subvectors ($k \times M = N$)

$$\underline{s}_i = \left[\begin{array}{ccccccc} \underline{s}_{i,0}^{\mathrm{T}} & | & \underline{s}_{i,1}^{\mathrm{T}} & | & \cdots & | & \underline{s}_{i,k-1}^{\mathrm{T}} \end{array} \right]^{\mathrm{T}} \tag{2.5}$$

An alternative representation is to view the partitions of $\underline{s}_i$ as columns of a signal matrix S_i

$$S_i = \left[\begin{array}{ccccccc} \underline{s}_{i,0} & | & \underline{s}_{i,1} & | & \cdots & | & \underline{s}_{i,k-1} \end{array} \right] \tag{2.6}$$

which are then transmitted sequentially, effectively as a single vector. Equation (2.6) will prove a more convenient form for manipulation of the expressions governing the SSMAMF. Thus, we could refer to the SSMAMF as having available a set of L $M \times k$ signal matrices to encode the data symbols

$$\left\{ S_i \right\} \quad i = 0, \ldots, L-1 \tag{2.7}$$

The dimension of the transmitted signal matrix is equal to the number of linearly independent columns (rank) of S_i and these columns form a set of basis vectors for a signal subspace. Instead of the single dimensional signal subspace effectively transmitted with the FVMAMF we now have the ability to transmit a k-dimensional signal subspace.

In the channel the signal is subject to noise. The noise vector $\underline{w}$ can be expressed as

$$\underline{w} = \left[\begin{array}{ccccccc} \underline{w}_0^{\mathrm{T}} & | & \underline{w}_1^{\mathrm{T}} & | & \cdots & | & \underline{w}_{k-1}^{\mathrm{T}} \end{array} \right]^{\mathrm{T}} \tag{2.8a}$$

$$W = \left[\begin{array}{ccccccc} \underline{w}_0 & | & \underline{w}_1 & | & \cdots & | & \underline{w}_{k-1} \end{array} \right] \tag{2.8b}$$

The noise corrupted signal arriving at the SSMAMF receiver can also be expressed in matrix form and is a function of both the signal matrix and the associated noise matrix

$$\begin{aligned} R_{SS} &= \left[\begin{array}{ccccccc} \underline{r}_0 & | & \underline{r}_1 & | & \cdots & | & \underline{r}_{k-1} \end{array} \right] \\ &= f_S(S_i, W) \end{aligned} \tag{2.9}$$

2.2 CHANNEL NOISE CHARACTERISTICS

The assumptions made concerning and the resulting characteristics of the noise in the communications channel play an integral role in the development of the MAMF receivers.

Definition: *The* ***transmission interval*** *is the time required for transmission of a single data symbol. It is defined to be, as a minimum, the time required to transmit a vector of length $2N$. This allows a gap, equal to the time needed to transmit a vector of length N, just prior to the arrival at the receiver of the corrupted signal which can be used to take samples of the channel noise.*

Given the above definition we assume that while the noise is in fact time-varying, it is ***wide-sense stationary*** (WSS) during the transmission interval. WSS implies that during this interval the mean value of the noise is independent of time and its correlation sequence depends only on the time difference between samples [1]. This means that the noise *characteristics* (statistics) remain the same for a single transmission interval. Obviously, the shorter the transmission interval the more valid our assumption. One effect of this is that restrictions are placed on the designer with respect to the maximum length attainable for the transmitted signal vector without violating the WSS assumption.

The remaining assumptions for the channel noise in this thesis are that the channel noise is ***additive, real, colored, and Gaussian*** with zero-mean and variance σ_w^2. Using the additive nature of the noise we can rewrite the noise corrupted signal vector and matrix of (2.4) and (2.9) arriving at the receiver for the FV and SSMAMF respectively as

$$\underline{r}_{FV} = \underline{s}_i + \underline{w} \tag{2.10}$$

$$R_{SS} = S_i + W \tag{2.11}$$

Note that R_{SS} is an $M \times k$ matrix whose columns are given by

$$\underline{r}_j = \underline{s}_{i,j} + \underline{w}_j \quad j = 0, \ldots, k-1 \tag{2.12}$$

The first and second order noise statistics (i.e. mean and correlation) can be written

$$E\{w_i\} = 0 \tag{2.13}$$

$$r_{ww,\tau} = E\{w_i w_{i+\tau}\} \quad \tau = 0, \ldots, N-1 \tag{2.14}$$

Obviously, if the noise is real, the autocorrelation sequence of (2.14) is also real. The autocorrelation sequence of any such noise is positive semi-definite [2,6]. A non-positive semi-definite or non-positive definite ($\Rightarrow$ negative definite) sequence does not represent an autocorrelation sequence.

Symmetric Toeplitz matrices formed from the noise correlation sequence will play a critical part in the design of both the FV and the SSMAMF. The following properties of an arbitrary $n \times n$ symmetric Toeplitz matrix R will be useful in various aspects of the development. Any properties involving the inverse of the matrix assume that R is non-singular. The elements of R are denoted r_{ij}.

1) R is persymmetric, by the definition of symmetric Toeplitz matrices (i.e., elements given by $r_{ij} = r_{ji} = r_{n+1-i,n+1-j}$) [28].

2) R^{-1} is persymmetric, but not necessarily Toeplitz [28].

3) $R = R^{\mathrm{T}}$ and $\left(R^{-1}\right)^{\mathrm{T}} = R^{-1}$, by definition of symmetric matrices.

4) R is similar to a diagonal matrix Λ whose elements are the eigenvalues of R through a transformation matrix U whose columns are the eigenvectors of R .

5) R is positive semi-definite as a result of being formed from a positive semi-definite correlation sequence [6].

6) R has n real eigenvalues by definition of symmetric matrices. The eigenvalues are all ≥ 0 by definition of positive semi-definite.

7) R has, or can be made to have, n orthonormal eigenvectors [3,15,28].

8) If n is odd and R has distinct eigenvalues then it has $(n+1)/2$ symmetric eigenvectors and $(n-1)/2$ skew symmetric eigenvectors. If n is even and R has distinct eigenvalues then it has $n/2$ symmetric and $n/2$ skew symmetric eigenvectors [16]. A vector $\underline{v}$ is defined as symmetric if it satisfies $J\underline{v} = \underline{v}$ and skew-symmetric if $J\underline{v} = -\underline{v}$ where J represents the exchange matrix with ones along the anti-diagonal and zeros elsewhere.

9) If R has multiple eigenvalues then the corresponding eigenvectors are neither unique, nor do they necessarily possess any symmetry. They may be chosen symmetric or skew-symmetric if desired.

2.3 AUTOCORRELATION FUNCTION ESTIMATORS

We are concerned with channel noise which is time-varying but assumed to be WSS during the transmission interval. Due to the continually varying nature of the noise, the noise autocorrelation function (ACF) associated with the transmission of any arbitrary bit is **not known *a priori*** and must be estimated in some fashion. The estimate is constructed from noise samples w_k, taken in the gap between symbol transmissions just prior to the arrival of the corrupted signal.

Definition: *An estimator is said to be asymptotically* ***consistent*** *if it produces an estimate which approaches the actual value of the desired parameter as the length of the data sequence used in the estimation procedure approaches infinity.*

Definition: *An estimator is said to be* ***unbiased (biased)*** *if the expected value of the estimate is equal (unequal) to the desired parameter.*

A consistent estimator for the ACF is desirable in that the resulting estimates converge to the actual ACF as more samples are added to the data sequence. Unfortunately, due to the WSS assumption we are restricted to fairly short record lengths which may produce poor or inaccurate estimates of the actual ACF. In §2.2 the noise correlation matrix R is defined as positive semi-definite. Therefore, we would prefer estimators which produce positive semi-definite estimates of the ACF. On a practical level, a correlation estimate which is not positive semi-definite generates an estimated correlation matrix R with non-positive eigenvalues. Negative eigenvalues would correspond to the physically impossible situation of negative noise power at some frequencies. One reason for the use of a biased rather than an unbiased estimator would be to guarantee a positive semi-definite R [3,4] for any data length available.

2.3.1 Moving Average (MA) Estimators

Moving average (all zero) estimators may produce an estimate of the ACF

directly from the finite length data sequence. The moving average estimator considered in this work is the biased ACF estimator. The biased estimator was compared with the unbiased, diagonal, triangular, exponential, and minimum norm moving average estimators [4] and found to yield the highest average and the lowest standard deviation for SNRI under conditions of white, lowpass and bandpass noise. The biased estimate of the noise autocorrelation sequence can be obtained from the noise sequence w_k of length N using

$$\hat{r}_{ww,l} = \frac{1}{N} \sum_{k=0}^{N-l-1} w_k w_{k+l} \qquad l = 0,\ldots,N-1 \tag{2.15}$$

Note that since the noise sequence is assumed to be real

$$\hat{r}_{ww,l} = \hat{r}_{ww,-l} \tag{2.16}$$

Unless specified otherwise an estimated quantity is denoted by $\hat{}$, throughout this thesis. As indicated by its name the estimator is biased

$$E\{\hat{r}_{ww,l}\} \neq r_{ww,l} \tag{2.17}$$

The estimator will uphold our WSS assumption by producing a positive semi-definite estimate of the ACF [4].

There are two primary advantages to the use of this biased estimator. First, the estimator uses the entire data sequence. This is of particular importance in MAMF design which relies heavily on estimated noise correlations. Second, the biased estimator requires comparatively few calculations [3].

2.3.2 Autoregressive (AR) Estimators

Autoregressive (AR) or all-pole estimators model the data sequence as the output of an AR filter driven by white noise. Once the model parameters have been estimated the corresponding estimate of the autocorrelation sequence can be generated using a method [17] which involves initializing the autocorrelation

sequence as the solution to a system of equations and then extending this sequence recursively to any arbitrary length. An alternative is to apply the backward Levinson algorithm to generate the correlation sequence. The specific AR estimators considered are the Autocorrelation Method, the Burg Method, the Covariance Method, the Modified Covariance Method and the Recursive Maximum Likelihood Method. All these methods are approximate maximum likelihood estimators (MLE) and they perform comparably on large data records. Their performance on short data records varies due to differences in the algorithms. Algorithms for each method abound [6].

In keeping with our WSS assumption for the channel noise, we desire the AR technique used to produce a stable filter (all poles inside the unit circle) which would result in a positive semi-definite correlation estimate. An unstable model could correspond to a non-stationary noise process. With this in mind the Covariance and Modified Covariance Methods are suspect as they can produce filter models with unstable poles. The other three methods are guaranteed to produce stable filter models [6].

The AR techniques generate a model based on an assumed order. Underestimating the model order will restrict the resulting correlation sequence and may produce poor results. To minimize this effect the model order should be chosen high enough but not too high given the length of the data sequence available. A rule of thumb often used is to choose the model order to be between $N/3$ and $N/2$. More sophisticated order selection techniques may be used [6].

Computationally the AR estimators impose a "modest" burden while one may take advantage of the structure of their governing equations to reduce this burden [6]. Regardless, whether the model parameters are to be estimated first and then used to determine the estimate of the noise autocorrelation sequence or whether the backward Levinson algorithm is used, the computational requirements are greater than for the moving average estimator described in §2.3.1.

2.4 MOVING AVERAGE MATCHED FILTER (MAMF) BASED RECEIVER

In any communication system the ultimate goal of the receiver is to determine which signal, if any, is present at a given time. Recall that the received signal consists of both the transmitted signal and the additive channel noise. It would seem reasonable, in terms of our ability to detect the transmitted signal, to seek a method of reception which would enhance the signal relative to the noise.

Typically, a receiver attempting to achieve the above goal might consist of two stages. The first stage consists of processing or *filtering* to enhance the signal relative to the noise and the second stage consists of determining or *detecting* which of the signals would most likely have been transmitted given the results of the filtering stage.

A more general version of this receiver could be described in terms of three stages rather than two as seen in Figure 3. The first or *pre-filtering* stage represents processing occurring prior to the second or filtering stage which is still followed by the detection stage. We shall restrict the operations of the first stage to be linear and thus have all the properties associated with a linear operator. Note that the two stage system is obtained if the pre-filtering stage is defined as a unity gain.

In this thesis we shall use for the filtering stage ***matched filters*** which provide a method of accomplishing signal enhancement in terms of the ratio of signal energy to noise energy (SNR). Specifically, matched filters maximize the OSNR relative to some fixed ISNR for a given detection time n_0. They are optimal in this sense but the design process does not guarantee either stability or causality of the resulting filter. To remove this potential problem we restrict ourselves to ***moving average matched filters*** (MAMF). The MAMF is an all-zero filter (all poles lie at the origin) guaranteed to be both causal and stable. A MAMF is potentially sub-optimal when compared to a general autoregressive moving average (ARMA) matched filter in that it may not achieve the absolute maximum OSNR. However, it is optimal given the restriction of only allowing a moving average solution to the problem.

We define the time n_0 (maximum OSNR) to be $N-1$ where N is the length of the transmitted signal vector (or the impulse response of the filter). Should the OSNR be greater than the ISNR we have a SNRI greater than unity and the filtering process has improved our chances of determining the signal vector that was actually transmitted. Conversely, if the SNRI is less than unity we have *degraded* the signal relative to the noise and reduced the probability of determining the transmitted signal vector. Variables such as signal design and type of colored noise existing in the channel will affect the SNRI.

The final stage of the receiver or the *detector* actually makes the decision as to which signal vector was in fact most likely to have been sent. While our ability to detect the transmitted signal vector is tied closely to the SNRI of the MAMF, the practical measure of performance for the detection scheme is in terms of the number of decision errors made or the bit error rate (BER).

We will develop the equations characterizing the more general three stage MAMF based receiving system shown in Figure 3. The actual pre-filtering operations used in the FVMAMF and SSMAMF systems will be defined and incorporated into the general receiver formulation.

2.4.1 MAMF Characteristics

Define the impulse response of a MAMF in vector form as

$$\underline{h} = \begin{bmatrix} h_0 & h_1 & \cdots & h_{N-1} \end{bmatrix}^{\mathrm{T}} \tag{2.18}$$

The noise corrupted signal vector defined in time reverse order as described in §2.1 is

$$\underline{r} = \underline{s}_i + \underline{w} \tag{2.19}$$

We have restricted the pre-filtering stage to be some linear operation $\mathcal{L}(\cdot)$. Due to its linear nature the output of the block operating on the noise corrupted signal vector of (2.19) can be expressed as

$$\begin{aligned}\tilde{\underline{r}} &= \mathcal{L}(\underline{r}) \\ &= \mathcal{L}(\underline{s}_i + \underline{w}) \\ &= \mathcal{L}(\underline{s}_i) + \mathcal{L}(\underline{w}) \\ &= \tilde{\underline{s}}_i + \tilde{\underline{w}} \end{aligned} \tag{2.20}$$

The output of the MAMF at time $n > 0$ is given by

$$y_n = \sum_{l=0}^{N-1} h_l \tilde{r}_{n-l} \tag{2.21}$$

and at the time of interest $n = n_0 = N - 1$

$$\begin{aligned} y_{N-1} &= \sum_{l=0}^{N-1} h_l \tilde{r}_{N-1-l} \\ &= \underline{h}^{\mathrm{T}} \tilde{\underline{r}} \\ &= \underline{h}^{\mathrm{T}} (\tilde{\underline{s}}_i + \tilde{\underline{w}}) \\ &= \underline{h}^{\mathrm{T}} \tilde{\underline{s}}_i + \underline{h}^{\mathrm{T}} \tilde{\underline{w}} \\ &= \underline{s}'_i + \underline{w}' \end{aligned} \tag{2.22}$$

Note that (2.22) is nothing more than the superposition of the output of the filter due to the input signal and that due to the noise, measured at time $N - 1$.

2.4.2 Theoretical Performance of a MAMF

Recall that the transmitted signal vector and the channel noise vector were designated $\underline{s}_i$ and $\underline{w}$ respectively and that we defined, at the output of the pre-filtering stage, a new signal vector $\tilde{\underline{s}}_i$ and its associated noise vector $\tilde{\underline{w}}$ (Figure 3).

This will provide the general formulation applicable to any three stage receiver system regardless of the linear operation of the pre-filtering stage. The performance of the MAMF receiver system is characterized by its SNRI or the ratio of OSNR to ISNR.

$$\text{SNRI} = \frac{\text{OSNR}}{\text{ISNR}} \tag{2.23}$$

The ISNR of the MAMF is measured ***at the input to the receiver system*** (see Figure 3) and given by the ratio of signal energy to channel noise power

$$\text{ISNR} = \frac{E_{\underline{s}_i}}{P_{\underline{w}}} \tag{2.24}$$

Signal energy is determined at transmission and equal to a constant value E. The noise by assumption is WSS and its power is equal to its autocorrelation at lag 0. With this we can rewrite (2.24)

$$\text{ISNR} = \frac{E}{r_{ww,0}} \tag{2.25}$$

The OSNR of the MAMF is given by

$$\text{OSNR} = \frac{E_{\underline{s}'}}{P_{\underline{w}'}} \tag{2.26}$$

The output of the MAMF at time $N-1$ was shown in (2.22). The energy in the output due to the deterministic signal $\underline{\tilde{s}}_i$

$$E_{\underline{s}'} = \left(\underline{h}^{\mathrm{T}} \underline{\tilde{s}}_i \right)^2 \tag{2.27}$$

The output power due to the noise $\underline{\tilde{w}}$ can be found as the power when no signal is present or as the output autocorrelation of the filtered noise at lag 0.

$$E\left\{y_{N-1}^2\right\} = E\left\{\left(\sum_{l=0}^{N-1} h_l \tilde{w}_{N-1-l}\right)^2\right\}$$

$$= E\left\{\sum_{l=0}^{N-1} h_l \tilde{w}_{N-1-l} \sum_{m=0}^{N-1} h_m \tilde{w}_{N-1-m}\right\}$$

$$= E\left\{\sum_{l=0}^{N-1} h_l \sum_{m=0}^{N-1} h_m \tilde{w}_{N-1-l} \tilde{w}_{N-1-m}\right\}$$

$$= \sum_{l=0}^{N-1} h_l \sum_{m=0}^{N-1} h_m E\left\{\tilde{w}_{N-1-l} \tilde{w}_{N-1-l+l-m}\right\}$$

$$= \sum_{l=0}^{N-1} h_l \sum_{m=0}^{N-1} h_m r_{\tilde{w}\tilde{w},l-m}$$

$$= \underline{h}^{\mathrm{T}} R_{\tilde{w}\tilde{w}} \underline{h} \tag{2.28}$$

$R_{\tilde{w}\tilde{w}}$ is the Toeplitz autocorrelation matrix for the noise $\underline{\tilde{w}}$ at the input to the MAMF. Substituting (2.27) and (2.28) into (2.26)

$$\text{OSNR} = \frac{\left(\underline{h}^{\mathrm{T}} \underline{\tilde{s}}_i\right)^2}{\underline{h}^{\mathrm{T}} R_{\tilde{w}\tilde{w}} \underline{h}} \tag{2.29}$$

The ISNR for an arbitrary transmitted bit is determined by the transmitted signal vector and the noise conditions currently existing in the channel. Maximization of the MAMF SNRI is achieved by maximizing the MAMF OSNR. Assume the noise is both known and fixed during the transmission interval and the power of the filtered noise at time $N-1$ is some constant $P_{\underline{w}'}$. Under these conditions maximizing OSNR is equivalent to maximizing the square root of the energy for the filtered signal at time $N-1$. We can apply the technique of Lagrange multipliers to maximize the output signal energy by variation of the impulse response of the MAMF, given the constraint of constant output noise power.

$$F(\underline{h}) = \left(\pm \underline{h}^{\mathrm{T}} \underline{\tilde{s}}_i \right) + \lambda \left(\underline{h}^{\mathrm{T}} R_{\tilde{w}\tilde{w}} \underline{h} - P_{\underline{w}'} \right)$$

$$= \left(\pm \underline{\tilde{s}}_i^{\mathrm{T}} \underline{h} \right) + \lambda \left(\underline{h}^{\mathrm{T}} R_{\tilde{w}\tilde{w}} \underline{h} - P_{\underline{w}'} \right) \tag{2.30}$$

Taking the partial derivative of (2.30) with respect to $\underline{h}$ and setting the result equal to zero

$$\frac{\partial F(\underline{h})}{\partial \underline{h}} = \pm \underline{\tilde{s}}_i + \lambda \left(R_{\tilde{w}\tilde{w}} \underline{h} + R_{\tilde{w}\tilde{w}}^{\mathrm{T}} \underline{h} \right) = \underline{0} \tag{2.31}$$

Recalling the properties of symmetric matrices in §2.2

$$\frac{\partial F(\underline{h})}{\partial \underline{h}} = \pm \underline{\tilde{s}}_i + \lambda \left(2 R_{\tilde{w}\tilde{w}} \underline{h} \right) = \underline{0} \tag{2.32}$$

Assuming that the correlation matrix is non-singular we can solve for the optimal impulse response $\underline{h}^{\dagger}$ ($\dagger$ denotes optimum) from

$$\underline{h}^{\dagger} = \left(\mp \frac{1}{2\lambda} \right) R_{\tilde{w}\tilde{w}}^{-1} \underline{\tilde{s}}_i \tag{2.33}$$

From (2.33) we can see that there are in fact two solutions for a given signal which yield the same OSNR. It is apparent from (2.29) that multiplying the optimum impulse response of the MAMF by an arbitrary constant does not affect OSNR and we can write

$$\underline{h}^{\dagger} = R_{\tilde{w}\tilde{w}}^{-1} \underline{\tilde{s}}_i \tag{2.34}$$

The optimum OSNR can be obtained by substituting (2.34) in (2.29)

$$\mathrm{OSNR}^{\dagger} = \frac{\left(\underline{\tilde{s}}_i^{\mathrm{T}} R_{\tilde{w}\tilde{w}}^{-1} \underline{\tilde{s}}_i \right)^2}{\underline{\tilde{s}}_i^{\mathrm{T}} R_{\tilde{w}\tilde{w}}^{-1} R_{\tilde{w}\tilde{w}} R_{\tilde{w}\tilde{w}}^{-1} \underline{\tilde{s}}_i}$$

$$= \tilde{\underline{s}}_i^{\,T} R_{\tilde{w}\tilde{w}}^{-1} \tilde{\underline{s}}_i \tag{2.35}$$

Using $\text{OSNR}^{\dagger}$ the $\text{SNRI}^{\dagger}$ from (2.23) is

$$\begin{aligned} \text{SNRI}^{\dagger} &= \frac{\text{OSNR}^{\dagger}}{\text{ISNR}} \\ &= \frac{\left(\tilde{\underline{s}}_i^{\,T} R_{\tilde{w}\tilde{w}}^{-1} \tilde{\underline{s}}_i \right)}{\frac{E}{r_{ww,0}}} \end{aligned} \tag{2.36}$$

Equation (2.36) represents the theoretical maximum SNRI of the MAMF for a given signal under the conditions of a known ACF.

Note that (2.35) is a quadratic form. This implies that the absolute maximum achievable output signal-to-noise ratio, $\text{OSNR}^{\ddagger}$, and thus $\text{SNRI}^{\ddagger}$ is obtained for a known ACF when the signal vector is chosen as an eigenvector corresponding to the minimum eigenvalue of $R_{\tilde{w}\tilde{w}}$ [9].

2.4.3 Practical Performance of a MAMF

In §2.4.2 the performance of a MAMF was presented under the condition that the ACF of the noise was known *a priori*. Since the noise is in fact time-varying it is unlikely that this condition would be met in practice. Instead we must sample the channel noise and estimate the noise characteristics during the specified transmission interval. Depending on the accuracy of the estimate the impulse response of the MAMF will vary from its optimal form in (2.34). The impulse response of the filter designed on the basis of estimated noise correlations is given by

$$\hat{\underline{h}} = \hat{R}_{\tilde{w}\tilde{w}}^{-1} \tilde{\underline{s}}_i \tag{2.37}$$

It is most likely that the transmitted signal vector $\underline{s}_i$ and hence $\tilde{\underline{s}}_i$ will not be optimal in any sense with respect to the noise. The estimated OSNR is obtained

by substituting (2.37) in (2.29)

$$\widehat{\text{OSNR}} = \frac{(\underset{\sim}{\tilde{s}}_i^{\,T} \hat{R}_{\tilde{w}\tilde{w}}^{-1} \underset{\sim}{\tilde{s}}_i)^2}{\underset{\sim}{\tilde{s}}_i^{\,T} \hat{R}_{\tilde{w}\tilde{w}}^{-1} R_{\tilde{w}\tilde{w}} \hat{R}_{\tilde{w}\tilde{w}}^{-1} \underset{\sim}{\tilde{s}}_i} \tag{2.38}$$

Note that (2.38) reduces to (2.35) if our estimate of the correlation matrix equals the actual correlation matrix. Since our choice of $\underset{\sim}{h}^{\dagger}$ was made to maximize the OSNR of the MAMF, the use of $\underset{\sim}{\hat{h}}$ will result in

$$\widehat{\text{OSNR}} \leq \text{OSNR}^{\dagger}$$

$\widehat{\text{SNRI}}$ can be obtained by substituting (2.38) into (2.23) and will also be less than or equal to $\text{SNRI}^{\dagger}$.

2.5 LINEAR COMBINATION

As mentioned in §2.1 the SSMAMF effectively transmits a k-dimensional signal subspace. This is the feature of the SSMAMF that distinguishes it from the FVMAMF. Upon arrival at the receiver the received signal vector plus noise is separated into its partitioned form. The linear operation of the pre-filtering stage (see Figure 4) is defined as that which creates the linear combination of the transmitted basis vectors. By linearly combining the basis vectors (columns of the signal matrix) we can achieve any vector in the transmitted signal subspace. Similarly, the additive channel noise will be linearly combined resulting in new noise characteristics. Note that for the FVMAMF the pre-processing block consists of a constant gain equal to 1.

2.5.1 Effects of Linear Combination on Signal Energy

The process of linearly combining the basis vectors representing the signal subspace is the key to the ability of the SSMAMF to *adapt* the signal vector to the currently existing noise conditions. However, some restriction is required with respect to the values that the combination coefficients may take on. Without a constraint we would of necessity have to search an infinity of possible solutions. Wilson suggests that the constraint be that the energy of the linearly combined signal be equal to the energy of the transmitted signal, a known predetermined constant fixed at the transmitter [3].

The energy of the transmitted signal is equal to the sum of the energies of the individual partitions

$$\begin{aligned} E_{\underline{s}_i} &= \underline{s}_i^{\mathrm{T}}\, \underline{s}_i \\ &= \sum_{j=0}^{k\text{-}1} \underline{s}_{i,j}^{\mathrm{T}}\, \underline{s}_{i,j} \\ &= E \end{aligned} \tag{2.39}$$

We define a coefficient vector $\underline{c}$ associated with the i-th transmitted signal matrix

$$\underline{c} = \begin{bmatrix} c_0 & c_1 & \cdots & c_{k-1} \end{bmatrix}^{\mathrm{T}} \tag{2.40}$$

Using (2.06) and (2.40) the linearly combined signal can be written as

$$\underset{\sim}{\tilde{s}}_i = S_i \, \underline{c} \tag{2.41}$$

The energy of the linearly combined signal $\underset{\sim}{\tilde{s}}_i$ is,

$$\begin{aligned} E_{\underset{\sim}{\tilde{s}}_i} &= \underset{\sim}{\tilde{s}}_i^{\mathrm{T}} \, \underset{\sim}{\tilde{s}}_i \\ &= \underline{c}^{\mathrm{T}} \, S_i^{\mathrm{T}} \, S_i \, \underline{c} \end{aligned} \tag{2.42a}$$

$$= \underline{c}^{\mathrm{T}} \begin{bmatrix} \underline{s}_{i,0}^{\mathrm{T}} \, \underline{s}_{i,0} & \underline{s}_{i,0}^{\mathrm{T}} \, \underline{s}_{i,1} & \cdots & \underline{s}_{i,0}^{\mathrm{T}} \, \underline{s}_{i,k-1} \\ \underline{s}_{i,1}^{\mathrm{T}} \, \underline{s}_{i,0} & \ddots & & \vdots \\ \vdots & & \ddots & \vdots \\ \underline{s}_{i,k-1}^{\mathrm{T}} \, \underline{s}_{i,0} & \cdots & \cdots & \underline{s}_{i,k-1}^{\mathrm{T}} \, \underline{s}_{i,k-1} \end{bmatrix} \underline{c} \tag{2.42b}$$

The resulting combination coefficient constraint with respect to maintaining energy equal to that in the transmitted signal vector can be written in terms of (2.39) and (2.42*a*)

$$\underline{c}^{\mathrm{T}} \, S_i^{\mathrm{T}} \, S_i \, \underline{c} = E \tag{2.43a}$$

The quadratic constraint of (2.43*a*) can also be written out as

$$\sum_{l=0}^{k-1} c_l^2 \, \underline{s}_{i,l}^{\mathrm{T}} \, \underline{s}_{i,l} + \sum_{\substack{l=0 \\ l \neq m}}^{k-1} \sum_{m=0}^{k-1} c_l c_m \, \underline{s}_{i,l}^{\mathrm{T}} \, \underline{s}_{i,m} = E \tag{2.43b}$$

Equation (2.43) describes a hyper-ellipsoid in k-space.

To this point we have made no assumptions regarding the columns of the signal matrix S_i. In general, we shall require that the columns of S_i be linearly independent so that we achieve the maximum dimension k for the transmitted signal subspace. The dimension of the transmitted signal subspace directly impacts the amount of computation necessary at the SSMAMF receiver. Thus, transmitting a signal matrix of less than full rank (i.e. S_i has linearly dependent columns) would result in redundant information and an increase in processing time at the receiver.

It is interesting to observe what occurs when some additional restrictions are imposed on the columns of the signal matrix. Suppose we add the assumption that the columns $\underline{s}_{i,j}$ have energy equal to 1 (i.e. form a normal set of basis vectors)

$$\underline{s}_{i,j}^{\mathrm{T}} \, \underline{s}_{i,j} \;=\; 1 \tag{2.44}$$

This modifies (2.43a) such that each element of the main diagonal of the matrix $S_i^{\mathrm{T}} S_i$ becomes equal to 1 while (2.43b) reduces to

$$\sum_{l=0}^{k-1} c_l^2 \;+\; \sum_{\substack{l=0 \\ l \neq m}}^{k-1} \sum_{m=0}^{k-1} c_l c_m \, \underline{s}_{i,l}^{\mathrm{T}} \, \underline{s}_{i,m} \;=\; k \tag{2.45}$$

Adding an orthogonality constraint for the columns of the transmitted signal matrix,

$$\underline{s}_{i,l}^{\mathrm{T}} \, \underline{s}_{i,m} \;=\; \delta_{l-m} \tag{2.46}$$

yields an identity matrix in (2.43a), and (2.45) reduces to

$$\sum_{l=0}^{k-1} c_l^2 \;=\; k \tag{2.47}$$

Equation (2.47) now describes a k-dimensional hyper-sphere. The latter is the constraint used in [3,5].

Another variant would be to require only the orthogonality constraint in which case the matrix of the quadratic form in (2.43a) becomes diagonal with

entries representing the energy placed in each of the columns of the transmitted signal matrix.

The more general form of the coefficient constraint expressed in (2.43) is of particular importance if we arbitrarily define as signal vector for the SSMAMF system a signal vector which is used in the FVMAMF system (i.e. for comparison purposes). There is no reason to expect that the desired FVMAMF signal vector partitions into signal vectors of equal energy (as required by (2.45) and (2.47)) or that these partitioned signal vectors will be orthogonal (as required by (2.47)).

2.5.2 Effects of Linear Combination on Noise Statistics

We linearly combine the incoming signal matrix in order to adapt the signal vector to the noise environment currently existing in the channel. This implies that the additive channel noise will also be linearly combined resulting in a new noise sequence with different characteristics. Since the noise correlation is heavily relied on in the design of a MAMF we must investigate the effect of the linear combination process on the noise statistics.

The linearly combined noise sequence can be written similarly to (2.41)

$$\underline{\tilde{w}} = W\,\underline{c} \tag{2.48a}$$

$$= \sum_{l=0}^{k-1} c_l\,\underline{w}_l \tag{2.48b}$$

Each element of the linearly combined noise vector can be expressed by writing out (2.48a) using (2.3) and (2.8)

$$\tilde{w}_l = \sum_{m=0}^{k-1} c_m\, w_{(k-m)M-l-1} \qquad 0 \le l \le M-1 \tag{2.49}$$

Taking the expected value of (2.49) and using the fact that the additive channel

noise was assumed in §2.2 to be zero mean

$$E\left\{ \tilde{w}_l \right\} = E\left\{ \sum_{m=0}^{k-1} c_m \, w_{(k-m)M-l-1} \right\}$$

$$= \sum_{m=0}^{k-1} c_m \, E\left\{ w_{(k-m)M-l-1} \right\}$$

$$= 0 \tag{2.50}$$

Thus, the linearly combined noise sequence will also be zero mean. Given that the input noise autocorrelation is denoted $r_{ww,l}$ the linearly combined noise correlation is generated as follows

$$r_{\tilde{w}\tilde{w},n} = E\left\{ \tilde{w}_l \tilde{w}_{l+n} \right\}$$

$$= E\left\{ \sum_{q=0}^{k-1} c_q \, w_{(k-q)M-l-1} \sum_{s=0}^{k-1} c_s \, w_{(k-s)M-l-1-n} \right\}$$

$$= E\left\{ \sum_{q=0}^{k-1} c_q \sum_{s=0}^{k-1} c_s \, w_{(k-q)M-l-1} \; w_{(k-s)M-l-1-n} \right\}$$

$$= \sum_{q=0}^{k-1} c_q \sum_{s=0}^{k-1} c_s \, E\left\{ w_{(k-q)M-l-1} \; w_{(k-s)M-l-1-n} \right\}$$

$$= \sum_{q=0}^{k-1} c_q \sum_{s=0}^{k-1} c_s \, r_{ww,\, qM-sM-n}$$

$$= \sum_{q=0}^{k-1} c_q \sum_{s=0}^{k-1} c_s \, r_{ww,\, M(q-s)-n} \tag{2.51a}$$

Since the noise is assumed real, we have from the properties of the autocorrelation function that $r_{ww,x} = r_{ww,-x}$ [18], thus

$$r_{\tilde{w}\tilde{w},n} = \sum_{q=0}^{k-1} c_q \sum_{s=0}^{k-1} c_s \, r_{ww,\, n+M(s-q)} \tag{2.51b}$$

$$= \underline{c}^{\mathrm{T}} W_{r,n} \underline{c} \qquad 0 \leq n \leq M-1 \tag{2.51c}$$

where $W_{r,n}$ is defined as

$$W_{r,n} = \begin{bmatrix} r_{ww,n} & r_{ww,n+M} & \cdots & r_{ww,n+M(k-1)} \\ r_{ww,n-M} & r_{ww,n} & \cdots & r_{ww,n+M(k-2)} \\ \vdots & \vdots & \ddots & \vdots \\ r_{ww,n-M(k-1)} & \cdots & \cdots & r_{ww,n} \end{bmatrix} \tag{2.51d}$$

Note that $W_{r,n}$ is Toeplitz. Since (2.51c) represents a scalar value,

$$r_{\tilde{w}\tilde{w},n} = \underline{c}^{\mathrm{T}} W_{r,n} \underline{c}$$

$$= \left(\underline{c}^{\mathrm{T}} W_{r,n} \underline{c}\right)^{\mathrm{T}}$$

$$= \underline{c}^{\mathrm{T}} W_{r,n}^{\mathrm{T}} \underline{c}$$

$$= \sum_{q=0}^{k-1} c_q \sum_{s=0}^{k-1} c_s \, r_{ww,\, n+M(q-s)}$$

$$= r_{\tilde{w}\tilde{w},-n} \tag{2.51d}$$

Equation (2.51d) shows that the linearly combined noise correlation is an even function or is reflection invariant.

Appendix A summarizes the expressions characterizing the FV and SSMAMF systems, with the effects of their respective pre-filtering stages included, for easy reference.

2.6 MAXIMIZATION OF OSNR

In the previous section we developed the governing expressions for the general three stage MAMF system. The pre-filtering stage of the FVMAMF is fixed as a constant gain of 1. There is no maximizing of the OSNR for this system once the signal vectors have been determined. The distinguishing feature of the SSMAMF is the pre-filtering stage which linearly combines the basis vectors of the transmitted signal. As a result, when the combination coefficients are varied through their allowable ranges, the linearly combined signal and noise change which causes the OSNR of the SSMAMF to change. Our goal is to find the coefficients $\underline{c}^{\dagger}$, that maximize the OSNR.

Equation (2.38) describes the OSNR of the SSMAMF under estimated conditions. Substituting (2.41) into (2.38) yields

$$\widehat{\mathrm{OSNR}}_{SS} = \frac{\left(\underline{c}^{\mathrm{T}} S_i^{\mathrm{T}} \widehat{R}_{\tilde{w}\tilde{w}}^{-1} S_i \underline{c}\right)^2}{\underline{c}^{\mathrm{T}} S_i^{\mathrm{T}} \widehat{R}_{\tilde{w}\tilde{w}}^{-1} R_{\tilde{w}\tilde{w}} \widehat{R}_{\tilde{w}\tilde{w}}^{-1} S_i \underline{c}} \tag{2.52}$$

In practice we do not have access to the actual correlation matrix $R_{\tilde{w}\tilde{w}}$ and cannot compute the noise power at the output of the SSMAMF. We shall instead assume that the output noise power is constant (as done in §2.4.2) and seek to maximize the numerator of (2.52) which represents the output signal energy of the MAMF at time $N-1$. Recall that both the linearly combined signal and the linearly combined noise correlation matrix are functions of the coefficient vector $\underline{c}$. Define a function

$$F(\underline{c}) = \underline{c}^{\mathrm{T}} S_i^{\mathrm{T}} \widehat{R}_{\tilde{w}\tilde{w}}^{-1} S_i \underline{c} \tag{2.53}$$

Observe that the function $F(\underline{c})$ is exactly equal to $\mathrm{OSNR}^{\dagger}$ if $\widehat{R}_{\tilde{w}\tilde{w}} = R_{\tilde{w}\tilde{w}}$. Assuming we have used a positive semi-definite correlation estimator in generating $\widehat{R}_{ww}$ and hence $\widehat{R}_{\tilde{w}\tilde{w}}$, $F(\underline{c})$ is greater than or equal to zero and maximizing $F(\underline{c})$ is equivalent to maximizing the output signal energy of the

SSMAMF. This is an important point with regard to choosing a correlation estimator. Under these conditions we can assume that $F(\underline{c})$ is bounded below by zero allowing us to ignore the possibility of negative values.

The maximization is subject to the energy constraint of (2.43)

$$\underline{c}^{\mathrm{T}} S_i^{\mathrm{T}} S_i \underline{c} = E$$

We now investigate several avenues for maximizing (2.53).

2.6.1 Brute Force Maximization

We can certainly attempt to find the maximum of $F(\underline{c})$ in a brute force fashion by varying the coefficients in accordance with the energy constraint. This method is computationally burdensome, particularly for systems with more than two coefficients. The resulting error in the solution is related to the step size used in incrementing each coefficient. The only significant problem arising in implementing this method is in varying the coefficients.

As mentioned in §2.5.1, the energy constraint of (2.43) describes a hyper-ellipse in k-space whose axes may not align with the coordinate axes of the system. The cross terms of the quadratic constraint indicate a rotation of the hyper-ellipse away from the coordinate axes which makes it more difficult, from a programming standpoint, to vary the coefficients through their allowable ranges. To eliminate this problem we apply a rotational coordinate transformation to the coefficient vector $\underline{c}$ which places the axes of the hyper-ellipse in line with the coordinate axes of the rotated system. This facilitates a more straightforward parametrization of the combination coefficients and corresponds to the diagonalization of the symmetric matrix $S_i^{\mathrm{T}} S_i$ [9] which can be achieved through its orthonormal eigenvector matrix V.

$$S_i^{\mathrm{T}} S_i = V \Lambda V^{\mathrm{T}} \tag{2.54}$$

Where Λ is the diagonal matrix containing the eigenvalues of $S_i^{\mathrm{T}} S_i$ as its entries.

Substituting (2.54) into (2.43) we obtain

$$E = \underline{c}^{\mathrm{T}} V \Lambda V^{\mathrm{T}} \underline{c}$$

$$= \underline{c}'^{\mathrm{T}} \Lambda \underline{c}' \tag{2.55}$$

The orthogonal coordinate transformation

$$\underline{c}' = V^{\mathrm{T}} \underline{c} \tag{2.56}$$

is a rotation as long as $det(V) = 1$. The ranges of each coefficient c'_i $(0 \leq i \leq k-1)$ are now easily obtained by setting the remaining coefficients equal to zero

$$c'_i = \pm \sqrt{\frac{E}{\lambda_i}} \tag{2.57}$$

Coefficients can then be incremented through their respective ranges. The coefficient vector $\underline{c}$ can be recovered from

$$\underline{c} = V \underline{c}' \tag{2.58}$$

2.6.2 Iterative Quadratic Maximization

An iterative method has been developed to maximize (2.53) based on the techniques for maximization of a standard quadratic form. Experimental results obtained thus far are promising with regards to its computational requirements and relative accuracy in finding the global extreme points of the maximizing function [7,8].

Given a standard quadratic form:

$$G(\underline{x}) = \underline{x}^{\mathrm{T}} A \underline{x} \tag{2.59}$$

where $\underline{x}$ is a $n \times 1$ vector of unknowns and A is a $n \times n$ constant matrix. The maximum (minimum) value of such an equation can be found by first finding the maximum (minimum) eigenvalue of the matrix A. Then, letting $\underline{x}$ be the eigenvector corresponding to the maximum (minimum) eigenvalue, we obtain the maximum (minimum) value of (2.59) [9]. This is subject to the constraint

$$\| \underline{x} \|^2 = \underline{x}^{\mathrm{T}} \underline{x} = \textit{constant}$$

In the SSMAMF communication system, the maximizing function is essentially a quadratic form. However, unlike the matrix A of (2.59), $\widehat{R}^{-1}_{\tilde{w}\tilde{w}}$ is not constant; it actually depends on the combination coefficient vector $\underline{c}$. This is the basis of the iterative method. The function $F(\underline{c})$, can be rewritten

$$F(\underline{c}) = \underline{c}^{\mathrm{T}} S_i^{\mathrm{T}} \widehat{R}^{-1}_{\tilde{w}\tilde{w}} S_i \underline{c}$$

$$= \underline{c}^{\mathrm{T}} \begin{bmatrix} \underline{s}^{\mathrm{T}}_{i,0} \widehat{R}^{-1}_{\tilde{w}\tilde{w}} \underline{s}_{i,0} & \underline{s}^{\mathrm{T}}_{i,0} \widehat{R}^{-1}_{\tilde{w}\tilde{w}} \underline{s}_{i,1} & \cdots & \underline{s}^{\mathrm{T}}_{i,0} \widehat{R}^{-1}_{\tilde{w}\tilde{w}} \underline{s}_{i,k-1} \\ \underline{s}^{\mathrm{T}}_{i,1} \widehat{R}^{-1}_{\tilde{w}\tilde{w}} \underline{s}_{i,0} & \underline{s}^{\mathrm{T}}_{i,1} \widehat{R}^{-1}_{\tilde{w}\tilde{w}} \underline{s}_{i,1} & \cdots & \underline{s}^{\mathrm{T}}_{i,1} \widehat{R}^{-1}_{\tilde{w}\tilde{w}} \underline{s}_{i,k-1} \\ \vdots & \vdots & \ddots & \vdots \\ \underline{s}^{\mathrm{T}}_{i,k-1} \widehat{R}^{-1}_{\tilde{w}\tilde{w}} \underline{s}_{i,0} & \underline{s}^{\mathrm{T}}_{i,k-1} \widehat{R}^{-1}_{\tilde{w}\tilde{w}} \underline{s}_{i,0} & \cdots & \underline{s}^{\mathrm{T}}_{i,k-1} \widehat{R}^{-1}_{\tilde{w}\tilde{w}} \underline{s}_{i,k-1} \end{bmatrix} \underline{c}$$

$$= \underline{c}^{\mathrm{T}} T(\underline{c}) \underline{c} \qquad (2.60)$$

Equation (2.60) now looks like a standard quadratic form with the exception that $T(\underline{c})$ is dependent on the coefficient vector and not a constant matrix. Note that $T(\underline{c})$ is symmetric.

The algorithm for the iterative quadratic method is based upon solving for the eigenvectors corresponding to the maximum eigenvalue of $T(\underline{c})$ and using this result as the new coefficient vector. The steps of the iteration are as follows

1) Choose arbitrary initial values for $\underline{c}_0$ within the allowed constraints.
2) Compute $F(\underline{c}_n)$ using (2.53).
3) Generate the inverse of the noise correlation matrix, i.e. $\hat{R}_{\tilde{w}\tilde{w}}^{-1}$.
4) Pre- and post-multiply $\hat{R}_{\tilde{w}\tilde{w}}^{-1}$ according to (2.60) to obtain $T(\underline{c}_n)$.
5) Compute the eigen decomposition of $T(\underline{c}_n)$.
6) Generate $\underline{c}_{n+1}$ by multiplying the normalized eigenvector corresponding to the maximum eigenvalue by an appropriate constant to satisfy the constraint of (2.43).
7) Compute $F(\underline{c}_{n+1})$ using (2.53).
8) Compute error criterion using $F(\underline{c}_{n+1})$ and $F(\underline{c}_n)$. If greater than tolerance repeat 3 - 8 using $\underline{c}_{n+1}$.

It has been observed that the value of $F(\underline{c})$ to which this algorithm converges can be lower than the actual function maximum as computed by the brute force approach, but can never exceed the actual maximum as long as the constraints on $\underline{c}$ are observed.

The algorithm may be modified to generate a minimization rather than a maximization by modifying step 6 such that the normalized eigenvector corresponding to the minimum eigenvalue of $T(\underline{c}_n)$ is used instead.

One possible advantage of this version of the algorithm is its incorporation of the signal matrix for the system into $T(\underline{c})$, which in a sense constrains our result within the available signal subspace. The initial value of the coefficient vector appears to have no major effect on the final convergence value of the routine, a matter which is of prime concern in using other methods of maximization.

A problem with this algorithm can be seen fairly easily in the case when the signal matrix S_i consists of two basis vectors (i.e. $k = 2$). In this case the matrix $T(\underline{c})$ is a 2×2 matrix. Should $T(\underline{c})$ become persymmetric, it yields two fixed eigenvectors. Therefore, the iterative quadratic algorithm has no choice but to accept one or the other as a solution. This solution can produce a very poor estimate of the maximum of the function $F(\underline{c})$ depending on the proximity of the

fixed eigenvectors to the desired solution $\underline{c}^{\dagger}$.

Another variation of this method can be generated by combining the terms of (2.53) in a slightly different manner

$$F(\underline{c}) = \underline{b}^{\mathrm{T}} \widehat{R}_{\widetilde{w}\widetilde{w}}^{-1} \underline{b} \tag{2.61}$$

where

$$\underline{b} = S_i \underline{c} \tag{2.62}$$

Here we apply the same algorithm as before using $\widehat{R}_{\widetilde{w}\widetilde{w}}^{-1}$ in place of $T(\underline{c})$. Once the eigenvector, $\underline{b}$, corresponding to the maximum eigenvalue is obtained we can solve the overdetermined system of equations given in (2.62) for the coefficient vector $\underline{c}$ in a least squares sense [10]. Potentially, problems may occur since the desired $\underline{b}$ may not be near the subspace $S_i \underline{c}$ regardless of the value of $\underline{c}$ for the given signal vectors in S_i.

2.6.3 Gradient Based Maximization

Another approach to maximizing the function in (2.53) is to use a method based on the gradient of the function. By determining the zeros of the gradient we have identified the extreme points of the maximizing function. We shall generate the general derivative expressions for a k-dimensional SSMAMF system using Lagrange multiplier techniques to incorporate the coefficient constraint directly into the function [24-27].

The function

$$F(\underline{c}) = \underline{c}^{\mathrm{T}} S_i^{\mathrm{T}} \widehat{R}_{\widetilde{w}\widetilde{w}}^{-1} S_i \underline{c}$$

is subject to the constraint on the combination coefficients

$$\underline{c}^{\mathrm{T}} S_i^{\mathrm{T}} S_i \underline{c} = E$$

Using a Lagrange multiplier, we can create a new function $G(\underline{c})$, by augmenting (2.53) with the coefficient constraint,

$$G(\underline{c}) = \underline{c}^{\mathrm{T}} S_i^{\mathrm{T}} \hat{R}_{\tilde{w}\tilde{w}}^{-1} S_i \underline{c} + \lambda(\underline{c}^{\mathrm{T}} S_i^{\mathrm{T}} S_i \underline{c} - E) \tag{2.63}$$

The update equation for the gradient method is

$$\underline{c}_{n+1} = \underline{c}_n + \underline{s}_n \tag{2.64}$$

The correction term $\underline{s}_n$ is found as the solution to

$$\nabla^2 G(\underline{c}_n)\, \underline{s}_n = -\nabla G(\underline{c}_n) \tag{2.65}$$

where

$$\nabla G(\underline{c}_n) = \left[\begin{array}{ccc} \frac{\partial}{\partial c_0} G & \cdots & \frac{\partial}{\partial c_{k-1}} G \quad \frac{\partial}{\partial \lambda} G \end{array} \right]^{\mathrm{T}} \quad \text{(Gradient)}$$

$$\nabla^2 G(\underline{c}_n) = \left[\begin{array}{ccc} \frac{\partial^2}{\partial c_0^2} G & \cdots & \frac{\partial^2}{\partial c_0 \partial c_{k-1}} G \quad \frac{\partial^2}{\partial c_0 \partial \lambda} G \\ \vdots & \ddots & \vdots \quad \vdots \\ \frac{\partial^2}{\partial c_{k-1} \partial c_0} G & \cdots & \frac{\partial^2}{\partial c_{k-1}^2} G \quad \frac{\partial^2}{\partial c_{k-1} \partial \lambda} G \\ \frac{\partial^2}{\partial \lambda \partial c_0} G & \cdots & \frac{\partial^2}{\partial \lambda \partial c_{k-1}} G \quad \frac{\partial^2}{\partial \lambda^2} G \end{array} \right] \quad \text{(Hessian)}$$

The Hessian is symmetric since

$$\frac{\partial^2}{\partial x \partial y} G(\underline{c}) = \frac{\partial^2}{\partial y \partial x} G(\underline{c}) \tag{2.66}$$

This method is a constrained maximization process and assumes that the maximizing function is twice continuously differentiable, a condition which is satisfied [11]. The matrix S_i is the only quantity independent of the combination coefficients. Appendix B contains the actual derivative expressions needed to compute (2.65).

The primary disadvantage of this method is that without an initial guess sufficiently close to the desired maximum of the function in the constrained space, the iterative approach based on (2.64) is just as likely to proceed towards a minimum extreme point as to a maximum extreme point [11]. Even with a good starting point there is some chance, depending on the nature of the maximum point in question, of the algorithm converging to a minimum point. Either the method of §2.6.1 or §2.6.2 may be used to generate the initial guess, though the potential disadvantages mentioned in their respective sections should be carefully considered. The advantages of the routine are its quite rapid convergence given a starting point near an extreme point (typically 4 iterations or less) and the fact that the error in the final convergence value is limited only by the tolerance criterion used.

2.7 MAXIMUM LIKELIHOOD DETECTION

The detection stage of the MAMF based receiver system follows the pre-filtering and filtering stages. It is here that the decision is made as to which signal was most likely transmitted. Obviously, we desire a decision-making process that identifies the corrupted signal in some optimal fashion based on the characteristics of the existing system. Such a detection scheme will be developed for the L-ary communication system using L arbitrary moving-average (MA) filters at the receiving end.

The ***maximum a posteriori*** (MAP) probability criterion is a form of hypothesis testing which can be applied as a detection scheme for the three stage MAMF receiver system. This can be developed as a special case of the more general *Bayes criterion* [13].

Assume an arbitrary MA filter $\underline{h}$ following an arbitrary linear pre-filtering operation $\mathcal{L}(\cdot)$ which operates on the received signal $\underline{r}$. The received signal is a noisy version of the signal,

$$\underline{r} = \underline{s}_i + \underline{w} \tag{2.67}$$

The vector $\underline{w}$ represents the additive colored noise and $\underline{s}_i$ the transmitted signal representing the L-ary symbol "i", $i = 0, 1, \ldots, L-1$. We can establish the following hypotheses for the received signal

$$\begin{aligned} H_0 &: \underline{r} = \underline{s}_0 + \underline{w} \\ H_1 &: \underline{r} = \underline{s}_1 + \underline{w} \\ &\vdots \\ H_{L-1} &: \underline{r} = \underline{s}_{L-1} + \underline{w} \end{aligned} \tag{2.68}$$

Bayes criterion minimizes the risk (average cost), $\overline{C}$, defined as

$$\overline{C} = \sum_{j=0}^{L-1} \sum_{k=0}^{L-1} C_{jk} P\left(D_j \mid H_k\right) P\left(H_k\right) \tag{2.69}$$

C_{jk} represents the cost associated with choosing the hypothesis H_j when in fact H_k is true, while $P(H_j)$ and $P(D_j \mid H_k)$ are respectively the *a priori* probability and conditional probability. Minimizing (2.69) implies that we select the hypothesis H_j that yields the smallest value of $\overline{C}$. The cost associated with hypothesis H_k for a given $L \times 1$ vector of samples $\underline{y}$ is

$$C_k = \sum_{j=0}^{L-1} C_{kj} P\left(H_j \mid \underline{y}\right) \tag{2.70}$$

where $P\left(H_j \mid \underline{y}\right)$ is the probability that hypothesis H_j is true given the samples $\underline{y}$. We can rewrite this probability as [13]

$$P\left(H_j \mid \underline{y}\right) = \frac{p_j(\underline{y})\, P(H_j)}{p(\underline{y})} \tag{2.71}$$

where $p_j(\underline{y})$ represents the probability density function associated with hypothesis H_j and $p(\underline{y})$ is the marginal density function for $\underline{y}$. Substituting (2.71) in (2.70), the cost of choosing hypothesis H_k becomes

$$C_k = \frac{\sum_{j=0}^{L-1} C_{kj}\, p_j(\underline{y})\, P(H_j)}{p(\underline{y})} \tag{2.72}$$

Since $p(\underline{y})$ has no dependence on the choice of hypothesis, the decision rule for Bayes test of multiple hypotheses is to choose the hypothesis H_k which yields the minimum β_k ($k = 0, 1, \ldots, L-1$), where

$$\beta_k = \sum_{j=0}^{L-1} C_{kj}\, p_j(\underline{y})\, P(H_j) \tag{2.73}$$

In a communications system we might typically consider the case where there is no cost associated with a correct decision and the costs for incorrect decisions are equal, i.e.

$$C_{jk} = \begin{cases} 1 & \forall\ j \neq k \\ 0 & j = k \end{cases} \tag{2.74}$$

Then (2.73) becomes

$$\beta_k = \sum_{\substack{j=0 \\ j \neq k}}^{L-1} p_j(\underline{y})\, P(H_j) \tag{2.75}$$

Let us assume (without loss of generality) that β_{k^*} is the smallest. Then for every $l \neq k^*$ we have

$$\beta_l - \beta_{k^*} = p_{k^*}(\underline{y})\, P(H_{k^*}) - p_l(\underline{y})\, P(H_l) > 0 \tag{2.76}$$

which implies that

$$p_{k^*}(\underline{y})\, P(H_{k^*}) > p_l(\underline{y})\, P(H_l) \tag{2.77}$$

Given the costs in (2.74), our decision rule is to choose the hypothesis H_{k^*} where

$$k^* = arg\left\{\max_k \left\{p_k(\underline{y})\, P(H_k)\right\}\right\} \tag{2.78}$$

The decision rule of (2.78) is in fact the MAP criterion for multiple hypotheses [13]. If we further assume that the probability of transmitting any of the L symbols is the same, then the a priori probabilities of the hypotheses are also equal and (2.78) reduces to

$$k^* = arg\left\{\max_k \left\{p_k(\underline{y})\right\}\right\} \tag{2.79}$$

We now need only evaluate the L density functions and select the hypothesis which generates the maximum value [13].

Associated with each decision is some chance or probability that an incorrect decision was made, typically referred to as the *probability of error*, P_e. The P_e can be computed from [13]

$$P_e = \sum_{j=0}^{L-1} \sum_{\substack{k=0 \\ k \neq j}}^{L-1} P\left(D_j \mid H_k\right) P\left(H_k\right) \tag{2.80}$$

Note that even if the *a priori* probabilities $P(H_k)$ are equal, (2.80) still requires a double summation of the L-fold integrals of the L-dimensional density functions, which is tedious to say the least.

To obtain the required probability density functions for the MAP criterion, we must determine the multivariate density function for the output of the L MA filters of length N when a particular signal $\underline{s}_i$ $(i = 0, 1, \ldots, L-1)$ in noise is present at the input to the three stage receiver system. We define an $L \times 1$ vector $\underline{y}$, whose elements are denoted by y_m $(1 \leq m \leq L)$, which represents the outputs of the L MA filters at the particular time $n_0 = N-1$. Given that the colored noise at the input to the system is assumed to be Gaussian, $\sim N(0, \sigma_w^2)$, the MA output vector will be distributed according to a multivariate Gaussian density function [18]. The form of this density function conditioned on $\underline{s}_i$ being present at the receiver system input is

$$p_i(\underline{y}) = \left((2\pi)^{L/2} |\Sigma|^{1/2}\right)^{-1} exp\left\{ -\frac{1}{2}\left(\underline{y} - \underline{\mu}^i\right)^{\mathrm{T}} \Sigma^{-1} \left(\underline{y} - \underline{\mu}^i\right) \right\} \tag{2.81}$$

where $\underline{\mu}^i$ is the mean of the MA output vector when $\underline{s}_i$ is present at the input to the three stage receiver and Σ is the covariance matrix of the output vector $\underline{y}$. The quadratic exponent in (2.81) is positive semi-definite [19].

Under the Gaussian assumption the decision rule of (2.79) can be modified by noting that the constant term is common to all L density functions. The hypothesis which maximizes (2.79) will also yield the maximum value of the exponential, or equivalently, yield the smallest absolute value of the quadratic exponent, i.e.

$$k^* = arg\left\{ \min_k \left\{ \frac{1}{2}\left(\underline{y} - \underline{\mu}^i\right)^{\mathrm{T}} \Sigma^{-1} \left(\underline{y} - \underline{\mu}^i\right) \right\} \right\} \tag{2.82}$$

For compactness in the notation that follows, we shall define a new variable $m^* = m - 1$. The noise is additive which allows us to express each element of the output vector as the superposition of the filtered signal and the filtered noise at time $N-1$, i.e.,

$$y_m = \underline{h}_{m^*}^{\mathrm{T}} \underline{\tilde{s}}_{m^* \mid i} + \underline{h}_{m^*}^{\mathrm{T}} \underline{\tilde{w}}_{m^*} \tag{2.83}$$

where $\underline{h}_j^{\mathrm{T}} \underline{\tilde{s}}_{j\,|\,i}$ is the output of the j-th MA filter due to the j-th pre-filtered signal $\underline{\tilde{s}}_{j\,|\,i}$, given that $\underline{s}_i$ is present at the pre-filter input. The term $\underline{h}_j^{\mathrm{T}} \underline{\tilde{w}}_j$ is the output of the j-th filter due to the j-th pre-filtered noise $\underline{\tilde{w}}_j$.

Using the linearity property of the expected value operator we can find the m-th element of the mean output vector $\underline{\mu}^i$, of the receiver system at $N-1$, when signal $\underline{s}_i$ is present at the input

$$\begin{aligned} \mu_m^i &= E\{ y_m \} \\ &= E\left\{ \underline{h}_{m^*}^{\mathrm{T}} \underline{\tilde{s}}_{m^*\,|\,i} + \underline{h}_{m^*}^{\mathrm{T}} \underline{\tilde{w}}_{m^*} \right\} \\ &= \underline{h}_{m^*}^{\mathrm{T}} \underline{\tilde{s}}_{m^*\,|\,i} + \underline{h}_{m^*}^{\mathrm{T}} E\left\{ \underline{\tilde{w}}_{m^*} \right\} \end{aligned} \tag{2.84}$$

The j-th pre-filtering operation was defined to be linear and is denoted $\mathcal{L}_j(\,\cdot\,)$, thus

$$\mu_m^i = \underline{h}_{m^*}^{\mathrm{T}} \mathcal{L}_{m^*}(\underline{s}_i) + \underline{h}_{m^*}^{\mathrm{T}} E\left\{ \mathcal{L}_{m^*}(\underline{w}) \right\} \tag{2.85}$$

Interchanging the expected value and pre-filtering operators and recalling that the signal $\underline{s}_i$ is deterministic while the mean value of the noise $\underline{w}$ is zero, we obtain

$$\begin{aligned} \mu_m^i &= \underline{h}_{m^*}^{\mathrm{T}} \mathcal{L}_{m^*}\left(\underline{s}_i \right) + \underline{h}_{m^*}^{\mathrm{T}} \mathcal{L}_{m^*}\left(E\{ \underline{w} \} \right) \\ &= \underline{h}_{m^*}^{\mathrm{T}} \mathcal{L}_{m^*}\left(\underline{s}_i \right) \end{aligned} \tag{2.86}$$

Observe that (2.86) is nothing more than the transmitted signal $\underline{s}_i$ which has been processed by the j-th pre-filter and the j-th MA filter.

The covariance matrix, at time $n_0 = N-1$, given that the signal $\underline{s}_i$ is present at the system input is denoted Σ and is generated as follows:

$$\begin{aligned} \Sigma &= E\left\{ \left(\underline{y} - \underline{\mu}^i \right) \left(\underline{y} - \underline{\mu}^i \right)^{\mathrm{T}} \right\} \\ &= E\left\{ \underline{y}\, \underline{y}^{\mathrm{T}} \right\} - \underline{\mu}^i \left(\underline{\mu}^i \right)^{\mathrm{T}} \end{aligned} \tag{2.87}$$

where each element Σ_{mn} $(1 \leq m,n \leq L)$ of the covariance matrix is given by

$$\Sigma_{mn} = E\left\{ y_m \, y_n^{\mathrm{T}} \right\} - \mu_m^i \left(\mu_n^i \right)^{\mathrm{T}} \tag{2.88}$$

Again for compactness, we define $n^* = n - 1$. The first term in (2.88) is

$$E\left\{ y_m \, y_n^{\mathrm{T}} \right\} = E\left\{ \left(\underline{h}_{m^*}^{\mathrm{T}} \left(\underline{\tilde{s}}_{m^* \mid i} + \underline{\tilde{w}}_{m^*} \right) \right) \left(\underline{h}_{n^*}^{\mathrm{T}} \left(\underline{\tilde{s}}_{n^* \mid i} + \underline{\tilde{w}}_{n^*} \right) \right)^{\mathrm{T}} \right\}$$

$$\begin{aligned} &= E\left\{ \underline{h}_{m^*}^{\mathrm{T}} \, \underline{\tilde{s}}_{m^* \mid i} \, \underline{\tilde{s}}_{n^* \mid i}^{\mathrm{T}} \, \underline{h}_{n^*} \right\} + E\left\{ \underline{h}_{m^*}^{\mathrm{T}} \, \underline{\tilde{s}}_{m^* \mid i} \, \underline{\tilde{w}}_{n^*}^{\mathrm{T}} \, \underline{h}_{n^*} \right\} \\ &\quad + E\left\{ \underline{h}_{m^*}^{\mathrm{T}} \, \underline{\tilde{w}}_{m^*} \, \underline{\tilde{s}}_{n^* \mid i}^{\mathrm{T}} \, \underline{h}_{n^*} \right\} + E\left\{ \underline{h}_{m^*}^{\mathrm{T}} \, \underline{\tilde{w}}_{m^*} \, \underline{\tilde{w}}_{n^*}^{\mathrm{T}} \, \underline{h}_{n^*} \right\} \end{aligned}$$

$$\begin{aligned} &= \underline{h}_{m^*}^{\mathrm{T}} E\left\{ \underline{\ell}_{m^*}(\underline{s}_i) \underline{\ell}_{n^*}^{\mathrm{T}}(\underline{s}_i) \right\} \underline{h}_{n^*} + \underline{h}_{m^*}^{\mathrm{T}} E\left\{ \underline{\ell}_{m^*}(\underline{s}_i) \, \underline{\ell}_{n^*}^{\mathrm{T}}(\underline{w}) \right\} \underline{h}_{n^*} \\ &\quad + \underline{h}_{m^*}^{\mathrm{T}} E\left\{ \underline{\ell}_{m^*}(\underline{w}) \underline{\ell}_{n^*}^{\mathrm{T}}(\underline{s}_i) \right\} \underline{h}_{n^*} + \underline{h}_{m^*}^{\mathrm{T}} E\left\{ \underline{\ell}_{m^*}(\underline{w}) \underline{\ell}_{n^*}^{\mathrm{T}}(\underline{w}) \right\} \underline{h}_{n^*} \end{aligned} \tag{2.89}$$

Again, interchanging the linear pre-filtering operator and the expected value operator along with knowing the noise vector $\underline{w}$ to be zero-mean and $\underline{s}_i$ to be deterministic allows us to write

$$\begin{aligned} E\left\{ y_m \, y_n^{\mathrm{T}} \right\} &= \underline{h}_{m^*}^{\mathrm{T}} \underline{\ell}_{m^*}(\underline{s}_i) \underline{\ell}_{n^*}^{\mathrm{T}}(\underline{s}_i) \underline{h}_{n^*} + \underline{h}_{m^*}^{\mathrm{T}} E\left\{ \underline{\ell}_{m^*}(\underline{w}) \underline{\ell}_{n^*}^{\mathrm{T}}(\underline{w}) \right\} \underline{h}_{n^*} \\ &= \mu_m^i \left(\mu_n^i \right)^{\mathrm{T}} + \underline{h}_{m^*}^{\mathrm{T}} \, R_{\tilde{w}_{m^*} \tilde{w}_{n^*}} \, \underline{h}_{n^*} \end{aligned} \tag{2.90}$$

where $R_{\tilde{w}_i \tilde{w}_j}$ is the cross-correlation matrix of the i-th pre-filtered noise and the j-th pre-filtered noise. Substituting (2.90) into (2.88) we have

$$\Sigma_{mn} = \underline{h}_{m^*}^{\mathrm{T}} \, R_{\tilde{w}_{m^*} \tilde{w}_{n^*}} \, \underline{h}_{n^*} \tag{2.91}$$

Note that the covariance matrix with elements described in (2.91) is independent

of which signal $\underline{s}_i$ is present at the input to the system.

Recalling the definition of the cross-correlation matrix in (2.90)

$$R_{\widetilde{w}_i\widetilde{w}_j} = E\left\{\underline{\ell}_i(\underline{w})\,\underline{\ell}_j^{\mathrm{T}}(\underline{w})\right\}$$

thus,

$$R_{\widetilde{w}_i\widetilde{w}_j}^{\mathrm{T}} = \left(E\left\{\underline{\ell}_i(\underline{w})\,\underline{\ell}_j^{\mathrm{T}}(\underline{w})\right\}\right)^{\mathrm{T}} \tag{2.92}$$

Using the fact that for a stochastic matrix A, $(E\{A\})^{\mathrm{T}} = E\{A^{\mathrm{T}}\}$, (2.92) can be written as

$$\begin{aligned} R_{\widetilde{w}_i\widetilde{w}_j}^{\mathrm{T}} &= E\left\{\left(\underline{\ell}_i(\underline{w})\,\underline{\ell}_j^{\mathrm{T}}(\underline{w})\right)^{\mathrm{T}}\right\} \\ &= E\left\{\underline{\ell}_j(\underline{w})\,\underline{\ell}_i^{\mathrm{T}}(\underline{w})\right\} \\ &= R_{\widetilde{w}_j\widetilde{w}_i} \end{aligned} \tag{2.93}$$

Since each element of the covariance matrix in (2.91) is a scalar we can write

$$\begin{aligned} \Sigma_{mn} &= \left(\underline{h}_{m^*}^{\mathrm{T}}\, R_{\widetilde{w}_{m^*}\widetilde{w}_{n^*}}\, \underline{h}_{n^*}\right)^{\mathrm{T}} \\ &= \underline{h}_{n^*}^{\mathrm{T}}\, R_{\widetilde{w}_{m^*}\widetilde{w}_{n^*}}^{\mathrm{T}}\, \underline{h}_{m^*} \end{aligned}$$

Applying (2.93), we find

$$\begin{aligned} \Sigma_{mn} &= \underline{h}_{n^*}^{\mathrm{T}}\, R_{\widetilde{w}_{n^*}\widetilde{w}_{m^*}}\, \underline{h}_{m^*} \\ &= \Sigma_{nm} \end{aligned} \tag{2.94}$$

Equation (2.94) shows that the covariance matrix is symmetric. The elements of the covariance matrix were given in (2.91) and required the pre-filtered cross-covariance matrix $R_{\widetilde{w}_i\widetilde{w}_j}$, a quantity we do not have access to in practice. We must instead use our estimate of the matrix and (2.91) becomes

$$\Sigma_{mn} = \underline{\hat{h}}^{\mathrm{T}}_{m^*} \hat{R}_{\tilde{w}_{m^*}\tilde{w}_{n^*}} \underline{\hat{h}}_{n^*}$$

$$= \underline{\tilde{s}}^{\mathrm{T}}_{m^*\,|\,m^*} \hat{R}^{-1}_{\tilde{w}_{m^*}\tilde{w}_{m^*}} \hat{R}_{\tilde{w}_{m^*}\tilde{w}_{n^*}} \hat{R}^{-1}_{\tilde{w}_{n^*}\tilde{w}_{n^*}} \underline{\tilde{s}}_{n^*\,|\,n^*} \qquad (2.95)$$

Appendix C contains the expressions for the mean vector and the covariance matrix applied specifically to the pre-filtering operations used in the FV and SSMAMF systems.

The density function of (2.81) contains the inverse of the covariance matrix. It would appear that the existence of this inverse would determine the existence of the density function itself. However, the density function can also be written as an L-fold integral (or the L-dimensional inverse Fourier transform) of the characteristic function which can always be computed [20]. Unfortunately, from a practical standpoint we do not desire to compute these multidimensional integrals. Anderson and Moore [20] suggest the use of the Moore-Penrose pseudo-inverse $\Sigma^{\#}$, an operation defined for an arbitrary matrix A as follows

$$A^{\#} A \underline{x} = \underline{x} \qquad \forall\, \underline{x} \in \mathcal{R}(A^{\mathrm{T}}) \qquad (2.96a)$$

$$A^{\#} \underline{x} = \underline{0} \qquad \forall \underline{x} \in \mathcal{N}(A^{\mathrm{T}}) \qquad (2.96b)$$

$\mathcal{R}(\cdot)$ and $\mathcal{N}(\cdot)$ represent respectively the range space and the null space of the argument matrix. Note that by the above definition, if A is nonsingular then $A^{\#} = A^{-1}$. Recall that Σ is a symmetric matrix and as such it can always be orthogonally diagonalized, i.e.,

$$\Sigma = V \Lambda V^{\mathrm{T}} \qquad (2.97)$$

V is the matrix of orthonormal eigenvectors and Λ is a diagonal matrix containing the eigenvalues λ_i of the covariance matrix. Realizing that V is non-singular and $V^{\#} = V^{-1} = V^{\mathrm{T}}$, we can apply the concept of a pseudo-inverse to (2.97) [21] and get

$$\Sigma^{\#} = \left(V \Lambda V^{\mathrm{T}}\right)^{\#}$$

$$= V \Lambda^{\#} V^{\mathrm{T}} \tag{2.98}$$

$\Lambda^{\#}$ is the diagonal matrix containing the pseudo-inverses of the eigenvalues defined as

$$\lambda_i^{\#} = \begin{cases} \frac{1}{\lambda_i} & \forall\, \lambda_i \neq 0 \\ 0 & \forall\, \lambda_i = 0 \end{cases} \tag{2.99}$$

The use of the pseudo-inverse for the covariance matrix allows us to evaluate the density function of (2.81) in all cases and it equals the actual inverse whenever it exists.

2.8 OPTIMUM SIGNAL VECTOR DESIGN

In §2.4.2 we developed the expression for $\text{OSNR}^{\dagger}$ (2.35). Achieving $\text{OSNR}^{\dagger}$ depends on the design of a signal vector that is optimum given the existing noise correlation matrix. This section is concerned with selecting such signal vectors for the FV and SSMAMF systems. It is shown that the SSMAMF can be "optimized" for multiple noise conditions and is in fact a generalization of the M-dimensional FVMAMF.

First, consider that the noise characteristics are assumed to be known. $\text{OSNR}^{\dagger}$ was given by

$$\text{OSNR}^{\dagger} = \underset{\sim}{\tilde{s}}_i^{\mathrm{T}} R_{\tilde{w}\tilde{w}}^{-1} \underset{\sim}{\tilde{s}}_i$$

Maximization of the quadratic expression for $\text{OSNR}^{\dagger}$ is achieved when the pre-filtered signal vector is chosen to be the eigenvector corresponding to the minimum eigenvalue of $R_{\tilde{w}\tilde{w}}$ [9].

The pre-filtering operation in the FVMAMF case consists of a unity gain. This implies that the signal vector be chosen as the eigenvector corresponding to the minimum eigenvalue of R_{ww}. The SSMAMF requires that the pre-filtered or linearly combined signal vector be chosen as the appropriate eigenvector of the linearly combined noise correlation matrix. Therefore, we must find the coefficient vector $\underset{\sim}{c}^{\dagger}$ which minimizes the smallest eigenvalue of $R_{\tilde{w}\tilde{w}}$.

Given $\underset{\sim}{c}^{\dagger}$ and the desired eigenvector $\underset{\sim}{v}_{\lambda_{min}}$ we must find a set of basis vectors for the signal subspace such that

$$S_i \, \underset{\sim}{c}^{\dagger} = \underset{\sim}{v}_{\lambda_{min}} \tag{2.100}$$

Observe that there are an infinite number of choices for the basis vectors. Constraints can be imposed to simplify the selection process (i.e. orthonormal set of basis vectors) but this is at the discretion of the designer.

One of the more interesting potentials of the SSMAMF system is its ability to be "optimized" for more than one type of noise. The FVMAMF has no

flexibility in terms of the transmitted signal vectors once the signal vector selection has been made. On the other hand, the SSMAMF can achieve any vector in the transmitted signal subspace satisfying the coefficient constraint.

We might anticipate that choosing the basis vectors of the SSMAMF to correspond to various noise conditions should allow us to select between the various noise conditions at the receiver. To show this assume that we have a signal matrix

$$S_i = \left[\begin{array}{ccccc} \underline{s}_{i,0} & | & \underline{s}_{i,1} & | & \cdots & | & \underline{s}_{i,k-1} \end{array} \right]$$

whose columns are chosen as signals which optimize an M-dimensional FVMAMF system under k different noise conditions. Each of these signals can be written in terms of the appropriate normalized eigenvector of its respective noise correlation matrix, i.e.

$$\underline{s}_{i,j} = \sqrt{\alpha_j} \cdot \underline{v}_j \qquad \Rightarrow \qquad \underline{s}_{i,j}^{\mathrm{T}} \underline{s}_{i,j} = \alpha_j \tag{2.101}$$

The total energy of the transmitted signal is equal to the sum of the energies of the columns of the signal matrix, thus

$$\sum_{j=0}^{k-1} \alpha_j = E$$

Assume that the current channel noise conditions match the j-th of the k conditions represented in the signal matrix. Certainly, one solution for the coefficients in maximizing the OSNR of the SSMAMF would be

$$c_l = C \delta_{l-j} \tag{2.102}$$

The constant can be determined by substituting (2.102) in (2.43) and solving for C

$$C = \pm \sqrt{\frac{E}{\alpha_j}} \tag{2.103}$$

The resulting linearly combined noise using these coefficients in (2.51) is

$$r_{\tilde{w}\tilde{w},n} = \left(\frac{E}{\alpha_j} \right) r_{ww,n} \tag{2.104}$$

Similarly the linearly combined noise correlation matrix becomes

$$R_{\tilde{w}\,\tilde{w}} = \left(\frac{E}{\alpha_j}\right) R_{ww} \tag{2.105}$$

and its inverse is

$$R_{\tilde{w}\,\tilde{w}}^{-1} = \left(\frac{\alpha_j}{E}\right) R_{ww}^{-1} \tag{2.106}$$

Using (2.103) and (2.106) in (2.35)

$$\begin{aligned}
\mathrm{OSNR}^{\dagger}_{SS,\,N=M\times k} &= \underline{c}^{\mathrm{T}} S_i^{\mathrm{T}} R_{\tilde{w}\,\tilde{w}}^{-1} S_i \underline{c} \\
&= \left(\pm\sqrt{\frac{E}{\alpha_j}}\,\underline{s}_{i,j}^{\mathrm{T}}\right)\left(\frac{\alpha_j}{E} R_{ww}^{-1}\right)\left(\pm\sqrt{\frac{E}{\alpha_j}}\,\underline{s}_{i,j}\right) \\
&= \underline{s}_{i,j}^{\mathrm{T}} R_{ww}^{-1} \underline{s}_{i,j} \\
&= \left(\sqrt{\alpha_j}\,\underline{v}_j^{\mathrm{T}}\right) R_{ww}^{-1} \left(\sqrt{\alpha_j}\,\underline{v}_j\right) \\
&= \alpha_j \left(\mathrm{OSNR}^{\dagger}_{FV,\,N=M}\right)
\end{aligned} \tag{2.107}$$

The optimum SNRI under these conditions

$$\begin{aligned}
\mathrm{SNRI}^{\dagger}_{SS,\,N=M\times k} &= \frac{\mathrm{OSNR}^{\dagger}_{SS,\,N=M\times k}}{\mathrm{ISNR}} \\
&= \frac{\alpha_j \left(\mathrm{OSNR}^{\dagger}_{FV,\,N=M}\right)}{\frac{E}{r_{ww,0}}}
\end{aligned}$$

$$= \left(\frac{\alpha_j}{E}\right)\left(\text{SNRI}^{\dagger}_{FV,N=M}\right) \tag{2.108}$$

Equation (2.108) indicates that the SSMAMF achieves the optimum SNRI for the M-dimensional FVMAMF given the j-th noise condition is assumed, weighted by the fraction of the total signal energy placed in the j-th column of the transmitted signal matrix. Two cases are of particular interest:

Case 1: $\alpha_l = E\delta_{l-j}$

The total signal energy is placed in a single column. For this degenerate case (2.108) becomes

$$\text{SNRI}^{\dagger}_{SS,N=M\times k} = \text{SNRI}^{\dagger}_{FV,N=M} \tag{2.109}$$

This shows that the M-dimensional FVMAMF is a special case of the more general $(M \times k)$-dimensional SSMAMF.

Case 2: $\alpha_l = 1 \qquad \forall\, l$

All basis vectors have norm equal to 1 (quite likely in practice). Thus,

$$\text{SNRI}^{\dagger}_{SS,N=M\times k} = \left(\frac{1}{k}\right)\left(\text{SNRI}^{\dagger}_{FV,N=M}\right) \tag{2.110}$$

Equation (2.110) shows that while we can optimize for multiple noise conditions with the SSMAMF, there is a tradeoff made relative to the number of basis vectors used. The higher the value of k, the more noise conditions which can be accounted for but the lower the maximum SNRI attainable for each noise condition.

3.0 SIMULATION DESCRIPTION

This chapter describes the methods and procedures used in simulating the FV and SSMAMF receiver systems. Simulation allows us to investigate the performance of both systems under a variety of conditions; conditions more easily changed in a computer environment than in practice. We choose to simulate a binary communication system with real data. For comparison of the FVMAMF and the SSMAMF systems we require that the length and total energy of the transmitted signal vectors be the same for both systems.

3.1 CHANNEL NOISE GENERATION

The additive channel noise was assumed in §2.2 to be real, colored, and Gaussian. In the simulations the colored noise was generated by driving an auto-regressive filter of order 2 (AR(2)) with white Gaussian noise, $\sim N(0,1)$. The coloring filter has a transfer function given by

$$\begin{aligned} \mathcal{H}(z) &= \frac{b_0}{1 - 2\rho\cos(\theta)z^{-1} + \rho^2 z^{-2}} \\ &= \frac{b_0}{\left(1 - \rho e^{j\theta} z^{-1}\right)\left(1 - \rho e^{-j\theta} z^{-1}\right)} \end{aligned} \tag{3.1}$$

The constant b_0 is defined such that the peak magnitude response of $\mathcal{H}(z)$ is unity, i.e.

$$b_0 = (1-\rho)\left|e^{j\theta} - \rho e^{-j\theta}\right| \tag{3.2}$$

$\mathcal{H}(z)$ has two zeros at the origin and a pair of poles with radius ρ and angles $\pm\theta$. The radius determines the bandwidth of the colored noise while the angle θ determines the center frequency. Without loss of generality, we define $T = 1$. For a given radius, we can shift the center frequency from 0 to π (half-sampling frequency π/T where $T = 1$) to investigate performance of the MAMF systems. Similarly, the radius can be changed to investigate the effects of various bandwidths. Unless otherwise specified, all simulations are run with a radius of $\rho = 0.95$, indicating narrowband colored noise.

Many of the cases examined involve comparing the SNRI of the MAMF when the colored noise ACF is known to when the colored noise ACF is estimated. The actual ACF of the colored noise for a given radius and angle can be computed directly from the AR coefficients [17]. The estimated ACF is computed from samples of the colored noise at the output of $\mathcal{H}(z)$. Since the coloring filter is an infinite impulse response (IIR) filter, the initial samples out of the filter are discarded to avoid transient effects. It was determined that the

maximum *memory depth* (time step at which the filter impulse response has decayed to 1% of its maximum value) was 220 time steps [5]. This allows the filter to reach an approximate steady state condition insuring the stationarity of the colored noise. We take the next $2N$ noise samples out of the filter; the first N for estimating the ACF of the colored noise; and the second N to be added to the transmitted signal vector. If a second signal vector is sent, we allow another 220 samples of colored noise to pass before taking the $2N$ samples to ensure the stationarity of the current noise samples and their independence from the previous set of noise samples. For our coloring filter, this is equivalent to allowing the noise correlation to decay to a point at which the samples are independent.

3.2 FVMAMF SIMULATION DESCRIPTION

In simulating a binary system we have a choice of two possible signal vectors to transmit

$$\left\{\underline{s}_i\right\} \quad i = 0,\ 1 \tag{3.03}$$

We define the length of the signal vectors to be $N = 8$ and have norm (energy) equal to 2. The length is purposely kept short in order to emphasize differences due to estimation of the noise characteristics as well as to maintain the idea of short term WSS of the noise. A total of 16 noise samples is generated using the coloring filter described earlier. The first 8 are assumed to be taken prior to the arrival of the noise corrupted signal vector at the receiver in order to estimate the noise characteristics and the second 8 are added to the transmitted signal vector. At the receiving end, an estimate of the channel noise correlation matrix is generated from the noise samples using one of the methods in §2.3. The FVMAMF (unity pre-filter) is designed using (A.3) and the resulting performance measures (OSNR and SNRI) of the filter can be calculated from (A.5). We can contrast the performance under estimated noise conditions by also computing the performance measures for a given noise condition assuming knowledge of the actual noise correlation.

In order to determine the number of bit errors, the output of the filter bank ($L = 2$) can be sent to the detector which is designed according to (C.1-3) and a determination made as to which signal was most likely to have been transmitted. Since the SNRI of a filter (once designed) is fixed, we can observe variations in the BER by adjusting the ISNR (and hence the OSNR). In doing this, the noise power is held constant and the signal energy scaled up or down in order to achieve the desired ISNR (2.24).

3.3 SSMAMF SIMULATION DESCRIPTION

In simulating a binary system we have a choice of two possible signal matrices to transmit

$$\left\{S_i\right\} \quad i = 0,\ 1 \tag{3.04}$$

We define the length of the basis signal vectors to be $M = 4$ and $k = 2$ ($k \times M = 2 \times 4 = 8 = N$) in order that the SSMAMF is comparable to the FVMAMF in terms of the length of the transmitted signal. The signal matrix is required to have a sum of the norms (energy) of the basis vectors equal to 2. For more exact comparison, the FVMAMF and SSMAMF are run simultaneously using identical transmitted signal vectors which allows us to use exactly the same noise samples for both systems (i.e. total of 16 noise samples is generated using the coloring filter and used as described in §3.2). At the receiving end, an estimate of the channel noise correlation matrix is generated from the noise samples using one of the methods in §2.3.

Given the noise correlation estimate, we use a 10 point brute force approach (§2.6.1) to initialize the gradient algorithm (§2.6.3, Appendix B) in order to determine which coefficient vector ($k = 2 \Rightarrow$ dimension($\underline{c}$) $= 2 \times 1$) maximizes the function of (2.53). The linearly combined noise correlation matrix (of dimension $M \times M = 4 \times 4$) can be obtained for a particular coefficient vector using (A.12). Equation (2.53) was evaluated in a brute force fashion at ten (10) equally spaced points encompassing the range of the combination coefficients (obtained from A.11). The coefficients generating the maximum value of (2.53) were selected as the starting point of the gradient algorithm. The gradient algorithm was allowed to run for two iterations, a number determined experimentally to produce a value of (2.53) sufficiently close to the maximum to produce no significant deviation in the resulting OSNR. A second reason that the gradient algorithm is allowed only a small number of iterations was to guard against the potential problem of the routine going off accidentally towards a minimum value of (2.53) or a slow convergence to a maximum of (2.53). This situation could presumably occur in practice due to particularly poor estimates of the noise

correlation or a particularly large gradient around the maximum. It should be mentioned that this rarely occurred in simulation.

Once the coefficient vector which maximizes (2.53) has been obtained, the MAMF can be designed using (A.10) and the performance measures under estimated noise conditions or assuming knowledge of the actual noise correlation can be found from (A.14) and (A.15). In order to determine the BER we can use the detection scheme described in §2.7, which can be implemented using (C.5-7) in Appendic C.

4.0 SIMULATION RESULTS

This chapter describes the actual trials conducted and presents the results. Absolute theoretical maximum SNRI ($\text{SNRI}^{\ddagger}$) is shown for both FV and SSMAMF systems for different system parameters (i.e. N, M, k). The two systems were then run side-by-side using identical transmitted signal vectors and additive channel noise for a variety of signal selections. Comparisons are made in terms of the SNRI under both actual and estimated channel noise conditions. These comparisons are shown graphically and as average differences relative to the absolute theoretical maximum of the FVMAMF.

When channel noise characteristics are estimated, the SNRI of a MAMF is a random variable obeying some distribution. Histograms of the SNRI under estimated noise conditions for several signals at a variety of colored noise center frequencies are shown.

Bit error results are presented in order to confirm the operation of the detector developed in §2.7 relative to a detection scheme derived solely for use in an optimal binary communication system [5].

4.1 SYSTEM THEORETICAL MAXIMUM SNRI

In this section we generate the absolute theoretical maximum value of SNRI ($SNRI^{\ddagger}$) for the FV and SSMAMF receiver systems across the range of colored noise center frequencies. For a given value of the colored noise center frequency θ, we can compute the actual noise correlation using the coefficients of the coloring filter [17].

In the case of the FVMAMF, the 8×8 correlation matrix can be formed for a particular θ and an eigen decomposition performed on the matrix. $SNRI^{\ddagger}$ of the FVMAMF receiver at this value of θ is defined as the inverse of the smallest eigenvalue of the 8×8 Toeplitz noise correlation matrix R_{ww} [3,9]. For the SSMAMF we vary the combination coefficients through their allowable ranges (given by the constraint of 2.43) in a brute force fashion at each θ to find the mimimum possible eigenvalue of $R_{\widetilde{w}\,\widetilde{w}}$. Since this is dependent on the amount of energy present in each basis vector, we consider the simplified case when the basis vectors are assumed to be orthonormal. This reduces the constraint of (2.43) to that of a circle in the case of the two dimensional coefficient vector used in simulation. At each of 100 equally spaced points, the linearly combined noise correlation was generated, the 4×4 linearly combined noise correlation matrix formed and an eigen decomposition conducted. $SNRI^{\ddagger}$ of the SSMAMF is the inverse of the smallest eigenvalue of $R_{\widetilde{w}\,\widetilde{w}}$ found while varying the combination coefficients [3,9].

Figure 6 presents $SNRI^{\ddagger}$ for the FV ($N = 8$) and SSMAMF ($k = 2\perp$, $M = 4$ where $\perp$ indicates that the basis vectors are orthogonal). The loss in $SNRI^{\ddagger}$ of the SSMAMF realtive to $SNRI^{\ddagger}$ of the FVMAMF is readily apparent from the figure, and is roughly constant (~ 4 dB) across the spectrum of center frequencies. Both systems are symmetric about π (half-sampling) and $\pi/2$, with the highest values of SNRI appearing at $\theta = 0$ and π and the minimum value of SNRI occurring at $\theta = \pi/2$. Examination of the eigenvalues across the spectrum of colored noise center frequencies revealed that both the FVMAMF and the SSMAMF possessed multiple minimal eigenvalues (multiplicity 2) at $\theta = \pi/2$. This multiple eigenvalue accounts for the reduction in $SNRI^{\ddagger}$ and can be related to the pole location of the coloring filter. At $\theta = 0$ we have a double real pole

which separates as we move from 0 to π, becoming a conjugate pair and achieving maximum separation in the z-plane at $\theta = \pi/2$. The poles then move back towards a double real pole configuration at $\theta = \pi$. Similarly, the smallest eigenvalue and the next smallest eigenvalue approach one another as the poles move towards $\theta = \pm\pi/2$ until it becomes a multiple eigenvalue at that location. The two dimensional minimal noise eigenspace allows for an infinity of possible solutions to the optimum signal selection problem at this location (see §2.8).

Investigation of the minimal noise correlation eigenvectors (optimal signals) for colored noise center frequencies $0 \leq \theta \leq \pi$ revealed that for $0 \leq \theta < \pi/2$ the eigenvectors were all skew-symmetric while for $\pi/2 < \theta \leq \pi$ the eigenvectors were all symmetric. At $\theta = \pi/2$, since there is a two dimensional minimal noise eigenspace, we may select the eigenvectors to be symmetric or skew-symmetric if we so desire. This was true for both FV and SSMAMF.

It should also be noted that in the case of the SSMAMF the coefficient vector which yielded $\text{SNRI}^{\ddagger}$ was in **all** cases either

$$\underline{c}^{\ddagger} = \begin{bmatrix} 1 & 1 \end{bmatrix}^{T}$$

or

$$\underline{c}^{\ddagger} = \begin{bmatrix} 1 & -1 \end{bmatrix}^{T}$$

It is important to remember that in order to achieve the SNRI values shown, we would also need to use the optimum signal vector (scaled version of the eigenvector) at each point. The problem in practice is that we must choose one signal vector for transmission and not a continuum of signal vectors.

Figures 7 and 8 show $\text{SNRI}^{\ddagger}$ of the FV and SSMAMF receiver systems for several different values of $N = 4, 8, 16$ and $M = 4, 8, 16$ (for $k = 2$) respectively. In both cases we can see that as the filter length is increased the $\text{SNRI}^{\ddagger}$ curve shifts upward, indicating the improvement in noise cancellation that occurs with increasing filter length. However, we can also observe that there is little difference between the curves of the FVMAMF for $N = 8$ and $N = 16$, as well as the curves of the SSMAMF for $M = 8$ and $M = 16$ (which would correspond to $N = 16$ and $N = 32$ when $k = 2$). This implies that there would be little

additional noise cancellation for the increase in filter length (though the additional length would require more noise samples and potentially a better estimate of the noise correlation).

In Figures 9 and 10 we wished to examine the effect of adding basis vectors on $\text{SNRI}^{\ddagger}$ for the SSMAMF. Figure 9 shows the case when the basis vectors are orthogonally constrained and we increase the number of vectors from the degenerate case of $k = 1$ to $k = 3$. In §2.8 we showed that the SSMAMF was in fact a generalization of the FVMAMF of length M. Therefore, in the degenerate case where the all signal energy is placed in one basis vector, $\text{SNRI}^{\ddagger}$ for the SSMAMF ($M = 4,\ k = 2$) is equal to the $\text{SNRI}^{\ddagger}$ of the FVMAMF of length $N = M$. Figure 10 shows the effect of additional basis vectors for the SSMAMF (by applying (2.110)) using as a starting point the degenerate case when $\text{SNRI}^{\ddagger}$ is that of the FVMAMF of length 4 (see Figure 7). Figures 9 and 10 are very similar in SNRI values and in fact differ only in the first or second decimal places (the orthogonally constrained version being marginally higher). The significance of this is in the computational aspects required to produce both figures. In Figure 9 we must compute the minimal eigenvalue of the linearly combined noise correlation matrix over the entire range of allowable combination coefficients. This must be repeated over the entire spectrum of colored noise center frequencies, which for $k \geq 3$ can be very tedious and time consuming. Conversely, in Figure 10 we need only compute the minimal eigenvalue of the 4×4 noise correlation matrix for the FVMAMF over the range of colored noise center frequencies and divide this by k to obtain the SNRI curves. While this was hardly the original intent of the exercise, it does appear as if it provides a simple and less computationally burdensome method of generating approximate versions of $\text{SNRI}^{\ddagger}$ shown in Figure 9.

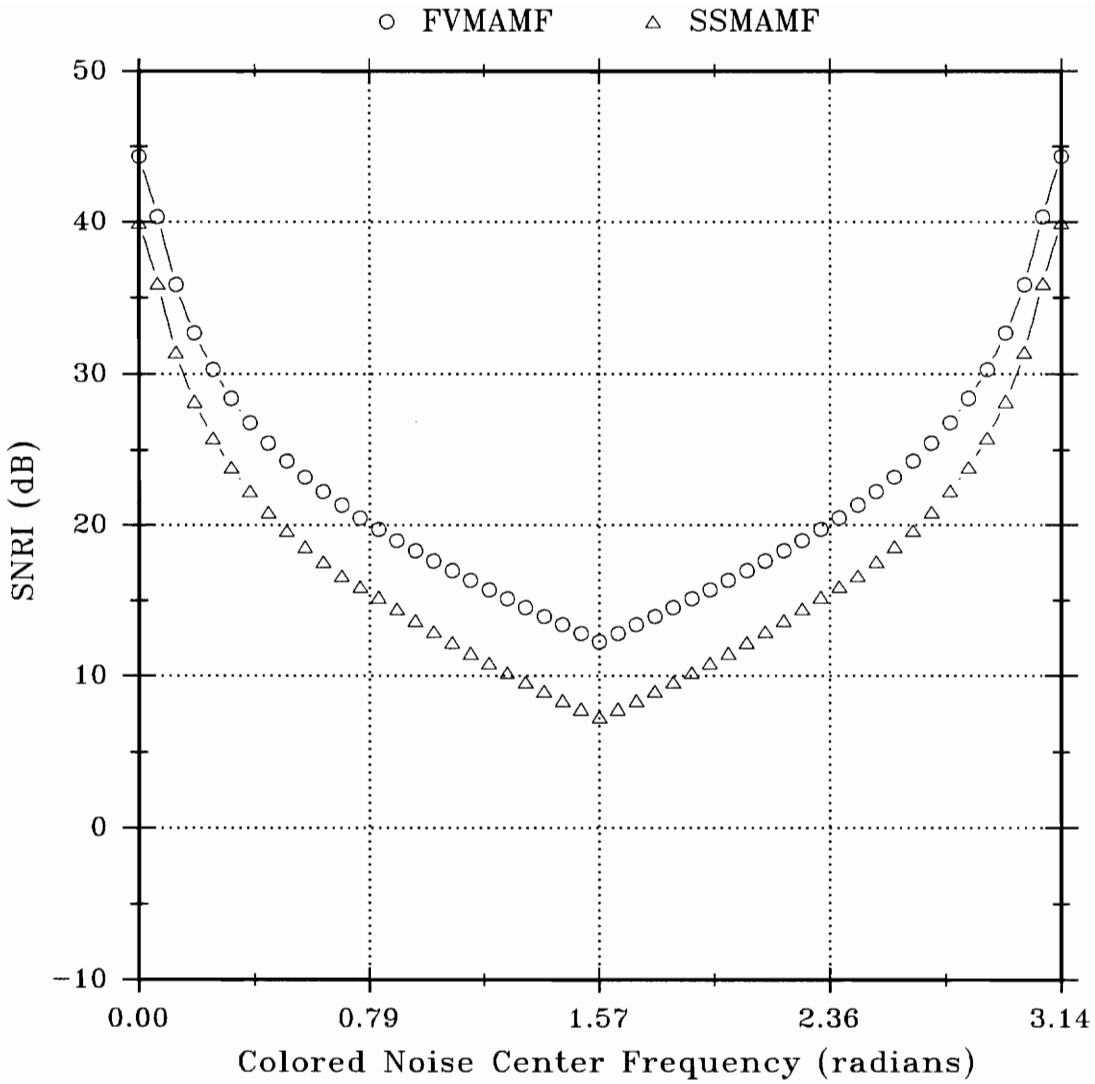

FIGURE 6: $\text{SNRI}^{\ddagger}$ for FVMAMF ($N = 8$) and $\text{SNRI}^{\ddagger}$ for the orthogonally contrained SSMAMF ($k = 2 \perp$, $M = 4$).

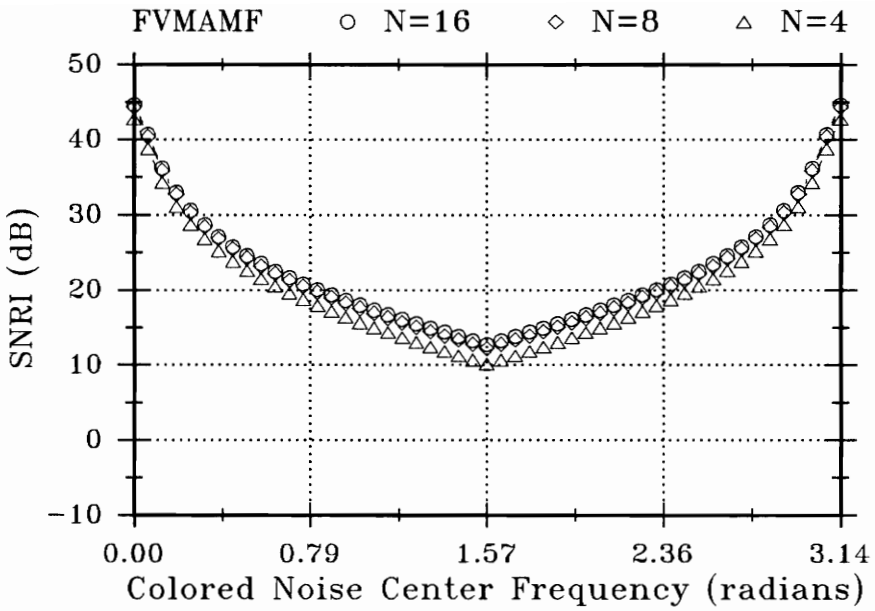

FIGURE 7: SNRI‡ for FVMAMF of lengths $N = 4$, 8, 16.

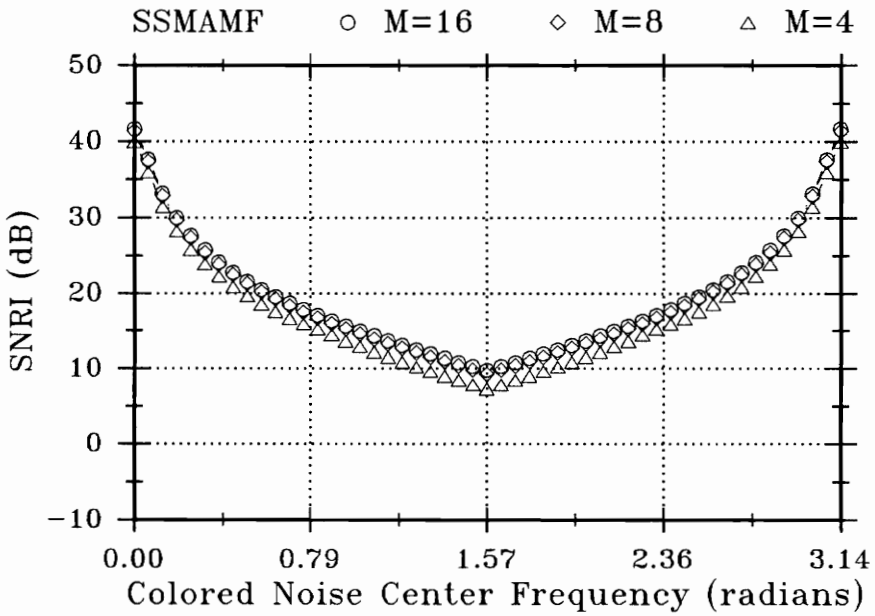

FIGURE 8: SNRI‡ for the orthogonally constrained SSMAMF ($k = 2 \perp$ with $M = 4$, 8 and 16).

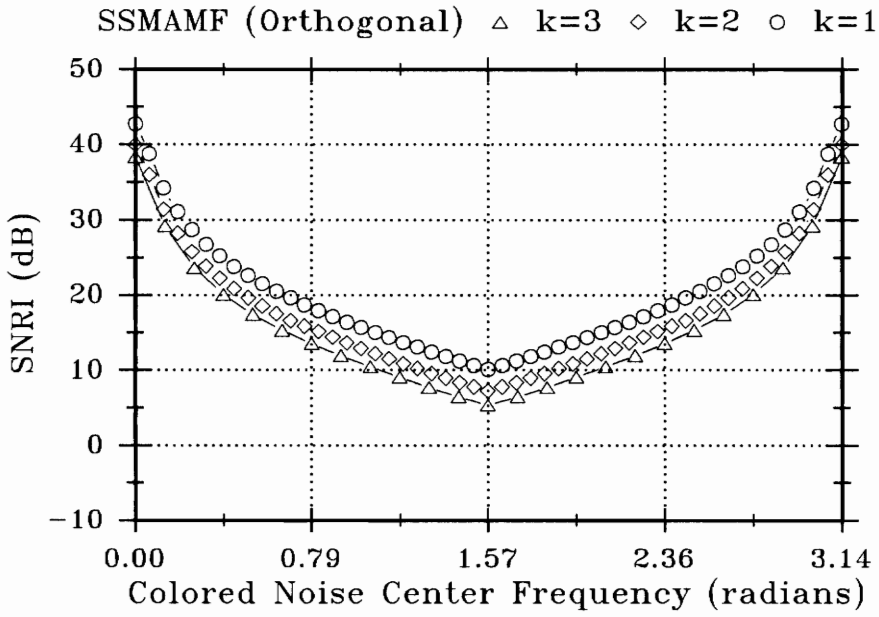

FIGURE 9: $\text{SNRI}^{\ddagger}$ **for the orthogonally constrained SSMAMF** ($k = 1$, 2, **and 3** $\perp$ **with** $M = 4$).

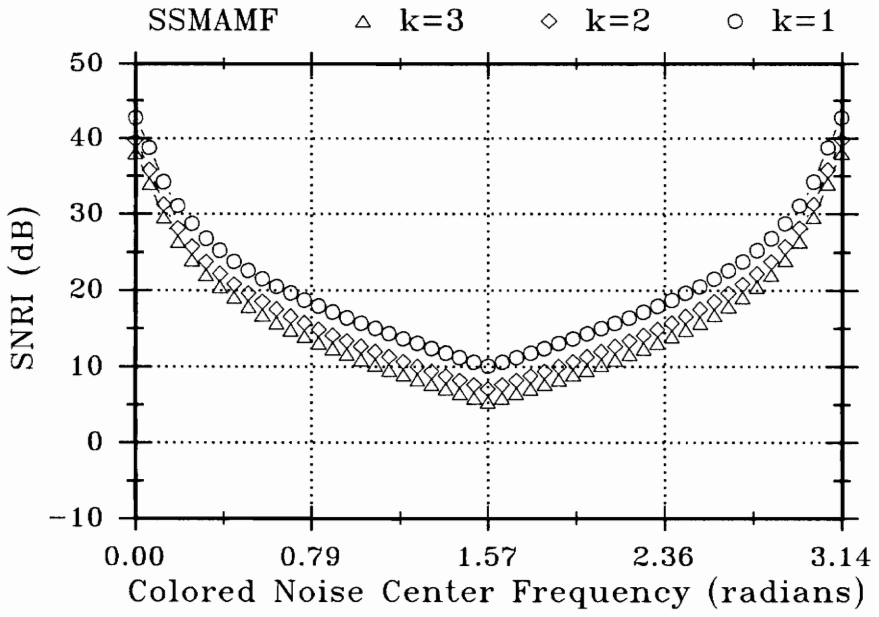

FIGURE 10: $\text{SNRI}^{\ddagger}$ **for the SSMAMF** ($k = 1$, 2, 3 **with** $M = 4$).

4.2 SYSTEM SNRI RESPONSE TO SELECTED SIGNALS

We now begin to investigate the performance of the FV and SSMAMF in terms of SNRI when using actual signals. We shall refer to a signal as *robust* (with respect to changing colored noise center frequencies) when its SNRI response maintains a close relationship to the $\text{SNRI}^{\ddagger}$ curve. Obviously, the ideal robust signal would produce a SNRI response which would closely follow the $\text{SNRI}^{\ddagger}$ curve **even when the noise ACF is estimated.**

As mentioned earlier, each signal is run concurrently in both systems using identical additive colored channel noise. The trials are conducted first using knowledge of the actual noise ACF which generates an upper bound on the SNRI attainable for that particular signal. The trial is then rerun using estimated noise ACF (generated from 8 samples of channel noise with the classical biased estimator) and repeated a total of 1000 times with different colored noise sequences at 21 discrete colored noise center frequencies ($\theta = n\pi/20$, $n = 0, 1, \ldots, 20$). The arithmetic mean of the SNRI ($\overline{\text{SNRI}}$) for the 1000 repetitions is computed at each θ and plotted against the discrete colored noise center frequency.

Each plot will show $\text{SNRI}^{\ddagger}$ of the FVMAMF ($N = 8$) and the performance of the actual system (FVMAMF or SSMAMF) using both actual and estimated ACF. Note that even the SSMAMF is shown with $\text{SNRI}^{\ddagger}$ of the FVMAMF since that represents the highest values achievable by either system and provides a good reference point for contrasting the two systems.

In the first sequence of four simulations (#'s 1-4) we deal with signals which are chosen for the FVMAMF in some fashion. Figures 11, 13 and 15 (simulations 1-3) show the FVMAMF SNRI response when the signal is chosen as that which optimizes the FVMAMF at discrete colored noise center frequencies of $\theta = 0$, $\pi/4$, and $\pi/2$ respectively. Figures 12, 14 and 16 show the SSMAMF SNRI response to the same signals. Recall that there is a two dimensional minimal noise eigenspace at $\theta = \pi/2$, implying that the signal chosen for simulation at this center frequency is not unique. Figures 17 and 18 (simulation 4) show the FV and SSMAMF SNRI responses when the signal was selected again to be optimal for

the FVMAMF system at $\theta = \pi/2$. However, in this case a trial and error search was conducted in the two dimensional minimal noise eigenspace in order to find a signal vector which would produce a more or less symmetric SNRI response for the FVMAMF about $\pi/2$ under estimated noise ACF. The transmitted signal vectors used in these four simulations are shown in Table I. Note that the optimal signal vectors are skew-symmetric for $\theta = 0, \pi/4$. These two signals are very similar, differing only in the third decimal place accounting for the similarity of Figures 11 and 13. It should be mentioned that the optimum signals for the FVMAMF at $\theta = 3\pi/4$, and π are exactly the symmetric versions of the signals for $\theta = \pi/4$, and 0 respectively. These signals will produce an exact mirror image of the SNRI responses seen in Figure 11 (for $\theta = \pi$) and Figure 13 (for $\theta = 3\pi/4$). This is true for any optimum signals (and their SNRI responses) selected for colored noise center frequencies which are equally spaced to either side of $\theta = \pi/2$.

Table I: Signals used in Simulations 1-4

SIMULATION #			
1	2	3	4
0.098	0.118	0.347	0.394
-0.347	-0.348	0.188	2e-4
0.592	0.593	0.808	0.919
-0.721	-0.716	0.438	4e-4
0.721	0.716	0.808	0.919
-0.592	-0.593	0.438	4e-4
0.347	0.348	0.347	0.394
-0.098	-0.118	0.188	2e-4

From the figures for the FVMAMF (11, 13, 15, 17) we can see that the selected signals are in fact optimal (i.e. produce SNRI†) at the colored noise center frequencies for which they were selected when the actual noise ACF is used. We also observe from Figures 11-18 that the values of $\overline{\text{SNRI}}$ generated using estimated

noise ACF are always less than (or equal to) the value of $SNRI^{\dagger}$ generated using the actual noise ACF. However, $\overline{SNRI}$ at the center frequency of optimization is also very close to the value of $SNRI^{\dagger}$ at that center frequency.

Figures 11 and 13 are very robust with respect to $SNRI^{\ddagger}$ for $0 \leq \theta \leq \pi/2$. Unfortunately, this behavior changes for $\pi/2 < \theta \leq \pi$, where the SNRI falls off significantly from $SNRI^{\ddagger}$ and in fact achieves negative values (in dB). This indicates that the filtering process is actually degrading the signal relative to the noise, a condition which should be avoided.

Figure 15 is reasonably robust for $\pi/2 \leq \theta \leq \pi$ but falls off significantly for $0 \leq \theta \leq \pi/2$. While this signal does not match as closely in its respective interval as those for $\theta = 0$ and $\pi/4$, it also does not ever reach negative SNRI values. For this reason, when considering a signal which is robust to the entire spectrum of colored noise center frequencies, this signal would be preferable to those used to generate Figures 11 and 13.

In Figure 17 we tried to achieve the most robust response possible for the FVMAMF under conditions of estimated noise ACF. By linearly combining the two eigenvectors at $\theta = \pi/2$, we were able (by trial and error) to achieve a near symmetric SNRI response. Since the signal is optimal for $\pi/2$, it does approach $SNRI^{\ddagger}$ most nearly in this neighborhood but shows significant losses in SNRI relative to $SNRI^{\ddagger}$ around $\theta = 0$ and π. It is also interesting to note that the signals used in Figures 11 and 13 actually are able to achieve a value of $\overline{SNRI}$ much closer to $SNRI^{\ddagger}$ at $\theta = \pi/2$ than were either of the two optimum signals used to generate Figures 15 and 17. This indicates that the optimum signals at $\theta = \pi/2$ are not robust with respect to estimated noise ACF. Other attempts were made to achieve a robust response by combining the optimum signals for various colored noise center frequencies (eg. $\theta = 0$ and π, $\pi/4$ and $3\pi/4$, etc.) but produced very poor SNRI responses and were not included.

There is little discussion here relative to the SSMAMF responses of Figures 12, 14, 16 and 18. In all cases, when using the optimum signals for the FVMAMF, they produce lower SNRI curves than their FVMAMF counterparts. We do notice that the general shape or trend of the SSMAMF SNRI curve is very similar to the comparable FVMAMF curve.

The second sequence of simulations (#'s 5-7) selected optimum signals for the SSMAMF at several colored noise center frequencies. In solving for the minimal eigenvalue of the SSMAMF (i.e. SNRI‡) we determine the optimum coefficient vector $\underline{c}^{\ddagger}$ for the particular colored noise center frequency as well as the minimal eigenvector $\underline{v}_{min}$, of the linearly combined noise correlation. Knowing these two items, we can create two basis vectors with equal energy for the SSMAMF which when linearly combined using $\underline{c}^{\ddagger}$ will generate $\underline{v}_{min}$. Optimum signals for the SSMAMF were created in this manner for colored noise center frequencies of $\theta = 0$, $\pi/4$ and $\pi/2$. Again, be reminded that there exists a two dimensional minimal noise eigenspace at $\theta = \pi/2$. The SNRI responses for the FVMAMF using these signals are presented in Figures 19, 21 and 23 while those of the SSMAMF are shown in Figures 20, 22 and 24 (simulations 5-7). The signals used in the simulation are listed in Table II.

Table II: Signals used in Simulations 5-7

SIMULATION #		
5	6	7
0.345	0.451	0.996
0.000	0.000	0.000
0.939	0.893	0.000
0.000	0.000	0.087
0.000	0.000	0.000
0.939	0.893	0.087
0.000	0.000	0.996
0.345	0.451	0.000

The first thing to observe in comparing Figure 19 with Figure 20 and Figure 21 with Figure 22, is that when using these optimum signals for the SSMAMF and the actual noise ACF, the FVMAMF produces a higher SNRI

curve over the entire spectrum of colored noise center frequencies. The second item of interest in the case of the actual noise ACF is that the SNRI responses are all nearly symmetric about $\theta = \pi/2$. This would indicate the potential for a robust signal and at this point certainly seems to indicate that the FVMAMF is superior even when using the SSMAMF optimum signals. Fortunately (for me), when the noise ACF is estimated, the situation is reversed and we see that these signals for the SSMAMF are very robust in the case of the SSMAMF while significant degradation in performance occurs for the FVMAMF. In fact, the SSMAMF maintains a very close relationship with its SNRI curve using the actual noise ACF. $\overline{\text{SNRI}}$ matches almost exactly the value of the SSMAMF SNRI‡ at the point of optimization and in fact is close to the SSMAMF SNRI‡ over the entire spectrum of center frequencies. The ability of the SSMAMF to achieve this symmetry is primarily due to its ability to manipulate or adapt the signal at the receiver. Recall that the optimum signals for $0 \leq \theta \leq \pi/2$ are skew-symmetric and for $\pi/2 \leq \theta \leq \pi$ they are symmetric. Essentially, the SSMAMF can, within limits, change the form of the linearly combined signal to be either symmetric or skew-symmetric depending on the existing noise conditions and produce a reasonably symmetric SNRI curve.

Using an arbitrarily selected optimum signal for $\theta = \pi/2$ produces fairly poor results although the SNRI curve of Figure 24 is more or less symmetric about $\pi/2$. It is fairly obvious that this is inferior to either of the two signals used to create Figures 20 and 22.

The final sequence of simulations investigates the idea of optimizing the SSMAMF for multiple noise conditions. Hopefully, based on §2.8 this will provide a robust SNRI response over the range of colored noise center frequencies. This final group is broken into two parts; 1) Simulation #'s 8-12 use the minimal eigenvectors for the FVMAMF ($N = 4$) at some center frequencies as basis vectors; and 2) Simulation #'s 13-17 use minimal eigenvectors for the orthogonally constrained SSMAMF ($k = 2 \perp, M = 4$) at some center frequencies as basis vectors. The only restriction placed upon the vectors was that they form a normal basis set (i.e. they were not required to be orthogonal, although certain combinations did lead to an orthonormal set). Signals used in parts 1) and 2) are shown in Table III.

Table III: Signals used in Simulations 8-17

SIMULATION #									
8	9	10	11	12	13	14	15	16	17
0.229	0.229	0.229	0.500	0.275	0.244	0.244	0.244	-0.704	0.319
-0.669	-0.669	-0.669	-0.500	-0.651	-0.664	-0.664	-0.664	-0.062	-0.631
0.669	0.669	0.669	0.500	0.651	0.664	0.664	0.664	-0.704	0.631
-0.229	-0.229	-0.229	-0.500	-0.275	-0.244	-0.244	-0.244	-0.062	-0.319
0.229	0.500	0.500	0.500	0.275	0.244	-0.704	-0.062	-0.062	0.319
0.669	-0.500	0.500	0.500	0.651	0.664	-0.062	0.704	0.704	0.631
0.669	0.500	0.500	0.500	0.651	0.664	-0.704	-0.062	-0.062	0.631
0.229	-0.500	0.500	0.500	0.275	0.244	-0.062	0.704	0.704	0.319

Figures 25 and 26 (simulation #8) show the FV and SSMAMF SNRI curves when the basis vectors are selected as the minimal eigenvectors of the FVMAMF of length 4 at $\theta = 0$ and π. Note that the eigenvector for $\theta = \pi$ is the symmetric version of the skew-symmetric eigenvector for $\theta = 0$ and the pair do form an orthonormal basis set. The FVMAMF shows a reasonable symmetry about $\theta = \pi/2$, but the SSMAMF is once again even more so. Under estimated noise ACF, the SSMAMF maintains a SNRI which is almost a (small) constant difference from the SNRI when using the actual noise ACF. Again, this is also quite close to the SSMAMF SNRI‡ from $0 \leq \theta \leq \pi$.

The SNRI responses in Figures 27 and 28 (simulation 9) result from a signal using as basis vectors the FVMAMF ($N = 4$) minimal eigenvector at $\theta = 0$ and an arbitrary skew-symmetric minimal eigenvector at $\theta = \pi/2$. Figures 29 and 30 (simulation 10) are similar but with a different choice for the minimal eigenvector at $\theta = \pi/2$ (symmetric). Note that the basis vectors for simulation 10 are orthonormal while those of simulation 9 are not. In Figure 28 we see that without the orthogonal constraint on the basis vectors, we can locally exceed the orthogonally constrained SNRI‡ (Figure 6), but pay the price in losing our robust SNRI response over all θ (i.e. Figure 28 begins to resemble Figure 12) and even

produce negative values of SNRI ($\Rightarrow$ degradation of SNR). Figure 30 is somewhat better, showing a more or less robust response, though easily better from $0 \leq \theta \leq \pi/2$ than in the remainder of the curve. This is due to our providing in the basis vectors optimum solutions for this interval.

Two minimal eigenvectors spanning the two dimensional minimal noise eigenspace at $\theta = \pi/2$ were used to produce the SNRI curves of the FV and the SSMAMF seen in Figures 31 and 32 (simulation 11) respectively. Note that these are the symmetric and skew-symmetric versions of the vector and they are orthonormal. This signal leads to a SNRI curve for the SSMAMF that is approximately symmetric, but is far more robust around $\theta = \pi/2$ than on the edges (i.e. $\theta \approx 0$ and π).

Figures 33 and 34 (simulation 12) show the SNRI response of the FV and SSMAMF when the basis vectors are chosen as the minimal eigenvectors of the FVMAMF ($N = 4$) at $\theta = \pi/4$ and $3\pi/4$. Once again we see a very robust response under estimated noise ACF.

Simulations 13-17 duplicate simulations 8-12 using instead the optimum signals (minimal eigenvector of the linearly combined noise correlation matrix) for the SSMAMF when orthogonally constrained and the SNRI results are presented in the same order in Figures 35-44. The only notable difference in the SNRI responses is when two basis vectors spanning the two dimensional minimal noise eigenspace at $\theta = \pi/2$ are used. The two vectors lie within the same space as the two used in simulation 11 (Figures 31 and 32). The SNRI response in Figure 42 has more variation across θ than the SNRI response of Figure 32. This merely indicates that care must be taken when selecting basis vectors from this 2-D space since they most certainly do not produce identical results.

Figures 35 and 36 (simulation 13) are almost indistinguishable from Figure 25 and 26 which is not too surprising considering that the basis vectors are quite close. A comparable situation occurs for Figures 43 and 43 (simulation 17) when compared with Figures 33 and 34 for the same reason.

The FV and SSMAMF SNRI responses are seen respectively in Figures 37 and 38 (simulation 14) for basis vectors chosen as the minimal eigenvector for the SSMAMF ($k = 2 \perp$, $M = 4$) and a vector from the 2-D minimal noise space at

$\theta = \pi/2$. Similarly for Figures 39 and 40 (simulation 15) using another vector from the 2-D space. There is little difference in the SSMAMF responses but the FVMAMF response of Figure 37 is significantly better than that of Figure 39.

While it can not be seen from these figures, it should be pointed out that in the cases where we attempted to take advantage of the multiple optimization capability of the SSMAMF, the maximization routine did in fact converge to the solution given in §2.8 for actual noise ACF at the optimization center frequency. When the estimated noise ACF is used, we can see from Figure 44 that $\overline{\text{SNRI}}$ does approach more closely the SNRI around the optimization center frequencies of $\theta = \pi/4$ and $3\pi/4$ when the actual ACF is used.

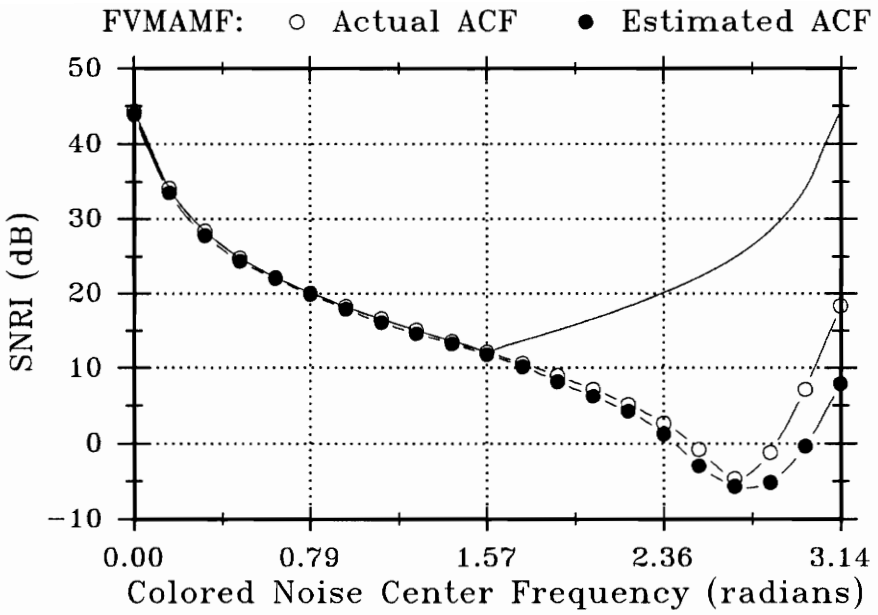

FIGURE 11: SNRI† and $\overline{\text{SNRI}}$ of the FVMAMF using the FVMAMF optimum signal for a colored noise center frequency $\theta = 0$.

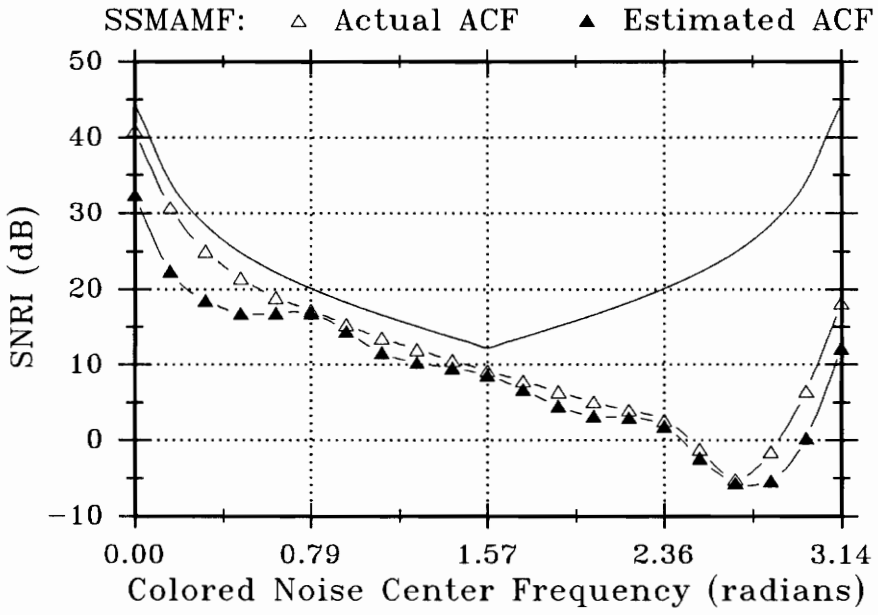

FIGURE 12: SNRI† and $\overline{\text{SNRI}}$ of the SSMAMF using the FVMAMF optimum signal for a colored noise center frequency $\theta = 0$.

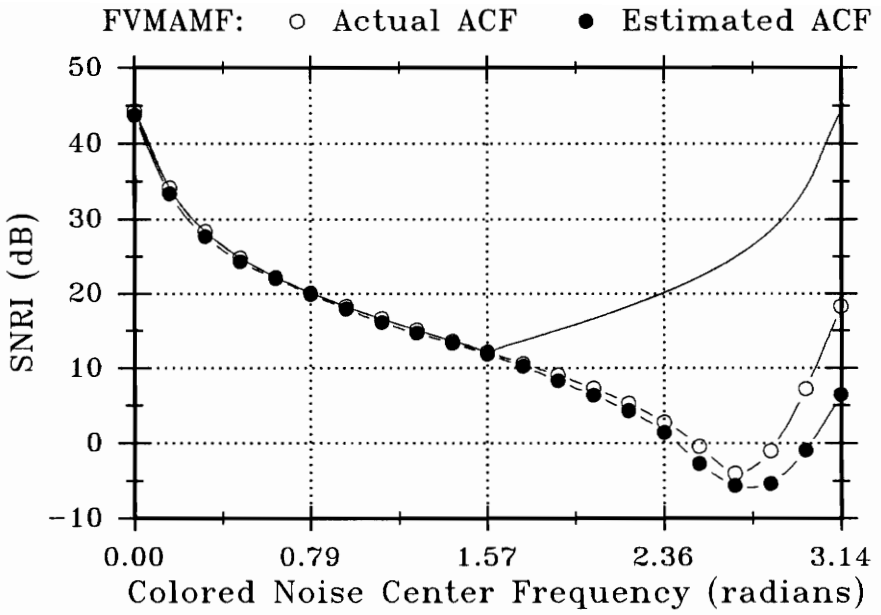

FIGURE 13: SNRI† and $\overline{\text{SNRI}}$ of the FVMAMF using the FVMAMF optimum signal for a colored noise center frequency $\theta = \pi/4$.

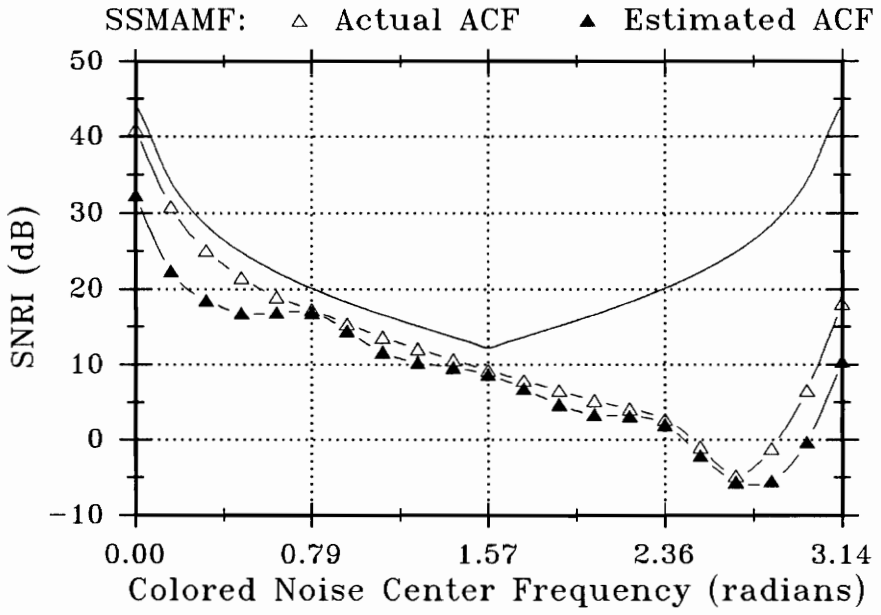

FIGURE 14: SNRI† and $\overline{\text{SNRI}}$ of the SSMAMF using the FVMAMF optimum signal for a colored noise center frequency $\theta = \pi/4$.

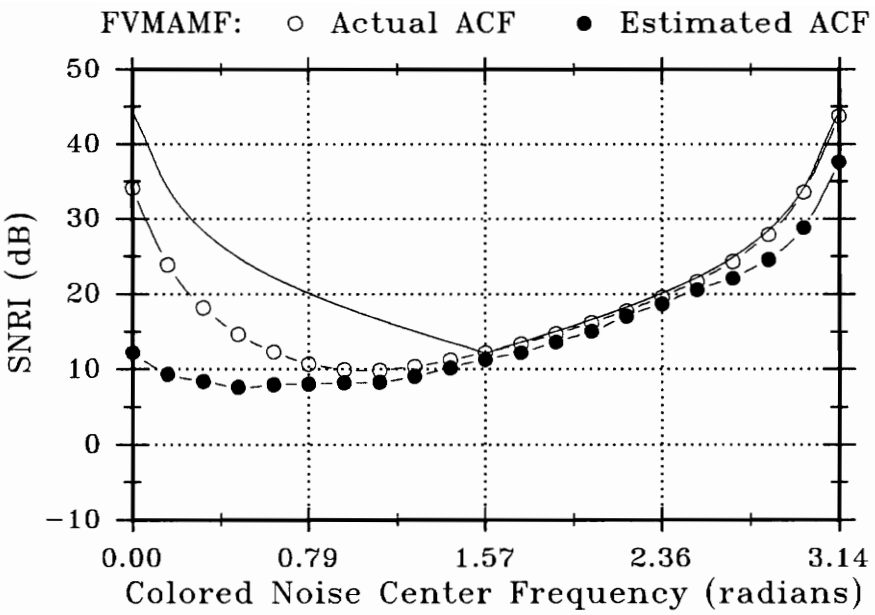

FIGURE 15: SNRI† and $\overline{\text{SNRI}}$ of the FVMAMF using a FVMAMF optimum signal for a colored noise center frequency $\theta = \pi/2$.

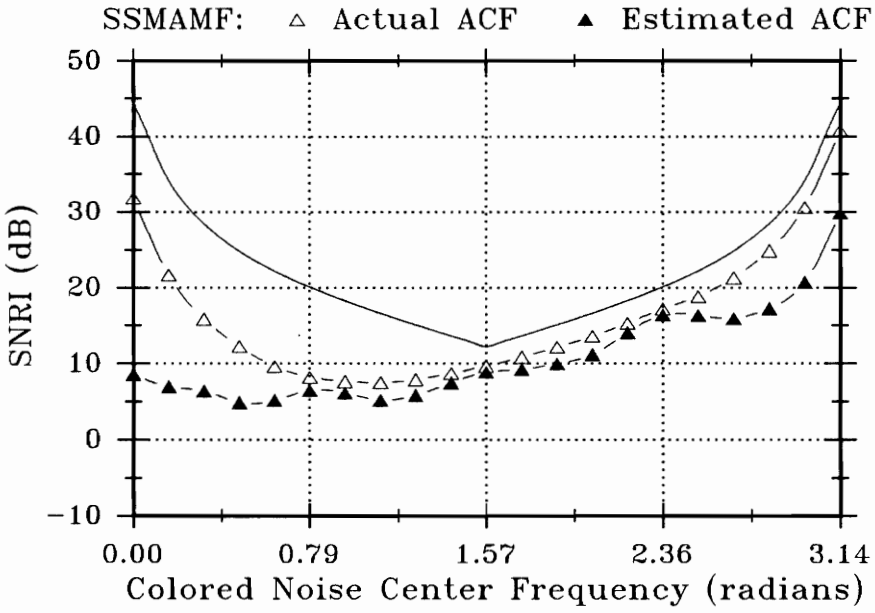

FIGURE 16: SNRI† and $\overline{\text{SNRI}}$ of the SSMAMF using a FVMAMF optimum signal for a colored noise center frequency $\theta = \pi/2$.

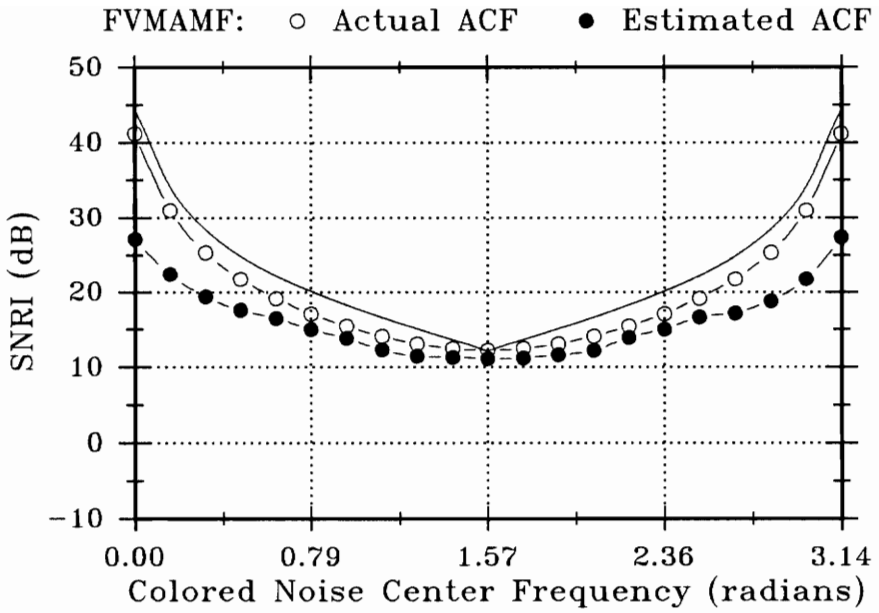

FIGURE 17: $SNRI^{\dagger}$ and $\overline{SNRI}$ of the FVMAMF using a FVMAMF optimum signal for a colored noise center frequency $\theta = \pi/2$ ($\sim$ balanced $\overline{SNRI}$).

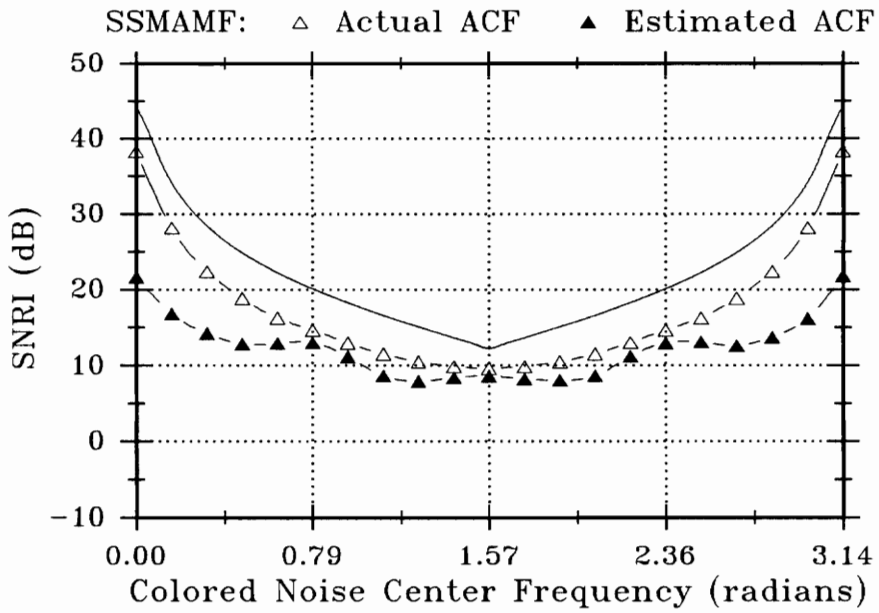

FIGURE 18: $SNRI^{\dagger}$ and $\overline{SNRI}$ of the SSMAMF using a FVMAMF optimum signal for a colored noise center frequency $\theta = \pi/2$.

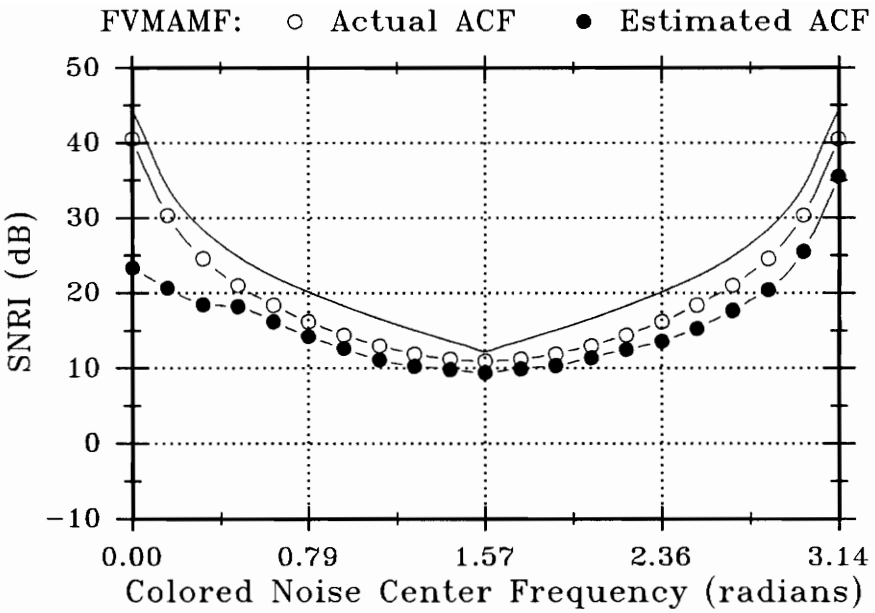

FIGURE 19: $SNRI^{\dagger}$ and $\overline{SNRI}$ of the FVMAMF using the SSMAMF optimum signal for a colored noise center frequency $\theta = 0$.

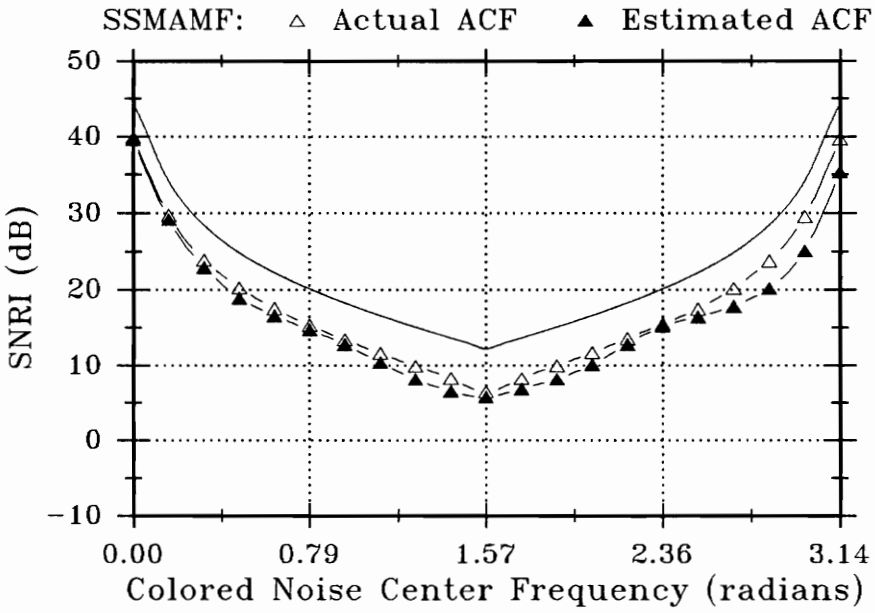

FIGURE 20: $SNRI^{\dagger}$ and $\overline{SNRI}$ of the SSMAMF using the SSMAMF optimum signal for a colored noise center frequency $\theta = 0$.

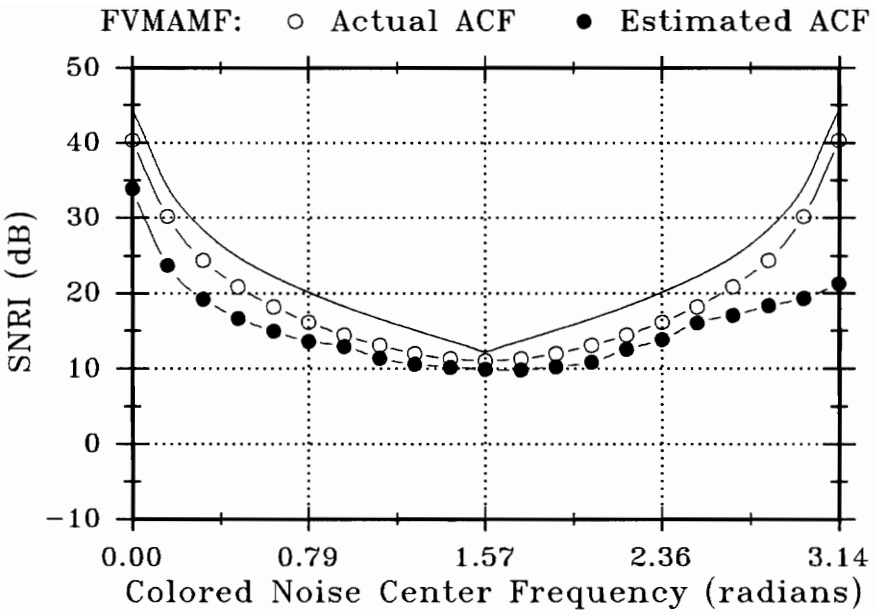

FIGURE 21: $SNRI^{\dagger}$ and $\overline{SNRI}$ of the FVMAMF using the SSMAMF optimum signal for a colored noise center frequency $\theta = \pi/4$.

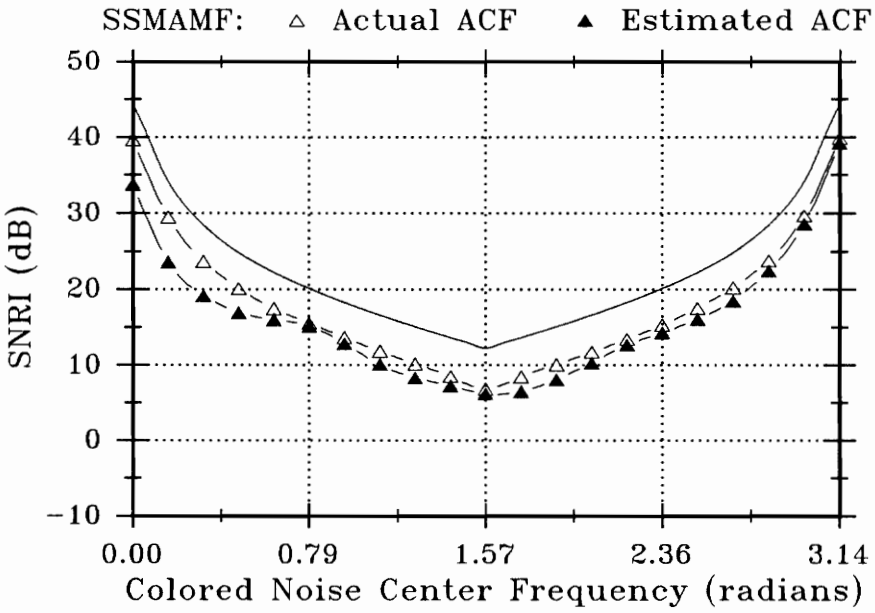

FIGURE 22: $SNRI^{\dagger}$ and $\overline{SNRI}$ of the SSMAMF using the SSMAMF optimum signal for a colored noise center frequency $\theta = \pi/4$.

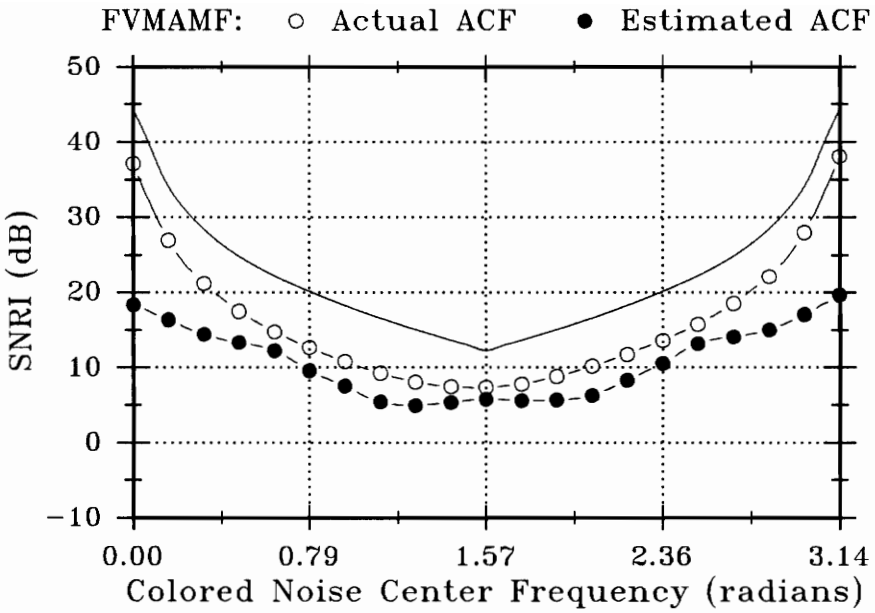

FIGURE 23: SNRI† and $\overline{\text{SNRI}}$ of the FVMAMF using a SSMAMF optimum signal for a colored noise center frequency $\theta = \pi/2$.

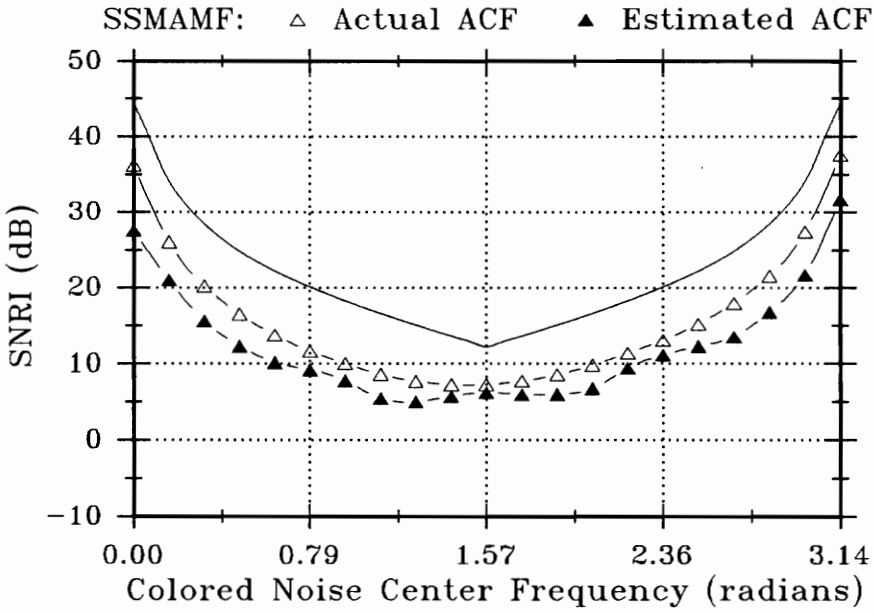

FIGURE 24: SNRI† and $\overline{\text{SNRI}}$ of the SSMAMF using a SSMAMF optimum signal for a colored noise center frequency $\theta = \pi/2$.

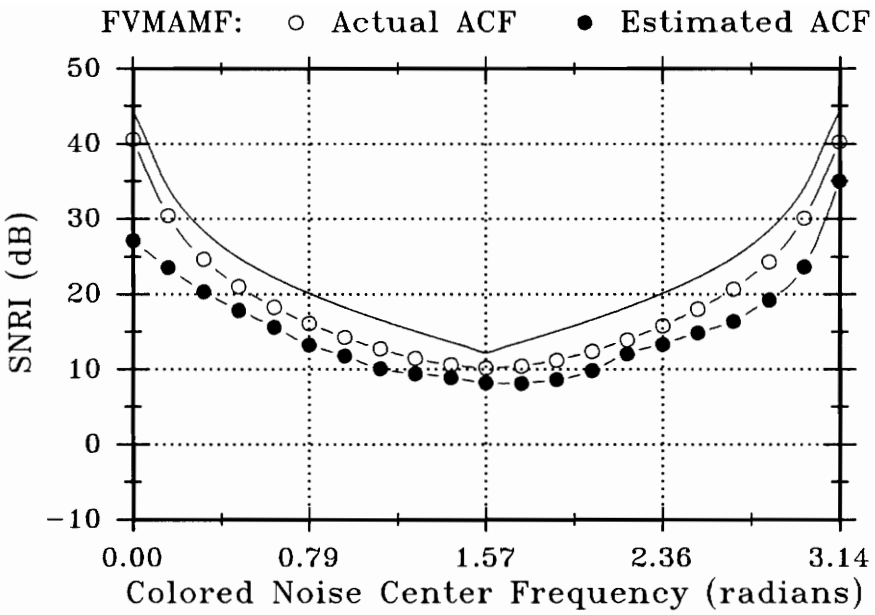

FIGURE 25: $\text{SNRI}^{\dagger}$ and $\overline{\text{SNRI}}$ of the FVMAMF using the concatenated FVMAMF ($N = 4$) optimum signals for a colored noise center frequency $\theta = 0$ and π.

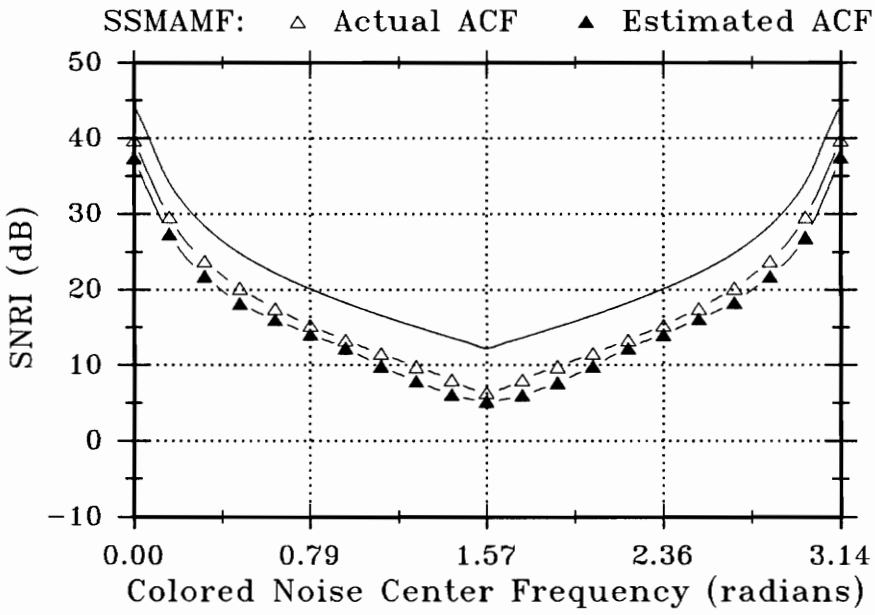

FIGURE 26: $\text{SNRI}^{\dagger}$ and $\overline{\text{SNRI}}$ of the SSMAMF using the concatenated FVMAMF ($N = 4$) optimum signals for a colored noise center frequency $\theta = 0$ and π.

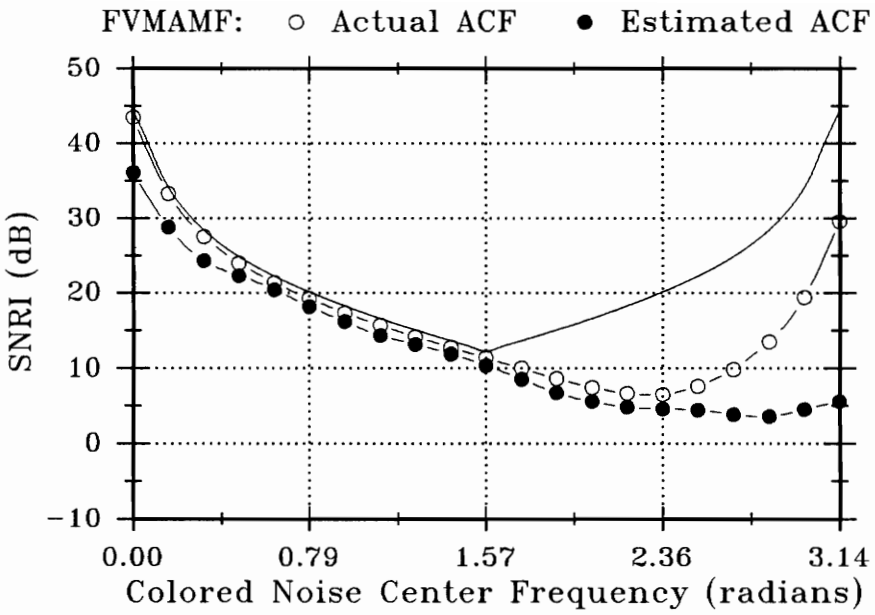

FIGURE 27: $\text{SNRI}^{\dagger}$ and $\overline{\text{SNRI}}$ of the FVMAMF using the concatenated FVMAMF ($N = 4$) optimum signals for a colored noise center frequency $\theta = 0$ and $\pi/2$ (#1).

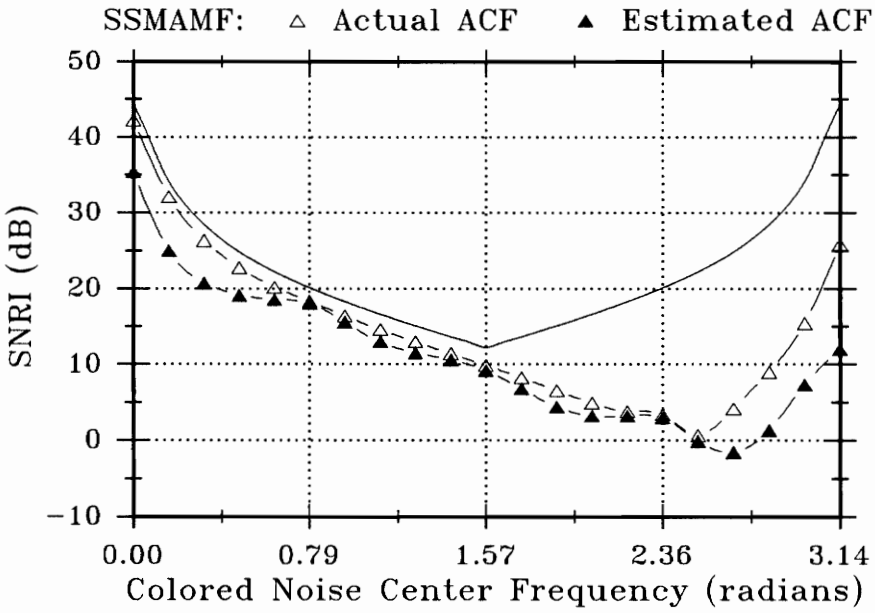

FIGURE 28: $\text{SNRI}^{\dagger}$ and $\overline{\text{SNRI}}$ of the SSMAMF using the concatenated FVMAMF ($N = 4$) optimum signals for a colored noise center frequency $\theta = 0$ and $\pi/2$ (#1).

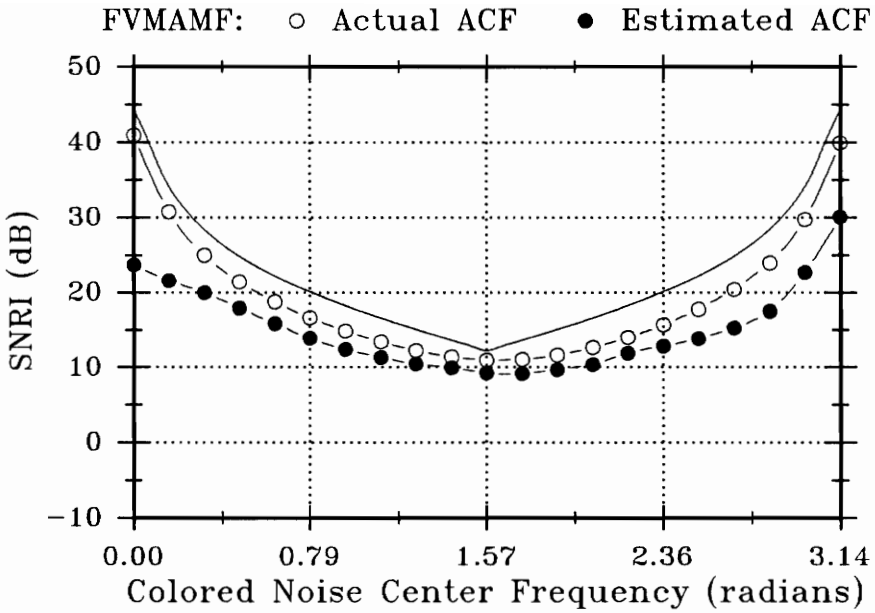

FIGURE 29: $\text{SNRI}^{\dagger}$ and $\overline{\text{SNRI}}$ of the FVMAMF using the concatenated FVMAMF ($N = 4$) optimum signals for a colored noise center frequency $\theta = 0$ and $\pi/2$ (#2).

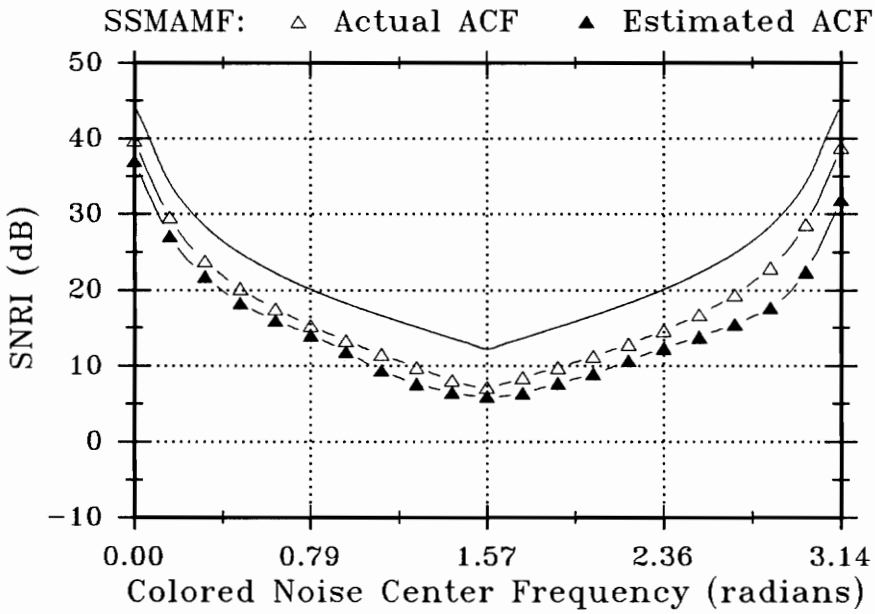

FIGURE 30: $\text{SNRI}^{\dagger}$ and $\overline{\text{SNRI}}$ of the SSMAMF using the concatenated FVMAMF ($N = 4$) optimum signals for a colored noise center frequency $\theta = 0$ and $\pi/2$ (#2).

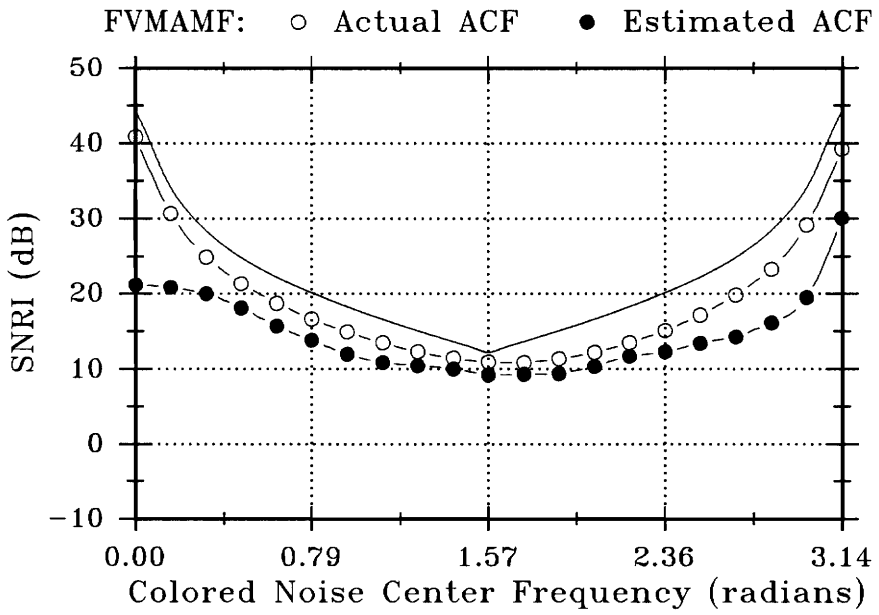

FIGURE 31: $\text{SNRI}^{\dagger}$ and $\overline{\text{SNRI}}$ of the FVMAMF using the concatenated FVMAMF ($N = 4$) optimum signals for a colored noise center frequency $\theta = \pi/2$ (#1) and $\pi/2$ (#2).

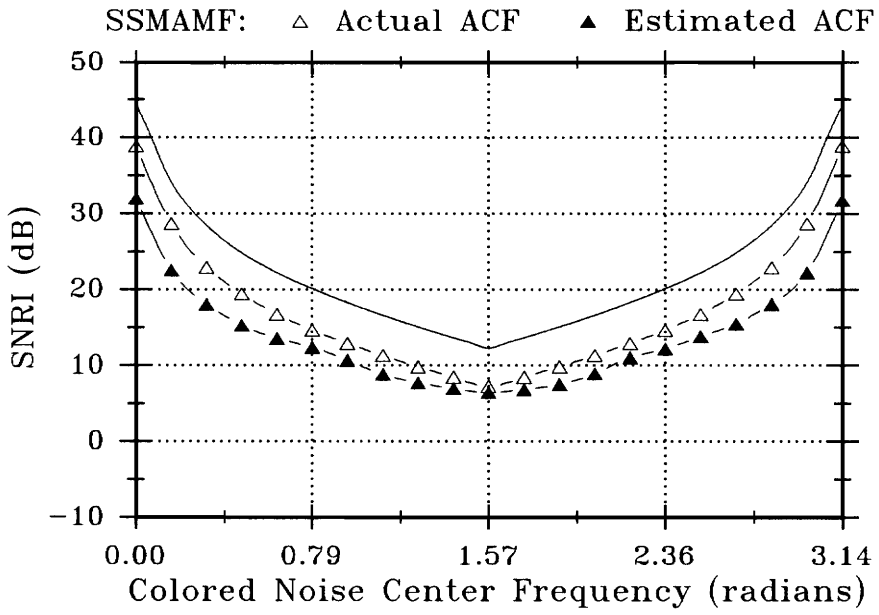

FIGURE 32: $\text{SNRI}^{\dagger}$ and $\overline{\text{SNRI}}$ of the SSMAMF using the concatenated FVMAMF ($N = 4$) optimum signals for a colored noise center frequency $\theta = \pi/2$ (#1) and $\pi/2$ (#2).

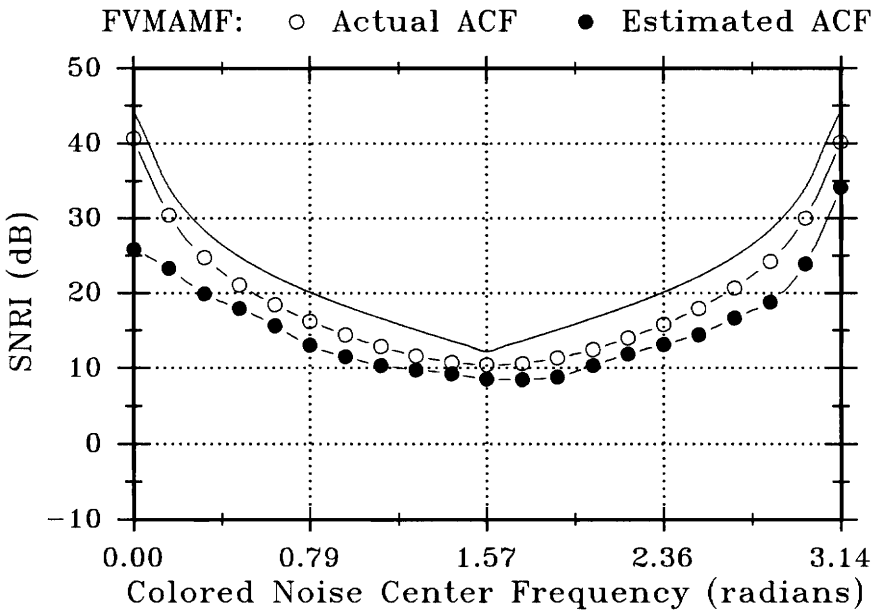

FIGURE 33: $\text{SNRI}^{\dagger}$ and $\overline{\text{SNRI}}$ of the FVMAMF using the concatenated FVMAMF ($N = 4$) optimum signals for a colored noise center frequency $\theta = \pi/4$ and $3\pi/4$.

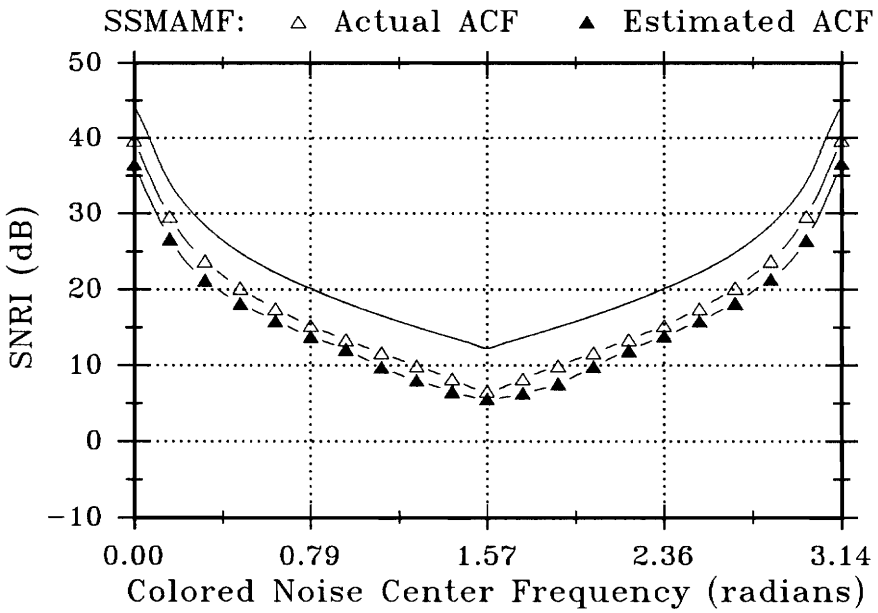

FIGURE 34: $\text{SNRI}^{\dagger}$ and $\overline{\text{SNRI}}$ of the SSMAMF using the concatenated FVMAMF ($N = 4$) optimum signals for a colored noise center frequency $\theta = \pi/4$ and $3\pi/4$.

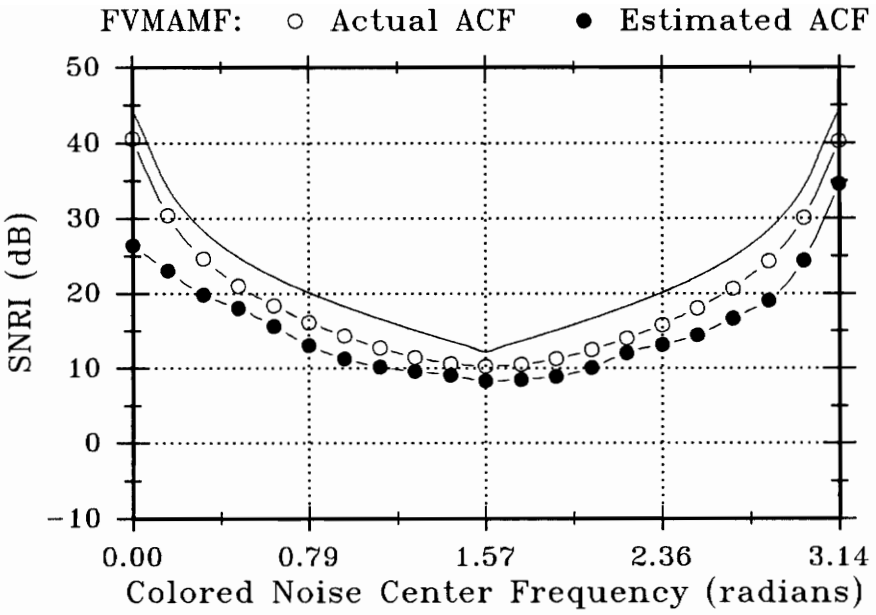

FIGURE 35: $SNRI^{\dagger}$ and $\overline{SNRI}$ of the FVMAMF using the concatenated orthogonally constrained SSMAMF ($k = 2\perp$, $M = 4$) optimum eigenvectors for a colored noise center frequency $\theta = 0$ and π.

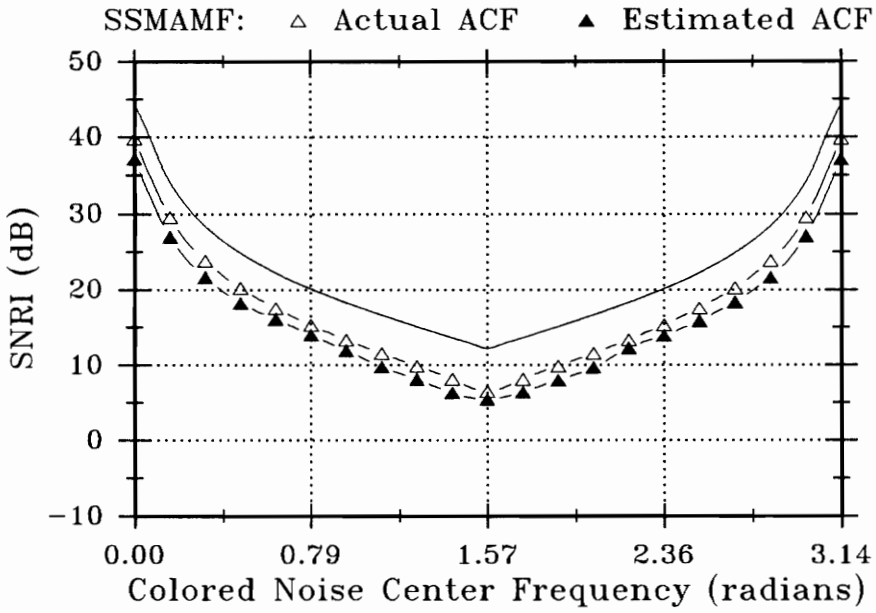

FIGURE 36: $SNRI^{\dagger}$ and $\overline{SNRI}$ of the SSMAMF using the concatenated orthogonally constrained SSMAMF ($k = 2\perp$, $M = 4$) optimum eigenvectors for a colored noise center frequency $\theta = 0$ and π.

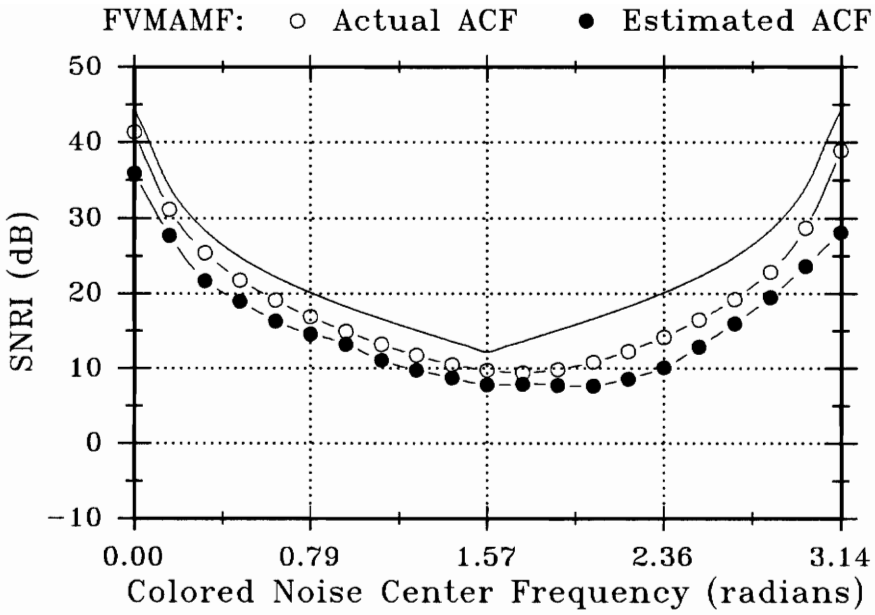

FIGURE 37: $SNRI^{\dagger}$ and $\overline{SNRI}$ of the FVMAMF using concatenated orthogonally constrained SSMAMF ($k = 2 \perp$, $M = 4$) optimum eigenvectors for a colored noise center frequency $\theta = 0$ and $\pi/2$ (#1).

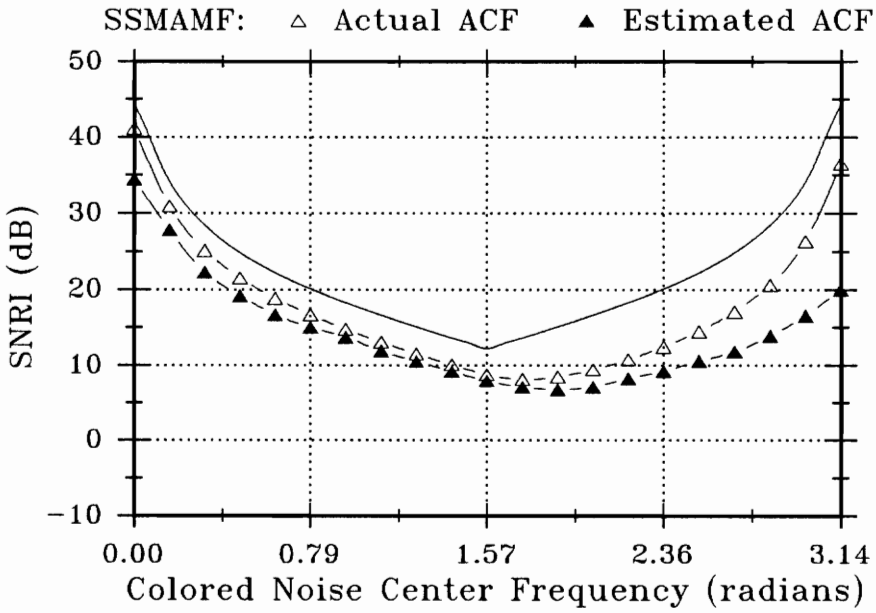

FIGURE 38: $SNRI^{\dagger}$ and $\overline{SNRI}$ of the SSMAMF using concatenated orthogonally constrained SSMAMF ($k = 2 \perp$, $M = 4$) optimum eigenvectors for a colored noise center frequency $\theta = 0$ and $\pi/2$ (#1).

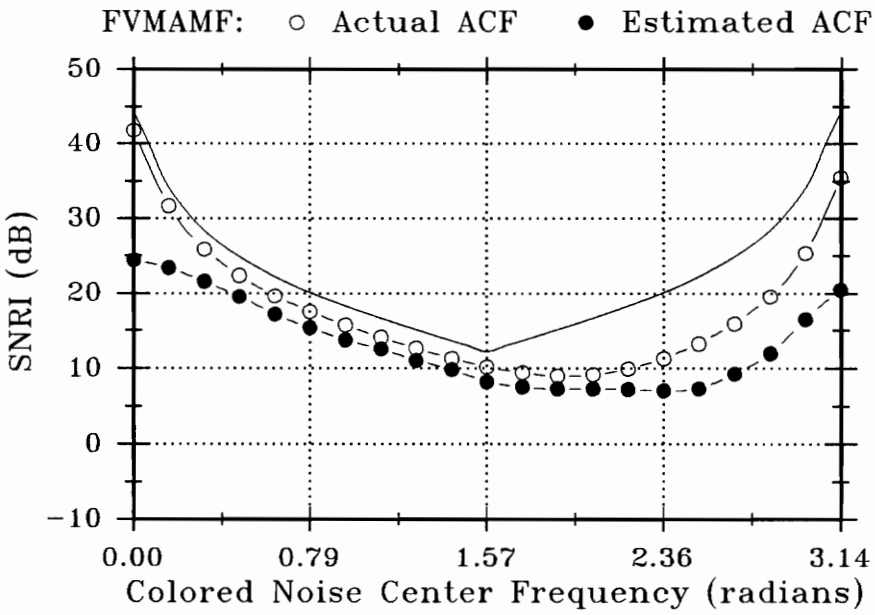

FIGURE 39: $SNRI^{\dagger}$ and $\overline{SNRI}$ of the FVMAMF using concatenated orthogonally constrained SSMAMF ($k = 2 \perp$, $M = 4$) optimum eigenvectors for a colored noise center frequency $\theta = 0$ and $\pi/2$ (#2).

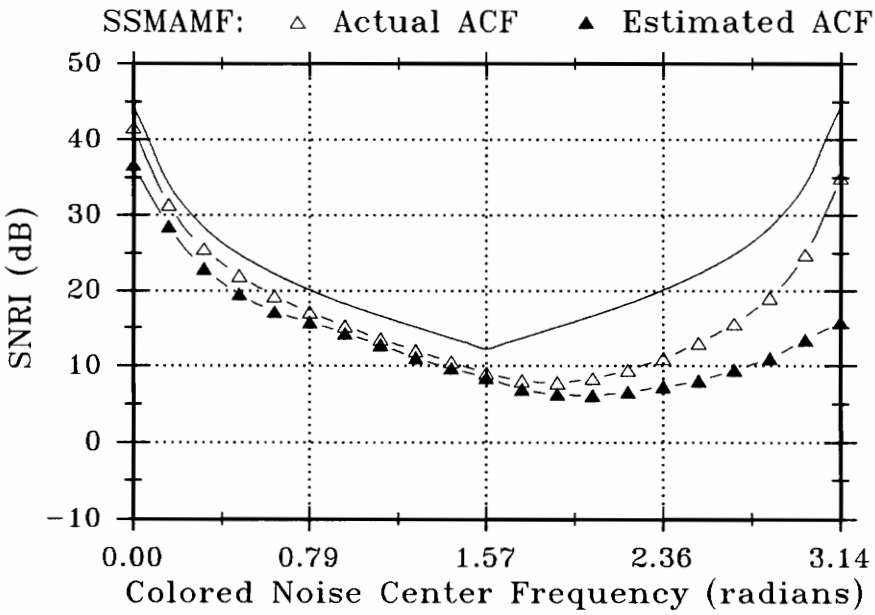

FIGURE 40: $SNRI^{\dagger}$ and $\overline{SNRI}$ of the SSMAMF using concatenated orthogonally constrained SSMAMF ($k = 2 \perp$, $M = 4$) optimum eigenvectors for a colored noise center frequency $\theta = 0$ and $\pi/2$ (#2).

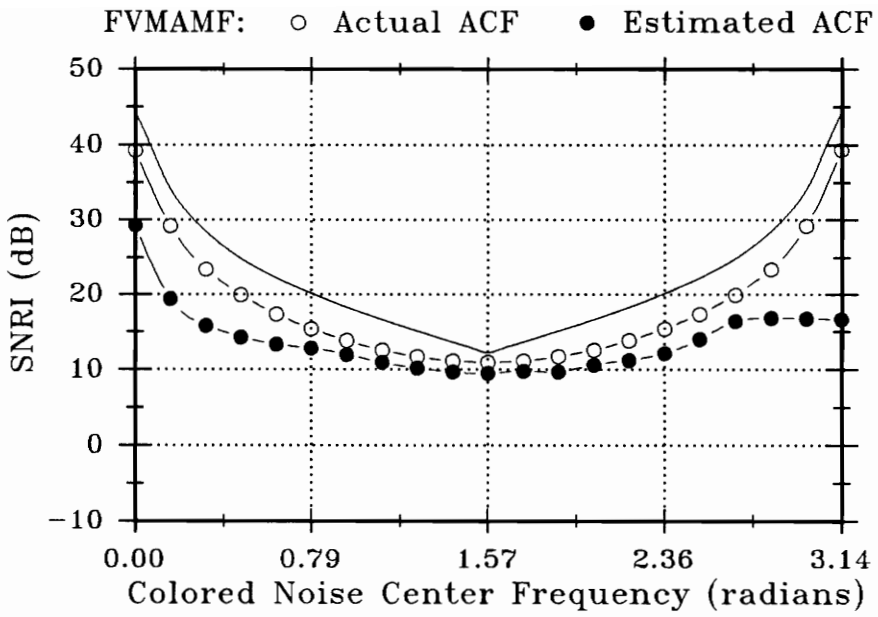

FIGURE 41: $SNRI^{\dagger}$ and $\overline{SNRI}$ of the FVMAMF using concatenated orthogonally constrained SSMAMF ($k = 2 \perp$, $M = 4$) optimum eigenvectors for a colored noise center frequency $\theta = \pi/2$ (#1) and $\pi/2$ (#2).

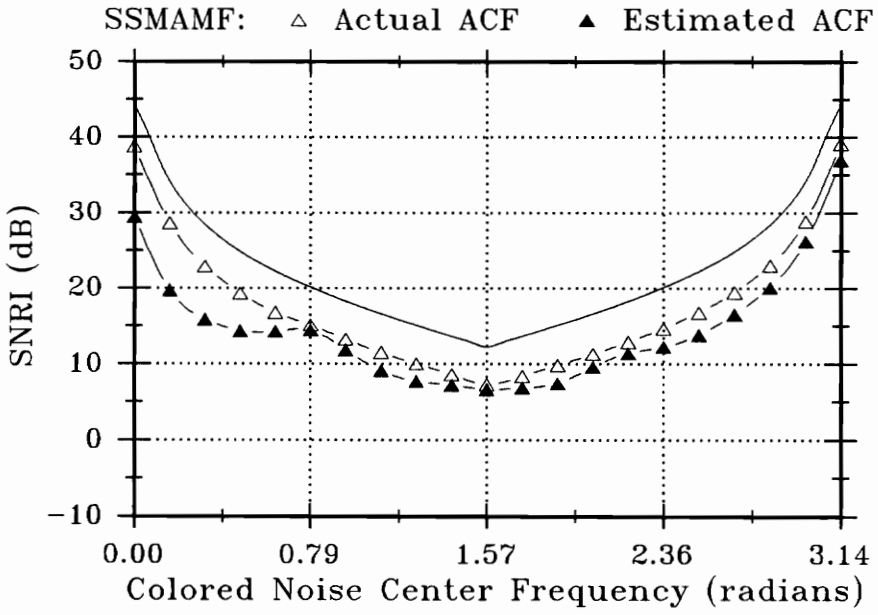

FIGURE 42: $SNRI^{\dagger}$ and $\overline{SNRI}$ of the SSMAMF using concatenated orthogonally constrained SSMAMF ($k = 2 \perp$, $M = 4$) optimum eigenvectors for a colored noise center frequency $\theta = \pi/2$ (#1) and $\pi/2$ (#2).

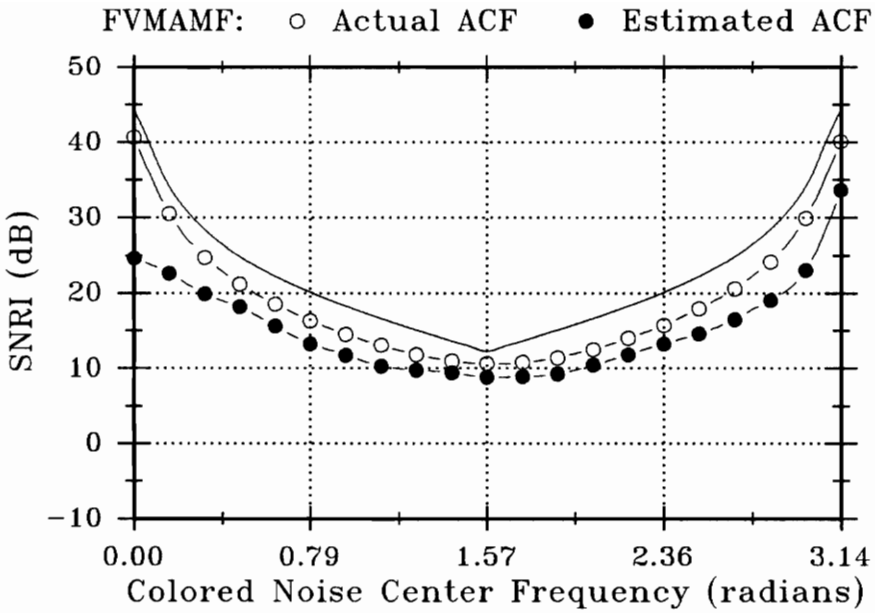

FIGURE 43: $SNRI^{\dagger}$ and $\overline{SNRI}$ of the FVMAMF using concatenated orthogonally constrained SSMAMF ($k = 2 \perp$, $M = 4$) optimum eigenvectors for a colored noise center frequency $\theta = \pi/4$ and $3\pi/4$.

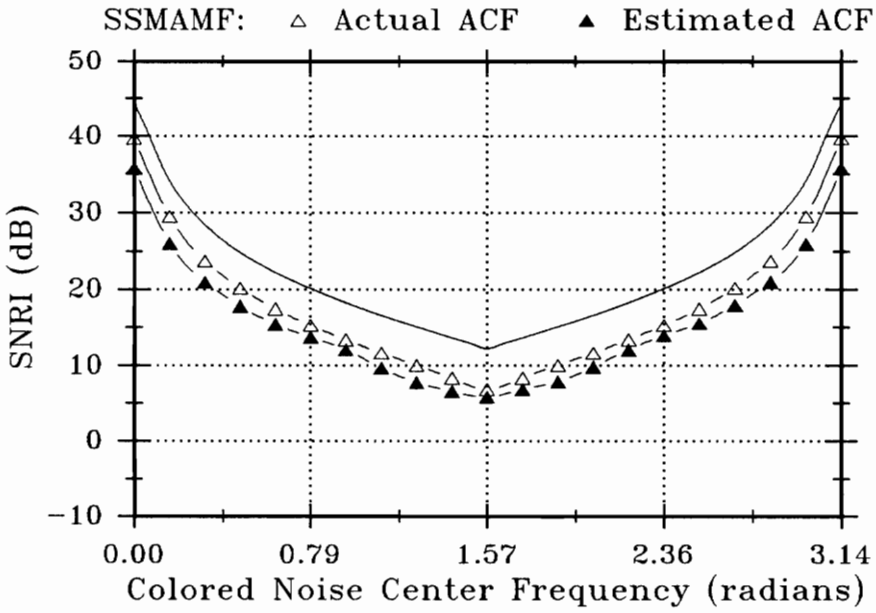

FIGURE 44: $SNRI^{\dagger}$ and $\overline{SNRI}$ of the SSMAMF using concatenated orthogonally constrained SSMAMF ($k = 2 \perp$, $M = 4$) optimum eigenvectors for a colored noise center frequency $\theta = \pi/4$ and $3\pi/4$.

4.3 "ROBUSTNESS" MEASURES

We now seek to quantify in some fashion the results seen in Figures 11-44 for somewhat easier comparison. Essentially, there are two types of robustness we would like to examine. The first is robustness against estimated noise characteristics which will involve comparing $\overline{\text{SNRI}}$ with $\text{SNRI}^{\dagger}$ for a given signal. A second item of interest is robustness against change in colored noise center frequency, or a comparison of $\overline{\text{SNRI}}$ with $\text{SNRI}^{\ddagger}$. For this second type we will compare $\overline{\text{SNRI}}$ of the FV and SSMAMF with $\text{SNRI}^{\ddagger}$ for the FVMAMF ($N = 8$) which represents the highest attainable value for either MAMF.

To assign a single number for each of these robustness measures, we compute the following differences (in dB),

$$d_{1i} = \text{SNRI}^{\dagger}(\theta_i) - \overline{\text{SNRI}}\,(\theta_i)$$

and

$$d_{2i} = \text{SNRI}^{\ddagger}(\theta_i) - \overline{\text{SNRI}}\,(\theta_i)$$

where $i = 1, \ldots, K$. For a given signal, the sample mean $\overline{d}_1$ measures the average difference between the SNRI using the actual noise ACF and the SNRI using estimated noise ACF at K discrete colored noise center frequencies. Similarly, the sample mean $\overline{d}_2$ measures the average difference between the absolute theoretical maximum SNRI of the FVMAMF ($N = 8$) and the SNRI for the given signal using estimated noise ACF at K discrete colored noise center frequencies. The K frequencies are equally spaced over $0 \leq \theta \leq \pi$, and we used a specific value of $K = 21$ (matching data presented in Figures 11-44).

The computed values of $\overline{d}_1$ and $\overline{d}_2$ and the sample standard deviations for simulations 1-17 are found in Tables IV and V respectively. The numbers are shown for each case as the average difference over the sample standard deviation. In examining the computed quantities $\overline{d}_1$ and $\overline{d}_2$, we should keep in mind that the best case scenario for these measures would be a value of 0 with 0 deviation. In such a situation, the MAMF in question would have identical performance using estimated or actual ACF (for $\overline{d}_1$) or would achieve $\text{SNRI}^{\ddagger}$ over all noise center frequencies (for $\overline{d}_2$). This is hardly likely in practice, nor is it the case in the

simulation results. However, we can search the results for the minimum values of $\overline{d}_i$ $(i = 1, 2)$ and the minimum values of the standard deviation of $\overline{d}_i$. These two are not necessarily found together for either the FV or SSMAMF (i.e. a signal generating the minimum $\overline{d}_i$ may have a large variance or vice-versa). Depending on the actual values involved, it is possible that a non-minimum value of $\overline{d}_i$ with a small variance would be preferable to the minimum value of $\overline{d}_i$ with a large variance.

Looking first at Table IV, we can see that while the FV and SSMAMF may produce comparable minimum values of $\overline{d}_1$ (~ 1.6 versus ~ 1.5 respectively), the SSMAMF stands out in simulations 8, 12, 13, and 17 with a significantly reduced value of the standard deviation ($\sigma = 0.4656$ to 0.8615) while in simulations 5-7, 10, 11, and 16 ($\sigma = 1.2150$ to 2.4419) the standard deviation is still less than or comparable to the smallest of the FVMAMF deviations ($\sigma = 2.0016$). Since the minimum average differences are roughly comparable, the reduced variance points to the SSMAMF as being more robust than the FVMAMF over the entire range of colored noise center frequencies, with respect to the practical situation where noise characteristics must be estimated from short data records. It is important to remember that $\overline{d}_1$ measures relative to the best achievable SNRI for a given signal ($\text{SNRI}^{\dagger}$) not the absolute theoretical maximum SNRI ($\text{SNRI}^{\ddagger}$). For example, "good" values of $\overline{d}_1$ do not show in any fashion whether or not the signal used yields negative values of $\overline{\text{SNRI}}$.

Table V gives us a measure ($\overline{d}_2$) of how robust the given signal is to changes in the colored noise center frequency. This quantity will yield information relating to the existence of negative $\overline{\text{SNRI}}$ values. For the FVMAMF we find the minimum value of $\overline{d}_2$ (6.8482) in simulation 4 but the smallest standard deviations in simulations 8 and 14 ($\sigma \approx 2.7$ with marginally higher values of $\overline{d}_2$). The SSMAMF once again provides smaller values of $\overline{d}_2$ and significantly smaller standard deviations. In simulations 5, 6, 8, 12, 13, and 17 we find values of $\overline{d}_2$ that are smaller or only slightly larger (~ 6.4 to 7.1) than those of the FVMAMF. The standard deviations in all cases are much smaller ($\sigma \sim 0.4$ to 1.6). The deviation indicates how well the particular SNRI curve follows the trend of the $\text{SNRI}^{\ddagger}$ curve and $\overline{d}_2$ shows how closely spaced the two curves are. From this we can say that the SSMAMF can be more robust than the FVMAMF

(under the practical situation where noise characteristics are estimated from short data records) with respect to SNRI‡. This is really quite remarkable when we consider that the SSMAMF goes into these simulations with an almost constant 4 dB lower SNRI‡ across the entire spectrum of colored noise center frequencies. If measured against its own lower SNRI‡, the minimum values of $\overline{d}_2$ would be low indeed.

Table IV: Measure $\overline{d}_1$ for Robustness when Colored Noise ACF is Estimated (shown as $\overline{d}_1$/std. dev)

Sim. #	FVMAMF	SSMAMF
1	$\frac{1.6193}{2.6274}$	$\frac{2.9140}{2.6772}$
2	$\frac{1.7772}{2.9230}$	$\frac{3.0685}{2.8623}$
3	$\frac{4.2422}{5.3500}$	$\frac{5.3965}{5.7177}$
4	$\frac{4.2744}{4.0462}$	$\frac{5.4156}{4.9412}$
5	$\frac{3.6727}{3.6976}$	$\frac{1.5458}{1.2150}$
6	$\frac{4.1097}{4.2276}$	$\frac{1.9485}{1.5916}$
7	$\frac{5.6533}{4.9842}$	$\frac{3.5406}{1.8211}$
8	$\frac{3.8081}{2.6771}$	$\frac{1.7729}{0.4656}$
9	$\frac{4.3349}{5.7318}$	$\frac{3.4774}{3.5919}$
10	$\frac{4.4479}{3.8194}$	$\frac{2.6911}{1.5731}$
11	$\frac{4.7209}{4.3868}$	$\frac{3.4270}{1.8731}$
12	$\frac{3.9715}{2.9668}$	$\frac{2.0219}{0.6367}$
13	$\frac{3.8954}{2.8240}$	$\frac{1.8488}{0.4871}$
14	$\frac{3.3617}{2.0016}$	$\frac{3.6580}{3.7512}$
15	$\frac{4.8734}{4.4845}$	$\frac{3.8859}{4.4340}$
16	$\frac{5.0914}{5.1691}$	$\frac{3.0820}{2.4419}$
17	$\frac{4.0674}{3.2953}$	$\frac{2.2365}{0.8615}$

Table V: Measure $\overline{d}_2$ for Robustness when Colored Noise ACF is Estimated (shown as $\overline{d}_2$/std. dev)

Sim. #	FVMAMF	SSMAMF
1	10.3807 / 13.5184	13.8545 / 10.7390
2	10.4678 / 13.6901	13.9059 / 10.9702
3	8.3852 / 8.7592	12.1355 / 8.4721
4	6.8482 / 4.5168	10.7019 / 5.5637
5	7.1722 / 3.9550	6.3770 / 1.2429
6	7.6733 / 4.5788	6.7428 / 1.5944
7	12.2987 / 5.1088	10.7761 / 2.3532
8	7.6168 / 2.7968	6.6968 / 0.5239
9	10.4255 / 10.5979	11.9677 / 9.6710
10	7.9878 / 4.1395	7.8336 / 1.7751
11	8.5073 / 4.7806	8.8150 / 1.9831
12	7.7037 / 3.1312	6.8977 / 0.5436
13	7.6769 / 5.8786	6.7526 / 0.4424
14	7.5795 / 2.7465	8.9356 / 5.1398
15	9.9311 / 6.0703	9.5120 / 6.6599
16	9.3354 / 5.7778	8.3816 / 2.5931
17	7.7509 / 3.4860	7.1068 / 0.7442

4.4 DISTRIBUTION OF $\overline{\text{SNRI}}$

Now that we have used the quantities $\overline{d}_1$ and $\overline{d}_2$ to help evaluate the "robustness" of the FV and SSMAMF, we need to briefly investigate the validity of the computations used. In order to do this, we will first investigate the empirical distribution of SNRI.

In computing $\overline{\text{SNRI}}$, we generate 1000 random colored noise sequences and add them to a particular signal. The computed SNRI is a random variable obeying some distribution. It is difficult to determine the theoretical distribution underlying these values since the computation involves the inverse of the noise (or linearly combined noise) correlation matrix. These values are then weighted by the signal (or linearly combined signal) and scaled by the ISNR for the system. We do know that the results are bounded above (in dB) by $\text{SNRI}^{\dagger}$ for the given signal but the lower bound is potentially $-\infty$ (in dB). Histograms are plotted for several illustrative data sets run at various colored noise center frequencies which show the variety of empirical distributions for SNRI that were observed in the simulations. The signal used in simulation 5 (see Table II) was run in both FV and SSMAMF to create the data points.

Figure 45 shows the distribution of SNRI for the SSMAMF at a colored noise center frequency $\theta = 0$. Note that this is the optimum signal for this particular colored noise. The points all lie within 2 dB of the $\text{SNRI}^{\dagger}$ for this frequency and are primarily clustered within several tenths of a dB of $\text{SNRI}^{\dagger}$ (~ 39.9 dB). The distribution is skewed left which is to be expected due to the upper bound represented by $\text{SNRI}^{\dagger}$. In general it was observed, from this and other similar sets, that the empirical distribution was "tight" when noise for which the optimum signal was selected was actually used in the simulation.

In Figure 46 we used noise with a colored noise center frequency $\theta = 3\pi/8$ with the SSMAMF. Here we see what looks to be a multi-modal distribution with one mode located at ~ 0 dB and the other at ~ 10 dB. Both appear to be one-sided distributions skewed to the left.

Figures 47 and 48 are plots of the histograms for the SNRI data of the SSMAMF using colored noise with a center frequency of $\theta = \pi/2$ and $5\pi/8$

respectively. Both distributions appear as one-sided distributions which are again skewed left although Figure 48 has greater spread in the data than Figure 47 (range ~ -3.7 dB to $\sim +10.9$ dB versus ~ -3.2 dB to $\sim +6.5$ dB).

We selected the data for the histograms in Figures 49 and 50 from the FVMAMF where the colored noise possessed a center frequency of $\theta = 0$ (Figure 49) and $\theta = \pi$ (Figure 50). The distribution of Figure 49 appears to be two-sided and skewed left while Figure 50 is two-sided but skewed less to the left ($\sim$ symmetric).

Since the SNRI is bounded above, it is fairly apparent that SNRI does not follow a Gaussian distribution. In fact, several of the figures (i.e. 46, 47 and 48) are not even two-sided. This brings to light the problem in computing the sample mean and sample standard deviation. Both of these estimators (for location and scale) are derived under the assumption that the underlying distribution of the data is Gaussian. Their performance using data drawn from some other distribution may produce results which are highly suspect as to their validity. In Figures 9-44 where we plot $\overline{\text{SNRI}}$ against colored noise center frequency, we may be creating values which are not truly representative of the data depending on the actual distribution of the data at that frequency. Since we are using a large number of data points to generate the average and since there are no points heading towards $-\infty$, we believe the results to be reasonably accurate.

More importantly, the standard deviation computed in Tables IV and V should only be used as a relative measure of comparison between the FV and SSMAMF (or in comparing one set of results for the SSMAMF with another set, etc.). It should be fairly obvious that the difference cannot be less than 0 dB. Considering simulation 1 for the FVMAMF (Table V) we can see the indicated problem since the mean difference is 10.3807 with a standard deviation σ=13.5184. Under the Gaussian assumption this would imply that $\approx 35\%$ of the data lies outside $\pm\sigma$ of the mean and $\approx 5\%$ of the data lies outside $\pm 3\sigma$ of the mean. This cannot apply to this situation since either condition claims significant probability of a negative difference occurring, a situation which cannot possibly happen. To reiterate, the standard deviations presented in Tables IV and V should only be used as a rough relative measure of comparison between the two data sets.

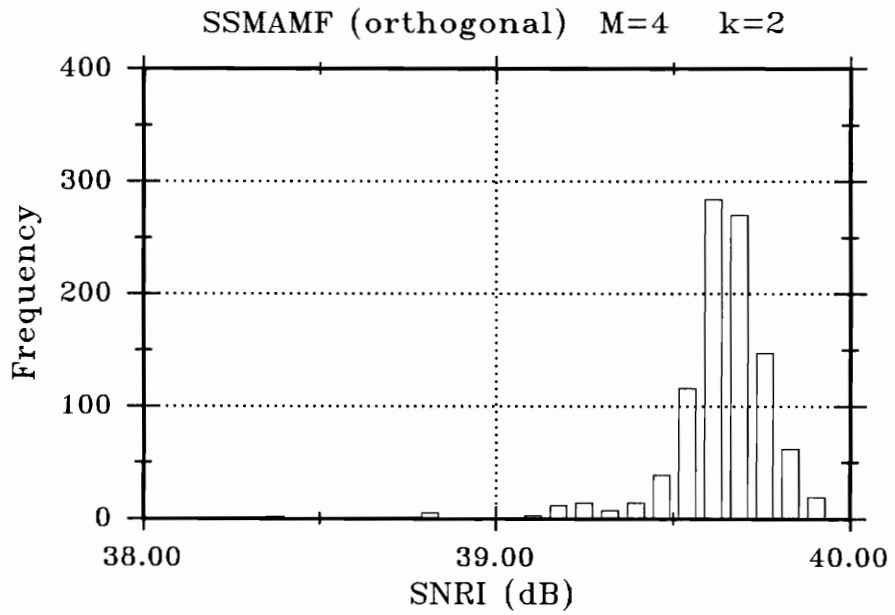

FIGURE 45: Histogram of SNRI data for SSMAMF run with colored noise having a center frequency $\theta = 0$. Signal was optimum for SSMAMF at $\theta = 0$.

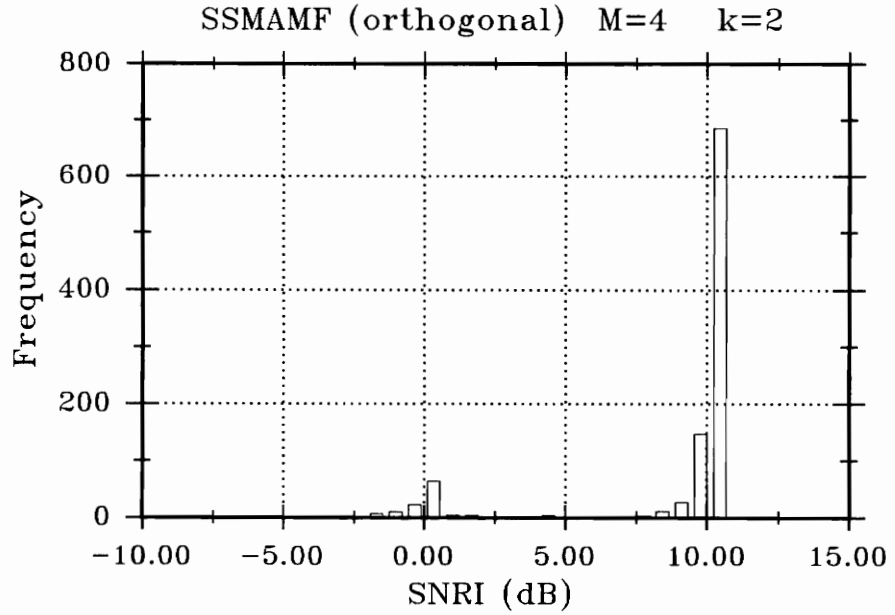

FIGURE 46: Histogram of SNRI data for SSMAMF run with colored noise having a center frequency $\theta = 3\pi/8$. Signal was optimum for SSMAMF at $\theta = 0$.

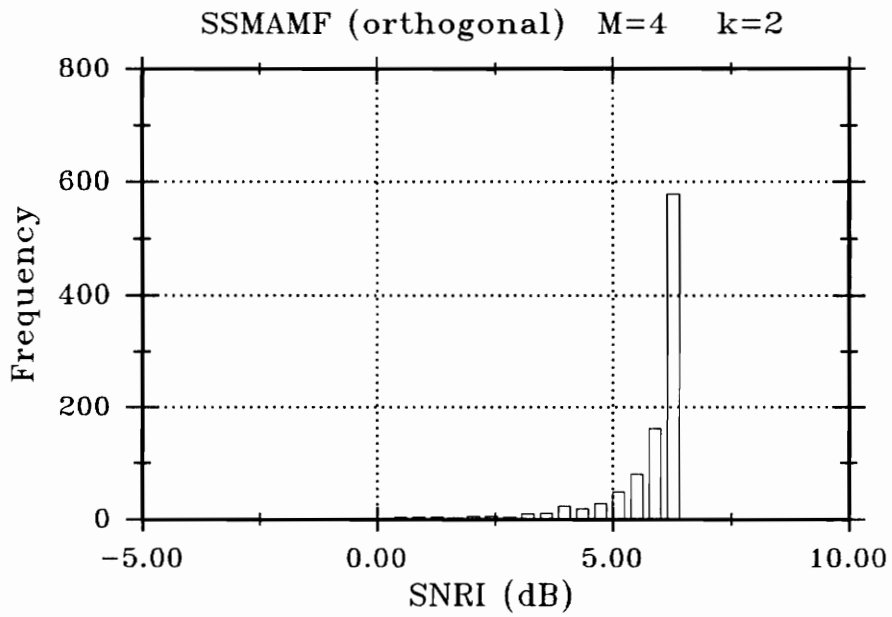

FIGURE 47: Histogram of SNRI data for SSMAMF run with colored noise having a center frequency $\theta = \pi/2$. Signal was optimum for SSMAMF at $\theta = 0$.

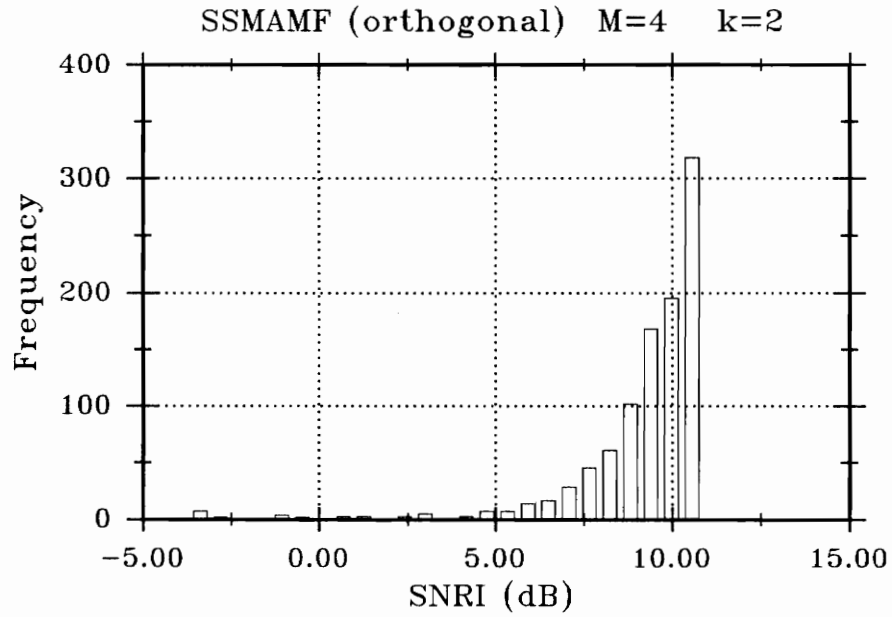

FIGURE 48: Histogram of SNRI data for SSMAMF run with colored noise having a center frequency $\theta = 5\pi/8$. Signal was optimum for SSMAMF at $\theta = 0$.

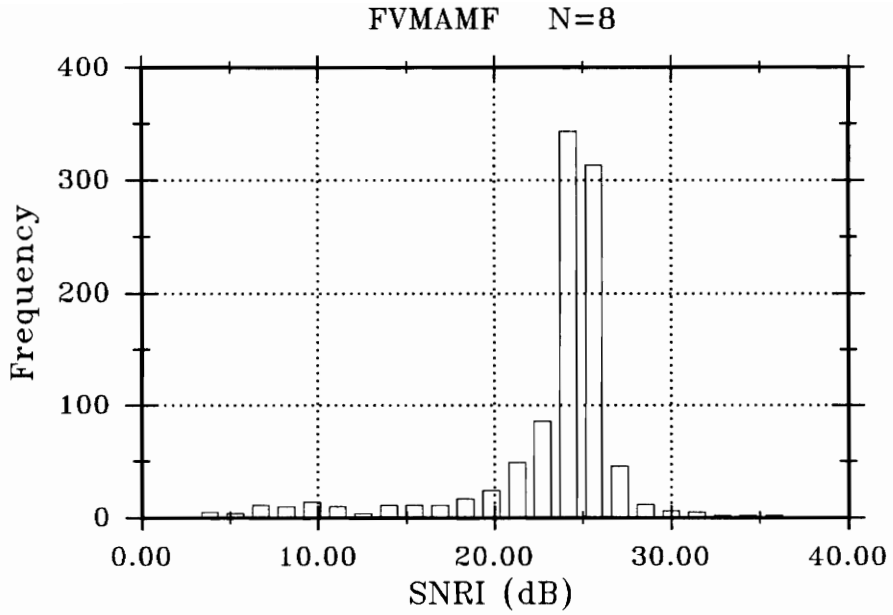

FIGURE 49: Histogram of SNRI data for FVMAMF run with colored noise having a center frequency $\theta = 0$. Signal was optimum for SSMAMF at $\theta = 0$.

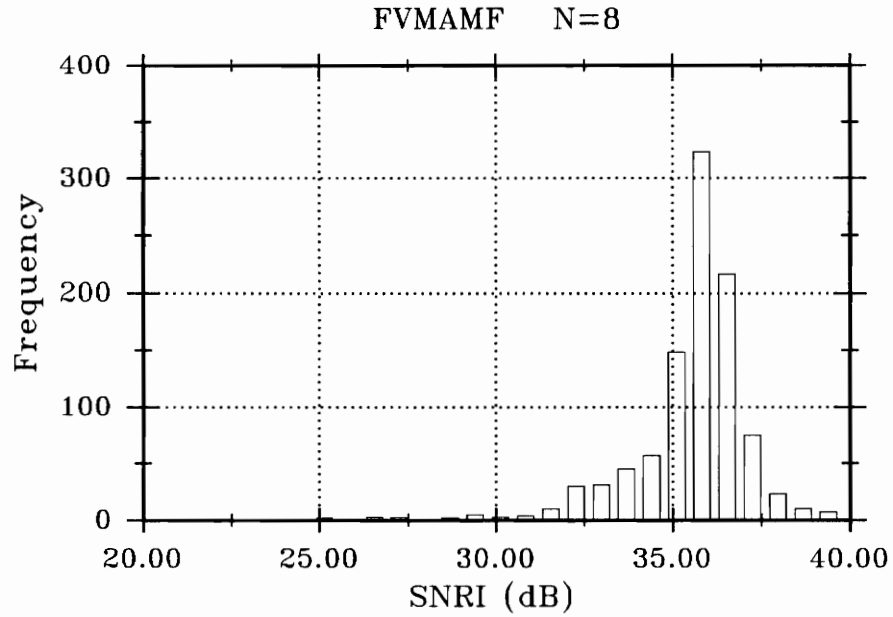

FIGURE 50: Histogram of SNRI data for SSMAMF run with colored noise having a center frequency $\theta = \pi$. Signal was optimum for SSMAMF at $\theta = 0$.

4.5 VERIFICATION OF MULTIVARIATE ML DETECTION SCHEME

In this section we verify the performance of the detection scheme presented earlier in §2.7, by running the SSMAMF communication system with the colored noise center frequency θ remaining at 0. Similar results for the FVMAMF were obtained but not included as they followed exactly the same trends and did not change the discussion in any fashion.

The first trial uses the optimal binary case ($\underline{s}_1 = -\underline{s}_0$) with the signal vector chosen to optimize the SSMAMF at a colored noise center frequency of 0 (Table II, simulation 5),

$$\underline{s}_0 = \begin{bmatrix} 0.34506 & 0.0 & 0.93858 & 0.0 & 0.0 & 0.93858 & 0.0 & 0.34506 \end{bmatrix}^T$$

Bit errors were generated for 5000 randomly transmitted symbols at an ISNR $= -40$dB using two different correlation estimators; a) Classical biased method; b) Burg method. The results are normalized to errors/1000 bits and are shown in Tables II-III. They confirm that the detection method of §2.7 and the detection method derived specifically for the optimal binary case [5] produce identical results under these conditions and that the results are comparable regardless of which estimator is used with errors $\sim$ balanced between symbols.

Table VI: Optimal Binary Detection Using Optimal Binary Detector [5]

CB Estimator			Burg Estimator		
Transmission Errors Made on:			Transmission Errors Made on:		
0's	1's	Total	0's	1's	Total
83.4	82.6	166	86	79.4	165.4

Table VII: Optimal Binary Detection Using General MA Detector

CB Estimator			Burg Estimator		
Transmission Errors Made on:			Transmission Errors Made on:		
0's	1's	Total	0's	1's	Total
83.4	82.6	166	86	79.4	165.4

In the second trial we chose signals which would not result in the optimal binary setup. The signal representing a "0" was that which optimized the FVMAMF system at $\theta = 0$ and the signal representing a "1" was chosen as that which optimized the SSMAMF system at $\theta = \pi/2$, i.e.

$$\underline{s}_0 = \begin{bmatrix} -0.09801 & 0.34705 & -0.59227 & 0.72054 & -0.72054 & 0.59227 & -0.34705 & 0.09801 \end{bmatrix}^T$$

$$\underline{s}_1 = \begin{bmatrix} 0.99617 & 0.0 & 0.0 & 0.08739 & 0.0 & 0.08739 & 0.99617 & 0.0 \end{bmatrix}^T$$

Bit errors were generated for 2500 randomly transmitted symbols at an ISNR $= -30$dB, again using the two estimators listed above. Results are normalized to errors/1000 bits transmitted and shown in Tables IV-V. These indicate that the detection scheme presented in this work can produce significantly fewer errors using the Burg estimator, yet this method and the optimal binary detector [5] yield comparable total errors using the classical biased estimator. Note that even though the total errors using the classical biased estimator are comparable, the new scheme produces balanced errors between the two symbols while the old method does not.

Table VIII: Non-Optimal Binary Detection Using Optimal Binary Detector [5]

CB Estimator			Burg Estimator		
Transmission Errors Made on:			Transmission Errors Made on:		
0's	1's	Total	0's	1's	Total
54.4	30	84.4	26.4	7.6	32

Table IX: Non-Optimal Binary Detection Using General MA Detector

CB Estimator			Burg Estimator		
Transmission Errors Made on:			Transmission Errors Made on:		
0's	1's	Total	0's	1's	Total
44.8	41.2	86	10	10.4	20.4

5.0 CONCLUSIONS AND RECOMMENDATIONS

We have presented a general development for the design of three stage MAMF receivers as well as a detection scheme which is applicable to a bank of L linear pre-filter and MAMF sections. We chose to create our transmitted signal vectors from k linearly independent partitions of length M (transmitted vector of length $N = k \times M$) in order to effectively transmit a k-dimensional subspace of the original M-dimensional signal subspace. At the receiver we apply a specific pre-filter which linearly combines these k partitions in order to maximize the OSNR of the MAMF (SSMAMF). The process of linearly combining the partitions results in a receiver system which can adapt the received signal in response to changes in the channel noise environment. This was contrasted with a receiver system (FVMAMF) which used a pre-filter defined as a unity gain, i.e. transmits a 1-dimensional subspace of the original N-dimensional signal subspace.

The reduction in the dimension of the original signal subspace for the SSMAMF through the partitioning of the transmitted signal vector yields absolute maximum SNRI ($\text{SNRI}^{\ddagger}$) which is lower by a significant amount than that of the FVMAMF (≈ 4 dB in the case of additive narrowband channel noise). $\text{SNRI}^{\ddagger}$ for both systems was demonstrated to increase with the increasing dimension of the MAMF and the SSMAMF was also shown to produce a decrease in $\text{SNRI}^{\ddagger}$ with an increasing number of partitions in the transmitted signal vector for a fixed length MAMF.

We presented methods by which optimum signal vectors for a particular type of colored noise could be generated for use in simulation of both FV and SSMAMF receivers. It was also demonstrated that the SSMAMF could utilize the columns of its signal matrix to provide optimum solutions to k arbitrary noise conditions.

Several alternatives were given to maximize the function approximating the OSNR of the SSMAMF. The gradient based approach proved to be the most accurate; it requires a decent initial guess for the combination coefficients. The gradient based approach requires a significant amount of computation when compared to the brute force approach in the 2-dimensional case simulated (approximately 3 or 4 times) but this may be reduced by numerically approximating the necessary derivatives. In higher dimensional versions of the SSMAMF, a brute force computation is hardly feasible and the usefulness of the gradient method should become more apparent.

The FV and SSMAMF were simulated to provide information as to their performance in terms of SNRI relative to one another. Optimum signals for a variety of narrowband colored noise conditions were used in both FV and SSMAMF and the SNRI and $\overline{\text{SNRI}}$ were computed across the spectrum of narrowband colored noise center frequencies. This yielded information on the system performance when the characteristics of the noise changed. The FVMAMF demonstrated superior performance for a particular colored noise center frequency when using its optimum signal vector for that location. It was observed that the performance degraded drastically in some cases when the noise center frequency was shifted, indicating that the FVMAMF was not particularly robust with respect to changing noise. In no case did the FVMAMF maintain a close and nearly constant relationship with its $\text{SNRI}^{\ddagger}$ curve. The SSMAMF when optimized for a particular colored noise, could maintain a reasonably constant relationship with little variation relative to $\text{SNRI}^{\ddagger}$ over all center frequencies. The average difference measures $\overline{d}_1$ and $\overline{d}_2$, as well as examination of the SNRI curves, showed that for several different transmitted signal vectors the SSMAMF produced more robust responses to the changing noise environment than the FVMAMF.

The SSMAMF was also demonstrated to produce robust performance with much smaller variance than the FVMAMF using the multiple optimization capability. It was seen that the process of linearly combining the transmitted signal partitions did achieve the locally optimum solution for the selected partitions in the case where actual knowledge of the noise ACF was assumed. It appeared that this solution held, even when estimating the noise ACF, as

evidenced by the SNRI plots which tended to approach $SNRI^{\ddagger}$ more closely at the multiple optimization points. More investigation is needed to confirm or deny the latter contention, perhaps with scatter plots of the coefficients at the solution to the maximization process.

We examined the distribution of SNRI when the colored noise ACF was estimated. Using histograms we saw that the empirical distributions, which are bounded above by the value of $SNRI^{\dagger}$, showed a variety of trends. The distribution at the center frequency for which the signal was selected was narrowly concentrated near $SNRI^{\dagger}$ (which equals $SNRI^{\ddagger}$ at this point). As we move farther away from the optimization center frequency, the distributions could be one-sided, two-sided (symmetric or non-symmetric), or even multi-modal. This makes the sample mean and sample standard deviations less representative as estimators of scale and location. The estimate of scale is of particular importance since it measures the spread of the SNRI data and we were unable to make a comparison (other than the few histograms) in this regard. Other methods of estimating these quantities should be pursued in order to allow a more accurate comparison between the FV and the SSMAMF (or the FV and the FVMAMF using different signal vectors, or the SSMAMF and the SSMAMF using different signal vectors).

The multivariate maximum likelihood detection method for an arbitrary bank of pre-filter and MA sections was verified against the optimal binary detector of [5] in the optimal binary communication case. It was shown to outperform the optimal binary detector when the optimal binary condition did not hold. The performance was demonstrated to be also dependent on the method of estimating the noise correlation. This is believed to be due to the fact that the Burg estimator imposes a structure on the correlation, by assuming a noise model, while the classical biased estimator merely acts on the noise samples. Certainly, the detector performance should be evaluated in cases where more than two signals may be transmitted since this is where it would be most valuable.

In general, the SSMAMF provides more robust response to changing narrowband noise environments than the FVMAMF when noise characteristics are estimated from short records. It adds computational complexity relative to the straighforward design of the FVMAMF but provides for adaptation of the signal to the existing channel noise conditions. This added complexity is significant in

the case of only two partitions, as used in our simulations, but it should not increase drastically for additional partitions when the gradient method is used in maximizing the approximation to the OSNR function. Since SNRI relates to the bit errors made in transmission [5], a SNRI response which maintains a closer relationship to $SNRI^{\ddagger}$ over the entire spectrum of colored noise center frequencies would provide more robust (better average) bit error rates as the noise environment changes. The SSMAMF and the multiple optimization of the SSMAMF need to be evaluated in more complex noise environments (i.e. multi-tone, ARMA generated colored noise).

In addition, since we have presented the development in terms of a general three stage receiver, there is an infinity of possible pre-filters which could be used in place of the linear combination process. A logical extension of this work would be to identify in some fashion a pre-filter that would produce robust SNRI results given some criterion of optimality. Another possibility is to have available a variety of pre-filters which could, for example, be developed for different noise environments and require a switching operation at the receiver based on estimated noise characteristics existing at a particular time. This was given a cursory examination for the FV and SSMAMF systems [5] with some success, but additional work remains.

APPENDIX

The appendix is intended to provide easy reference for various equations relating to the FV and/or SSMAMF systems. Specifically, Appendix A provides the equations with which we can design and characterize the performance of both MAMF systems. Appendix B summarizes the partial derivative expressions required in maximizing the OSNR of the SSMAMF using the Gradient method. Appendix C details the multivariate Gaussian density functions for use in the MAP detection scheme.

Appendix A - FV and SSMAMF Equations

FVMAMF

The FVMAMF has a pre-filtering section which is defined to be unity gain. Thus, the following relationships hold

$$\tilde{\underline{s}}_{FV,i} = \underline{s}_{FV,i} \tag{A.1}$$

$$\tilde{\underline{w}}_{FV} = \underline{w}_{FV} \tag{A.2}$$

Therefore, the pre-filtered noise correlation matrix $\widehat{R}_{\tilde{w}\tilde{w}} = \widehat{R}_{ww}$. The filter is designed for estimated noise conditions using

$$\underline{\widehat{h}}_{FV} = \widehat{R}_{ww}^{-1} \underline{s}_{FV,i} \tag{A.3}$$

We can rewrite the OSNR of (2.38) which assumes an estimated noise correlation

$$\widehat{\text{OSNR}}_{FV} = \frac{\left(\underline{s}_{FV,i}^{\text{T}} \widehat{R}_{ww}^{-1} \underline{s}_{FV,i} \right)^2}{\underline{s}_{FV,i}^{\text{T}} \widehat{R}_{ww}^{-1} R_{ww} \widehat{R}_{ww}^{-1} \underline{s}_{FV,i}} \tag{A.4}$$

The SNRI of the FVMAMF would be

$$\widehat{\text{SNRI}}_{FV} = \frac{\widehat{\text{OSNR}}_{FV}}{\frac{E}{r_{ww,0}}} \tag{A.5}$$

E represents the total energy of the transmitted signal. Note that if $\widehat{R}_{ww} = R_{ww}$ (A.4) reduces to

$$\text{OSNR}_{FV}^{\dagger} = \underline{s}_{FV,i}^{\text{T}} R_{ww}^{-1} \underline{s}_{FV,i} \tag{A.6}$$

where † denotes optimum. Equation (A.5) becomes

$$\mathrm{SNRI}_{FV}^{\dagger} = \frac{\underline{s}_{FV,i}^{\mathrm{T}} R_{ww}^{-1} \underline{s}_{FV,i}}{\frac{E}{r_{ww,0}}} \tag{A.7}$$

SSMAMF

The SSMAMF has a pre-filtering section that performs the process of linearly combining the received signal in noise. Thus, the following relationships hold from §2.5.1 and §2.5.2

$$\underset{i}{\tilde{\underline{s}}} = S_i \underline{c} \tag{A.8}$$

$$\underline{\tilde{w}} = W \underline{c} \tag{A.9}$$

The filter is designed under estimated noise conditions from

$$\underline{\hat{h}}_{SS} = \hat{R}_{\tilde{w}\tilde{w}}^{-1} \underline{\tilde{s}}_{SS,i} \tag{A.10}$$

The energy constraint for the linearly combined signal $\underline{\tilde{s}}$ is,

$$\underline{c}^{\mathrm{T}} S_i^{\mathrm{T}} S_i \underline{c} = E \tag{A.11}$$

We found in §2.5.2 that the linearly combined noise correlation sequence is

$$r_{\tilde{w}\tilde{w},n} = \sum_{q=0}^{k-1} c_q \sum_{s=0}^{k-1} c_s r_{ww,\, n+M(q-s)}$$

$$= \underline{c}^{\mathrm{T}} W_r \underline{c} \qquad 0 \leq n \leq M-1 \tag{A.12}$$

The noise was shown to be reflection invariant in §2.5.2,

$$r_{\tilde{w}\tilde{w},n} = r_{\tilde{w}\tilde{w},-n} \tag{A.13}$$

The output signal-to-noise ratio of the SSMAMF for estimated noise conditions is

$$\begin{aligned} \widehat{\mathrm{OSNR}}_{SS} &= \frac{\left(\underline{\tilde{s}}_{SS,i}^{\mathrm{T}} \widehat{R}_{\tilde{w}\tilde{w}}^{-1} \underline{\tilde{s}}_{SS,i}\right)^2}{\underline{\tilde{s}}_{SS,i}^{\mathrm{T}} \widehat{R}_{\tilde{w}\tilde{w}}^{-1} R_{\tilde{w}\tilde{w}} \widehat{R}_{\tilde{w}\tilde{w}}^{-1} \underline{\tilde{s}}_{SS,i}} \\ &= \frac{\left(\underline{c}^{\mathrm{T}} S_i^{\mathrm{T}} \widehat{R}_{\tilde{w}\tilde{w}}^{-1} S_i \underline{c}\right)^2}{\underline{c}^{\mathrm{T}} S_i^{\mathrm{T}} \widehat{R}_{\tilde{w}\tilde{w}}^{-1} R_{\tilde{w}\tilde{w}} \widehat{R}_{\tilde{w}\tilde{w}}^{-1} S_i \underline{c}} \end{aligned} \tag{A.14}$$

The SNRI of the SSMAMF would be

$$\widehat{\mathrm{SNRI}}_{SS} = \frac{\widehat{\mathrm{OSNR}}_{SS}}{\frac{E}{r_{ww,0}}} \tag{A.15}$$

Note that if $\widehat{R}_{\tilde{w}\tilde{w}} = R_{\tilde{w}\tilde{w}}$ (A.14) reduces to

$$\mathrm{OSNR}_{SS}^{\dagger} = \underline{c}^{\mathrm{T}} S_i^{\mathrm{T}} R_{\tilde{w}\tilde{w}}^{-1} S_i \underline{c} \tag{A.16}$$

and (A.15) becomes

$$\mathrm{SNRI}_{SS}^{\dagger} = \frac{\underline{c}^{\mathrm{T}} S_i^{\mathrm{T}} R_{\tilde{w}\tilde{w}}^{-1} S_i \underline{c}}{\frac{E}{r_{ww,0}}} \tag{A.17}$$

Appendix B - Derivative Terms for Gradient Algorithm

We defined in §2.6.3 an augmented function (2.63) for which we seek the maximum

$$G(\underline{c}) = \underline{c}^{\mathrm{T}} S_l^{\mathrm{T}} \hat{R}_{\tilde{w}\tilde{w}}^{-1} S_l \underline{c} + \lambda(\underline{c}^{\mathrm{T}} S_l^{\mathrm{T}} S_l \underline{c} - E) \tag{B.1}$$

which can be rewritten as

$$G(\underline{c}) = \underline{c}^{\mathrm{T}} S_l^{\mathrm{T}} \left(\hat{R}_{\tilde{w}\tilde{w}}^{-1} + \lambda \cdot \mathbf{I} \right) S_l \underline{c} - \lambda E \tag{B.2}$$

Taking the first derivative of (B.2) with respect to the coefficient c_i $(i = 0, 1, \ldots, k-1)$

$$\frac{\partial}{\partial c_i} G(\underline{c}) = g_1(\underline{c}) + g_2(\underline{c}) + g_3(\underline{c}) \tag{B.3}$$

where

$$g_1(\underline{c}) = \left(\frac{\partial}{\partial c_i} \underline{c}^{\mathrm{T}} \right) S_l^{\mathrm{T}} \left(\hat{R}_{\tilde{w}\tilde{w}}^{-1} + \lambda \cdot \mathbf{I} \right) S_l \underline{c} \tag{B.4}$$

$$g_2(\underline{c}) = \underline{c}^{\mathrm{T}} S_l^{\mathrm{T}} \left(\frac{\partial}{\partial c_i} \hat{R}_{\tilde{w}\tilde{w}}^{-1} \right) S_l \underline{c} \tag{B.5}$$

$$g_3(\underline{c}) = \underline{c}^{\mathrm{T}} S_l^{\mathrm{T}} \left(\hat{R}_{\tilde{w}\tilde{w}}^{-1} + \lambda \cdot \mathbf{I} \right) S_l \left(\frac{\partial}{\partial c_i} \underline{c} \right) \tag{B.6}$$

We observe that $g_1(\underline{c})$ and $g_3(\underline{c})$ are each others transpose. Since both terms are scalar valued, and the transpose of a scalar value is just that scalar value, we need only evaluate two of the derivative terms in (B.3). The first derivative term involving λ yields the coefficient constraint

$$\frac{\partial}{\partial \lambda} G(\underline{c}) = \underline{c}^{\mathrm{T}} S_l^{\mathrm{T}} S_l \underline{c} - E \tag{B.7}$$

The second partial of (B.2) with respect to the combination coefficients is

$$\frac{\partial^2}{\partial c_j \partial c_i} G(\underline{c}) = \frac{\partial}{\partial c_j} g_1(\underline{c}) + \frac{\partial}{\partial c_j} g_2(\underline{c}) + \frac{\partial}{\partial c_j} g_3(\underline{c}) \tag{B.8}$$

where:

$$\frac{\partial}{\partial c_j} g_1(\underline{c}) = \left(\frac{\partial^2}{\partial c_j \partial c_i} \underline{c}^{\mathrm{T}}\right) S_l^{\mathrm{T}} \left(\widehat{R}_{\tilde{w}\tilde{w}}^{-1} + \lambda \cdot \mathbf{I}\right) S_l \underline{c} + \left(\frac{\partial}{\partial c_i} \underline{c}^{\mathrm{T}}\right) S_l^{\mathrm{T}} \left(\frac{\partial}{\partial c_j} \widehat{R}_{\tilde{w}\tilde{w}}^{-1}\right) S_l \underline{c}$$

$$+ \left(\frac{\partial}{\partial c_i} \underline{c}^{\mathrm{T}}\right) S_l^{\mathrm{T}} \left(\widehat{R}_{\tilde{w}\tilde{w}}^{-1} + \lambda \cdot \mathbf{I}\right) S_l \left(\frac{\partial}{\partial c_j} \underline{c}\right) \tag{B.9}$$

$$\frac{\partial}{\partial c_j} g_2(\underline{c}) = \left(\frac{\partial}{\partial c_j} \underline{c}^{\mathrm{T}}\right) S_l^{\mathrm{T}} \left(\frac{\partial}{\partial c_i} \widehat{R}_{\tilde{w}\tilde{w}}^{-1}\right) S_l \underline{c} + \underline{c}^{\mathrm{T}} S_l^{\mathrm{T}} \left(\frac{\partial^2}{\partial c_j \partial c_i} \widehat{R}_{\tilde{w}\tilde{w}}^{-1}\right) S_l \underline{c}$$

$$+ \underline{c}^{\mathrm{T}} S_l^{\mathrm{T}} \left(\frac{\partial}{\partial c_i} \widehat{R}_{\tilde{w}\tilde{w}}^{-1}\right) S_l \left(\frac{\partial}{\partial c_j} \underline{c}\right) \tag{B.10}$$

$$\frac{\partial}{\partial c_j} g_3(\underline{c}) = \left(\frac{\partial}{\partial c_j} \underline{c}^{\mathrm{T}}\right) S_l^{\mathrm{T}} \left(\widehat{R}_{\tilde{w}\tilde{w}}^{-1} + \lambda \cdot \mathbf{I}\right) S_l \left(\frac{\partial}{\partial c_i} \underline{c}\right) + \underline{c}^{\mathrm{T}} S_l^{\mathrm{T}} \left(\frac{\partial}{\partial c_j} \widehat{R}_{\tilde{w}\tilde{w}}^{-1}\right) S_l \left(\frac{\partial}{\partial c_i} \underline{c}\right)$$

$$+ \underline{c}^{\mathrm{T}} S_l^{\mathrm{T}} \left(\widehat{R}_{\tilde{w}\tilde{w}}^{-1} + \lambda \cdot \mathbf{I}\right) S_l \left(\frac{\partial^2}{\partial c_j \partial c_i} \underline{c}\right) \tag{B.11}$$

Again observe the transpose of scalar values in (B.9) and (B.11). The second partials involving λ are

$$\frac{\partial}{\partial c_i \partial \lambda} G(\underline{c}) = \left(\frac{\partial}{\partial c_i} \underline{c}^{\mathrm{T}}\right) S_l^{\mathrm{T}} S_l \underline{c} + \underline{c}^{\mathrm{T}} S_l^{\mathrm{T}} S_l \left(\frac{\partial}{\partial c_i} \underline{c}\right) \tag{B.12}$$

$$\frac{\partial^2}{\partial \lambda^2} G(\underline{c}) = 0 \tag{B.13}$$

The derivative terms required in the above expressions are

a) $\frac{\partial}{\partial c_i}\underline{c}$

The form of the coefficient vector is,

$$\underline{c} = \begin{bmatrix} c_0 & c_1 & \cdots & c_{k-2} & c_{k-1} \end{bmatrix}^{\mathrm{T}}$$

thus

$$\frac{\partial}{\partial c_i}\underline{c} = \begin{bmatrix} 0 & \cdots & 0 & 1 & 0 & \cdots & 0 \end{bmatrix}^{\mathrm{T}} \tag{B.14}$$

The derivative is the $(i+1)$-th Euclidian basis vector $\underline{e}_{i+1}$, $i = 0,\ldots,k-1$ (vector of zeros except for a 1 in the $(i+1)$-th position).

b) $$\frac{\partial^2}{\partial c_j \partial c_i}\underline{c} = \underline{\mathbf{0}} \tag{B.15}$$

c) $\frac{\partial}{\partial c_i}\widehat{R}^{-1}_{\tilde{w}\tilde{w}}$

Using the following property of the derivative of a matrix inverse [14],

$$\frac{\partial}{\partial x}\boldsymbol{Y}^{-1} = -\boldsymbol{Y}^{-1}\left(\frac{\partial}{\partial x}\boldsymbol{Y}\right)\boldsymbol{Y}^{-1} \tag{B.16}$$

allows us to take the derivative of the linearly combined noise correlation matrix rather than of its inverse. The derivative of the real Toeplitz correlation matrix can be taken element by element, where each element is given by (2.51c)

$$r_{\tilde{w}\tilde{w},n} = \underline{c}^{\mathrm{T}} W_{r,n}\,\underline{c}$$

Taking the first derivative of (2.51c)

$$\frac{\partial}{\partial c_i} r_{\tilde{w}\tilde{w},n} = \left(\frac{\partial}{\partial c_i}\underline{c}^{\mathrm{T}}\right) W_{r,n}\,\underline{c} + \underline{c}^{\mathrm{T}} W_{r,n}\left(\frac{\partial}{\partial c_i}\underline{c}\right) \tag{B.17}$$

d) $\frac{\partial^2}{\partial c_j \partial c_i}\widehat{R}^{-1}_{\tilde{w}\tilde{w}}$

From (B.16)

$$\frac{\partial^2}{\partial y \partial x} \boldsymbol{Y}^{-1} = \frac{\partial}{\partial y}\left(\frac{\partial}{\partial x} \boldsymbol{Y}^{-1}\right)$$

$$= \frac{\partial}{\partial y}\left(-\boldsymbol{Y}^{-1}\left(\frac{\partial}{\partial x} \boldsymbol{Y}\right)\boldsymbol{Y}^{-1}\right)$$

$$= -\left(\frac{\partial}{\partial y}\boldsymbol{Y}^{-1}\right)\left(\frac{\partial}{\partial x} \boldsymbol{Y}\right)\boldsymbol{Y}^{-1} - \boldsymbol{Y}^{-1}\left(\frac{\partial^2}{\partial y \partial x}\boldsymbol{Y}\right)\boldsymbol{Y}^{-1}$$

$$-\boldsymbol{Y}^{-1}\left(\frac{\partial}{\partial x} \boldsymbol{Y}\right)\left(\frac{\partial}{\partial y}\boldsymbol{Y}^{-1}\right) \qquad \textbf{(B.18)}$$

The only quantity not yet computed is $\frac{\partial^2}{\partial y \partial x}\boldsymbol{Y}$, whose elements follow directly from (B.17)

$$\frac{\partial^2}{\partial c_j \partial c_i} r_{\tilde{w}\tilde{w},n} = \left(\frac{\partial^2}{\partial c_j \partial c_i}\underline{c}^{\mathrm{T}}\right) W_{r,n}\,\underline{c} + \left(\frac{\partial}{\partial c_i}\underline{c}^{\mathrm{T}}\right) W_{r,n}\left(\frac{\partial}{\partial c_j}\underline{c}\right)$$

$$+ \left(\frac{\partial}{\partial c_j}\underline{c}^{\mathrm{T}}\right) W_{r,n}\left(\frac{\partial}{\partial c_i}\underline{c}\right) + \underline{c}^{\mathrm{T}} W_{r,n}\left(\frac{\partial^2}{\partial c_j \partial c_i}\underline{c}\right)$$

Using (B.15) and the fact that all terms are scalars

$$\frac{\partial^2}{\partial c_j \partial c_i} r_{\tilde{w}\tilde{w},n} = \left(\frac{\partial}{\partial c_i}\underline{c}^{\mathrm{T}}\right) W_{r,n}\left(\frac{\partial}{\partial c_j}\underline{c}\right) + \left(\frac{\partial}{\partial c_j}\underline{c}^{\mathrm{T}}\right) W_{r,n}\left(\frac{\partial}{\partial c_i}\underline{c}\right)$$

$$= \left(\frac{\partial}{\partial c_i}\underline{c}^{\mathrm{T}}\right)\left(W_{r,n} + W_{r,n}^{\mathrm{T}}\right)\left(\frac{\partial}{\partial c_j}\underline{c}\right) \qquad \textbf{(B.19)}$$

Appendix C - Multivariate Gaussian Density Functions for L-ary MAP Detection

We defined an $L \times 1$ vector $\underline{y}$ consisting of the L MAMF filter outputs at time $n_0 = N - 1$. This appendix shows the effect of the FVMAMF and SSMAMF pre-filtering stages on the mean vector and covariance matrix required in the detection scheme of §2.7.

FVMAMF

The pre-filtering stage of the FVMAMF is defined as a unity gain. Under these conditions the estimated pre-filtered noise autocorrelations are all equal to a single matrix $\widehat{R}_{ww}$. Let m $(1 \leq m \leq L)$ denote the index of the vector and $m^* = m - 1$ $(0 \leq m^* \leq L - 1)$. Therefore, the m-th element of the mean vector conditioned on $\underline{s}_i$ being present at the system input (2.84) reduces to

$$\begin{aligned} \mu_m^i &= \underline{\widehat{h}}_{m^*}^{\mathrm{T}} \, \underline{s}_i \\ &= \underline{s}_{m^*}^{\mathrm{T}} \, \widehat{R}_{ww}^{-1} \, \underline{s}_i \end{aligned} \tag{C.1}$$

and the mn-th element of the covariance matrix $(1 \leq m,n \leq L, \;\; n^* = n - 1$ $0 \leq n^* \leq L - 1)$ is

$$\begin{aligned} \Sigma_{mn} &= \underline{\widehat{h}}_{m^*}^{\mathrm{T}} \, \widehat{R}_{w_{m^*} w_{n^*}} \, \underline{\widehat{h}}_{n^*} \\ &= \underline{s}_{m^*}^{\mathrm{T}} \, \widehat{R}_{w_{m^*} w_{m^*}}^{-1} \, \widehat{R}_{w_{m^*} w_{n^*}} \, \widehat{R}_{w_{n^*} w_{n^*}}^{-1} \, \underline{s}_{n^*} \end{aligned} \tag{C.2}$$

For the FVMAMF the cross-correlation matrix is equal to the autocorrelation matrix and (C.2) becomes

$$\Sigma_{mn} = \underline{s}_{m^*}^{\mathrm{T}} \, \widehat{R}_{ww}^{-1} \, \underline{s}_{n^*} \tag{C.3}$$

SSMAMF

The pre-filtering stage of the SSMAMF, defined in §2.5, yields a linearly combined signal for the $(m-1)$-th $(1 \leq m \leq L)$ SSMAMF assuming that the signal $\underline{s}_i$ is present at the pre-filter input.

$$\underline{\tilde{s}}_{m^* \mid i} = S_i \, \underline{c}_{m^*} \tag{C.4}$$

where $\underline{c}_j$ represents the combination coefficient vector which maximizes the OSNR of the j-th SSMAMF assuming that the signal $\underline{s}_j$ is present at the pre-filter input. The m-th element of the mean vector conditioned on signal $\underline{s}_i$ is

$$\begin{aligned} \mu_m^i &= \underline{\hat{h}}_{m^*}^{\mathrm{T}} \, \underline{\ell}_{m^*}(\underline{s}_i) \\ &= \underline{\hat{h}}_{m^*}^{\mathrm{T}} \, S_i \, \underline{c}_{m^*} \end{aligned} \tag{C.5}$$

The mn-th element of the covariance matrix is

$$\Sigma_{mn} = \underline{\hat{h}}_{m^*}^{\mathrm{T}} \, \hat{R}_{\tilde{w}_{m^*} \tilde{w}_{n^*}} \, \underline{\hat{h}}_{n^*} \tag{C.6}$$

In order to compute the Toeplitz cross-correlation matrix required for (C.6) we need to generate the cross-correlation between the $(m-1)$-th and the $(n-1)$-th linearly combined noises. This follows closely the development for the autocorrelation of the linearly combined noise in §2.5.2. Denote the l-th element of the i-th linearly combined noise as $\tilde{w}_{i,l}$, then

$$\begin{aligned} r_{\tilde{w}_i \tilde{w}_j, n} &= E\left\{ \tilde{w}_{i,l} \tilde{w}_{j,l+n} \right\} \\ &= E\left\{ \sum_{q=0}^{k-1} c_{i,q} \, w_{(k-q)M-l-1} \sum_{s=0}^{k-1} c_{j,s} \, w_{(k-s)M-l-1-n} \right\} \\ &= E\left\{ \sum_{q=0}^{k-1} c_{i,q} \sum_{s=0}^{k-1} c_{j,s} \, w_{(k-q)M-l-1} \, w_{(k-s)M-l-1-n} \right\} \end{aligned}$$

$$= \sum_{q=0}^{k-1} c_{i,q} \sum_{s=0}^{k-1} c_{j,s} E\left\{ w_{(k-q)M-l-1} \; w_{(k-s)M-l-1-n} \right\}$$

$$= \sum_{q=0}^{k-1} c_{i,q} \sum_{s=0}^{k-1} c_{j,s} r_{ww,\, qM-sM-n}$$

$$= \sum_{q=0}^{k-1} c_{i,q} \sum_{s=0}^{k-1} c_{j,s} r_{ww,\, M(q-s)-n} \qquad \text{(C.7}a\text{)}$$

Since the noise is assumed real, we have from the properties of the autocorrelation function that $r_{ww,x} = r_{ww,-x}$ [1], thus

$$r_{\tilde{w}_i \tilde{w}_j, n} = \sum_{q=0}^{k-1} c_{i,q} \sum_{s=0}^{k-1} c_{j,s} r_{ww,\, n+M(s-q)} \qquad \text{(C.7}b\text{)}$$

$$= \underline{c}_i^{\mathrm{T}} W_{r,n} \underline{c}_j \qquad 0 \leq n \leq M-1 \qquad \text{(C.7}c\text{)}$$

REFERENCES

[1] G. R. Cooper and C. D. McGillem, *Probabilistic Methods of Signal and System Analysis.* New York: Holt, Rinehart and Winston, Inc., 1971.

[2] A. Papoulis, *Probability, Random Processes, and Estimation Theory for Engineers.* New York: McGraw-Hill, 1984.

[3] J. M. Wilson, "Robust Communication in a Time-Varying Noisy Environment," M. S. Thesis, Virginia Polytechnic Institute and State University, Blacksburg, VA, November 1987.

[4] K. A. Becker, "Effects of Spectral Estimation on Matched Filter Design," M. S. Thesis, Virginia Polytechnic Institute and State University, Blacksburg, VA, May 1985.

[5] N. S. Kontoyannis, "Detector Design and Estimation for a Digital Communication System," M. S. Thesis, Virginia Polytechnic Institute and State University, Blacksburg, VA, July 1991.

[6] S. M. Kay, *Modern Spectral Estimation.* New Jersey: Prentice Hall,1988.

[7] Y. Bresler and A. Macovski, "Exact Maximum Likelihood Parameter Estimation of Superimposed Exponential Signals in Noise," *IEEE Transactions ASSP* **34**:5, pp. 1081-1089 (October 1986).

[8] R. Kumaresan, L. L. Scharf, and A. K. Shaw, "An Algorithm for Pole-Zero Modeling and Spectral Analysis," *IEEE Transactions ASSP* **34**:3, pp. 637-640 (June 1986).

[9] H. Anton, *Elementary Linear Algebra.* New York: Wiley & Sons, 1987.

[10] L. B. Jackson, *Digital Filters and Signal Processing.* Boston: Kluwer Academic Publishers, 1989.

[11] J. E. Dennis and R. B. Schnabel, *Numerical Methods for Unconstrained Optimization and Nonlinear Equations.* New Jersey: Prentice-Hall.

[12] K. Atkinson, *Elementary Numerical Analysis.* New York: Wiley & Sons, 1985.

[13] A. D. Whalen, *Detection of Signals in Noise.* New York: Academic Press, 1971.

[14] W. H. Beyer (Ed.), *CRC Standard Mathematical Tables.* Boca Raton: CRC Press, 1987.

[15] F. A. Graybill, *Introduction to Matrices with Applications in Statistics.* Belmont: Wadsworth Publishing Co., Inc., 1969.

[16] A. Cantoni and P. Butler, "Eigenvalues and Eigenvectors of Symmetric Centrosymmetric Matrices," *Linear Algebra and its Applications* **13**:3, pp. 275-288, 1976.

[17] J. Dugré, A. A. Beex and L. L. Scharf, "Generating Covariance Sequences and the Calculation of Quantization and Rounding Error Variances in Digital Filters," *IEEE Transactions ASSP* **28**:1, pp. 102-104 (February 1980).

[18] K. S. Shanmugan and A. M. Breipohl, *Random Signals: Detection, Estimation, and Data Analysis.* New York: Wiley & Sons, 1988.

[19] H. Stark and J. W. Woods, *Probability, Random Processes, and Estimation Theory for Engineers.* New Jersey: Prentice Hall, 1986.

[20] B. D. O. Anderson and J. B. Moore, *Optimal Filtering.* New Jersey: Prentice Hall, 1979.

[21] B. D. O. Anderson and J. B. Moore, *Optimal Control - Linear Quadratic Methods.* New Jersey: Prentice Hall, 1990.

[22] C. L. Weber, *Elements of Detection and Signal Design.* New York: Springer-Verlag, 1987.

[23] H. R. Raemer, *Statistical Communication Theory and Applications.* New Jersey: Prentice Hall, 1969.

[24] D. P. Bertsekas, *Constrained Optimization and Lagrange Multiplier Methods.* New York: Academic Press, 1982.

[25] D. A. Wismer and R. Chattergy, *Introduction to Nonlinear Optimization.* New York: North Holland, 1979.

[26] P. E. Gill and W. Murray (Ed.), *Numerical Methods for Constrained Optimization.* New York: Academic Press, 1974.

[27] G. Arfken, *Mathematical Methods for Physicists.* New York: Academic Press, 1970.

[28] J. Makhoul, "On the Eigenvectors of Symmetric Toeplitz Matrices," *IEEE Transactions ASSP* **29**:4, pp. 868-872 (August 1981).

[29] H. Taub and D. L. Schilling, *Principles of Communication Systems.* New York: McGraw-Hill, 1986.

VITA

Jerry Roger Mitchell, Jr. was born on October 29th, 1960 in Buffalo, NY, moved to Mayaguez, Puerto Rico in 1965 and to Palmyra, NY in 1968. He attended Palmyra Elementary School and graduated with honors from Palmyra-Macedon High School in 1978.

After one year of college at SUNY Geneseo, he decided to abandon his education in favor of the workplace. He was employed for ≈ 5 years with Mobil Chemical's Plastic Division in their Research and Development Center in Macedon, NY. Following his departure from Mobil, he entered MacMurray College in Jacksonville, IL where he continued his education for another year. He then re-entered the job market working for Wynn's Precision in Lynchburg, VA.

Finally, deciding to seriously continue his education he enrolled at Virginia Tech in the fall of 1987, completed his Bachelor of Science in Electrical Engineering in May of 1990, and remained to pursue his Masters degree.

He received the NY State Regents Scholarship, Konrad-Steinmetz Scholarship, and membership offers to a variety of honor societies. He is a member of IEEE Signal Processing, Communications, and Control Systems Societies and has been employed as a Graduate Project Assistant since May 1990.